STUDIES OF MAGNETIC MICROPULSATIONS WITH SPECIAL REFERENCE TO DISCRETE EMISSIONS IN THE VICINITY OF ONE CYCLE PER SECOND

VOLUME II

A Thesis presented for the
degree of Doctor of Philosophy.

University of Canterbury
1965

B. J. Fraser

LIST OF FIGURES

Figure

Figure 2.1. Block diagram of the micropulsation recording system. For the correlation of magnetic effects with individual meteors the meteor echo pulses were recorded on the chart recorder in place of the broad-band micropulsation signal.

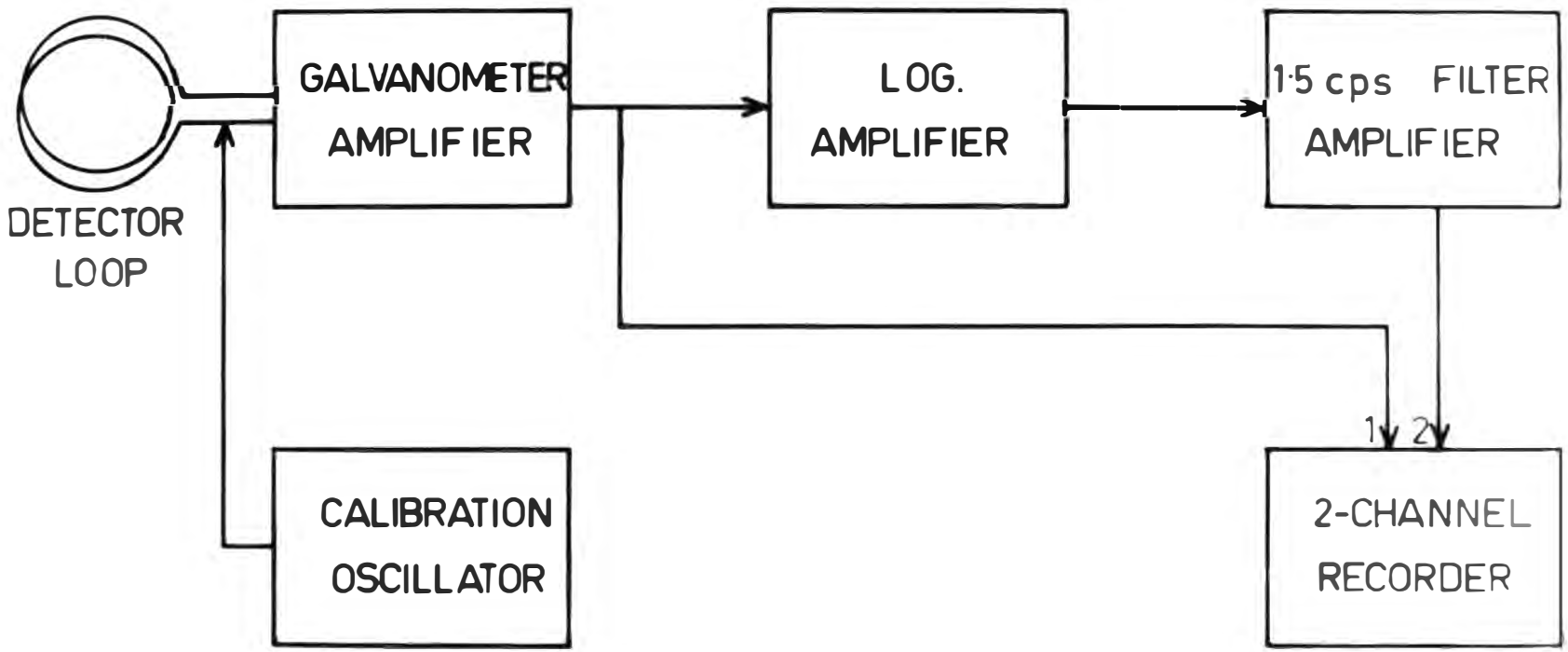
DETECTOR
LOOP
GALVANOMETER
AMPLIFIER
LOG.
AMPLIFIER
1·5 cps FILTER
AMPLIFIER
1
2
CALIBRATION
OSCILLATOR
2-CHANNEL
RECORDER

Figure 2.2. Micropulsation recording equipment frequency response curves.

Galvanometer-photocell amplifier ×

Semi-logarithmic amplifier △

1.5 cps filter amplifier with rise time of 3 sec. ○

1.5 cps filter amplifier with rise time of 1 sec. □

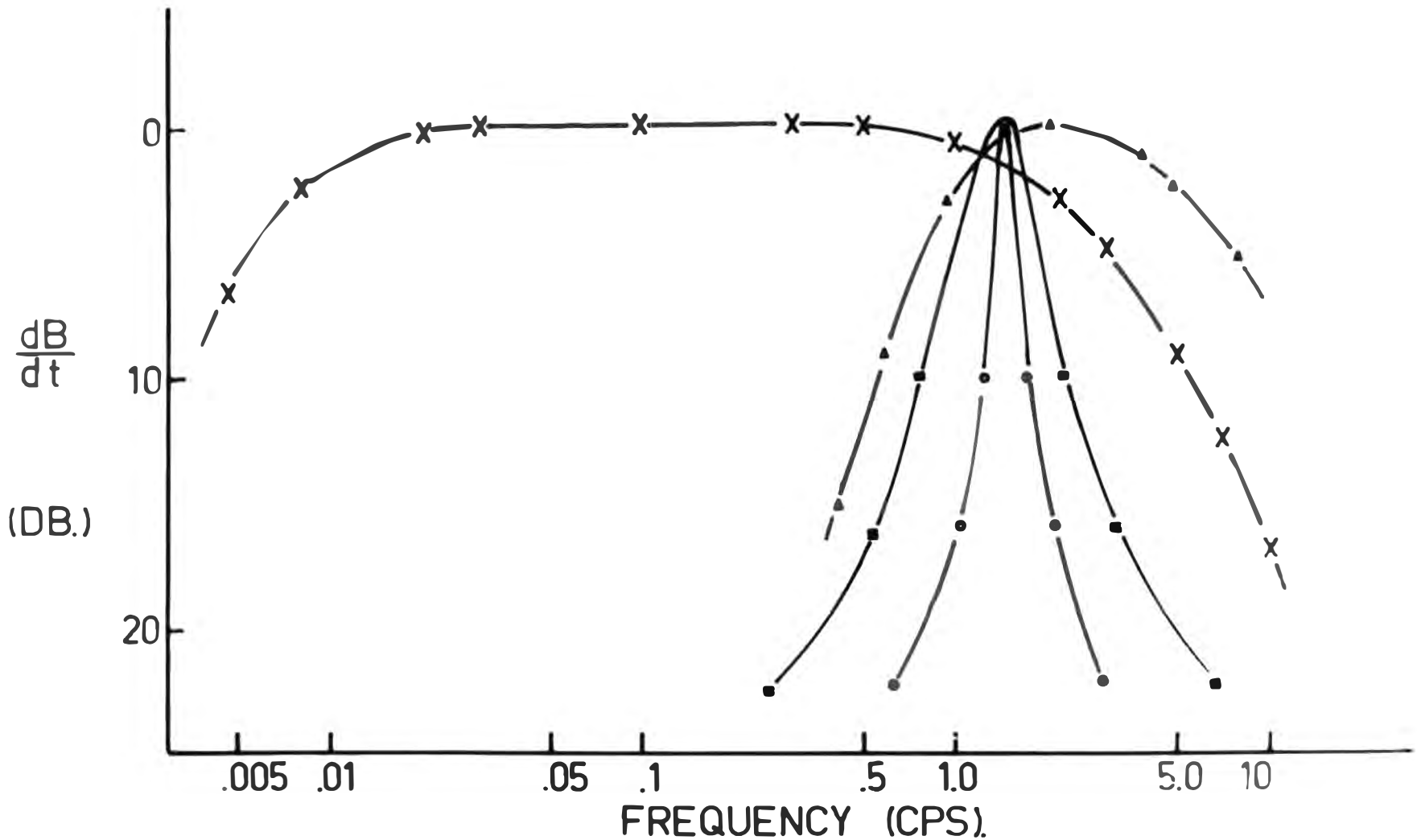
0
10
20
dB
dt
(DB.)
.005
.01
.05
.1
.5
1.0
5.0
10
FREQUENCY (CPS).

Figure 2.3. Meteor rates recorded simultaneously by film and chart displays for the night of April 30 - May 1, 1962.

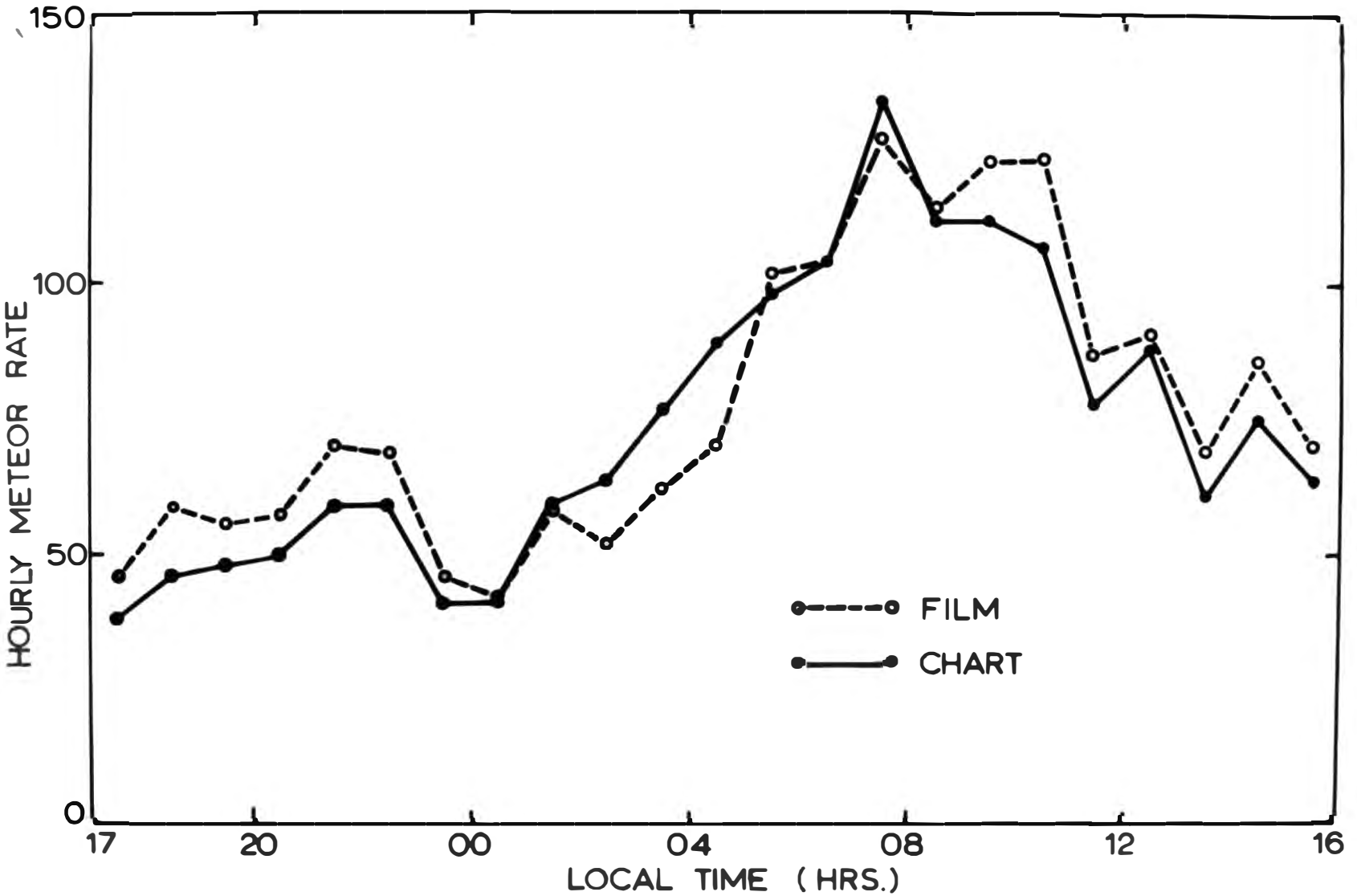
150
100
50
0
HOURLY METEOR RATE
FILM
CHART
17
20
00
04
08
12
16
LOCAL TIME (HRS.)

Figure 2.4. Mean hourly all-sky meteor rates for the period March 5-16, 1962.

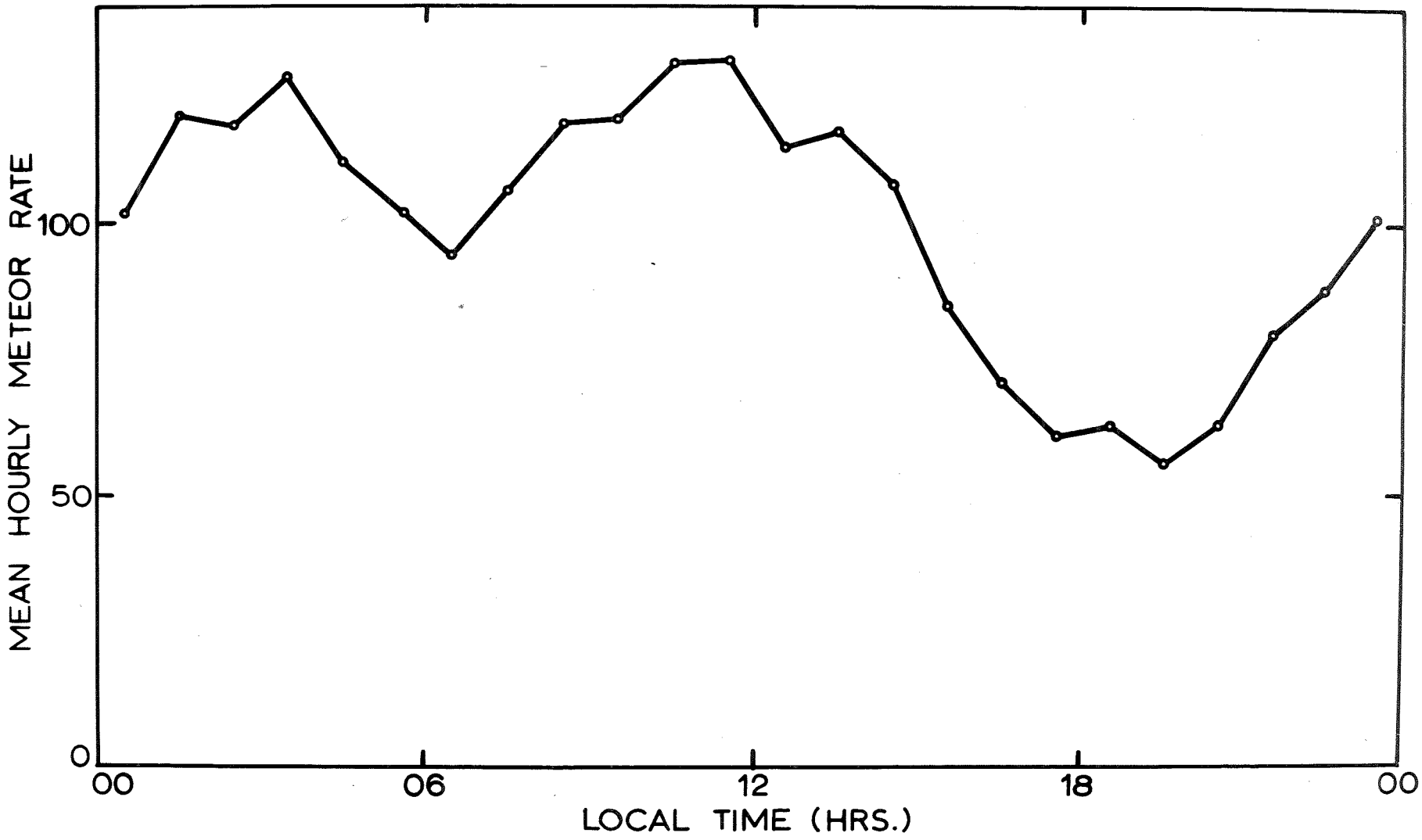
MEAN HOURLY METEOR RATE
100
50
0
00
06
12
18
00
LOCAL TIME (HRS.)

Figure 2.5. Comparison of mean hourly all-sky meteor rates and mean 1.5 cps micropulsation occurrence rates over the period March 5-16, 1962.

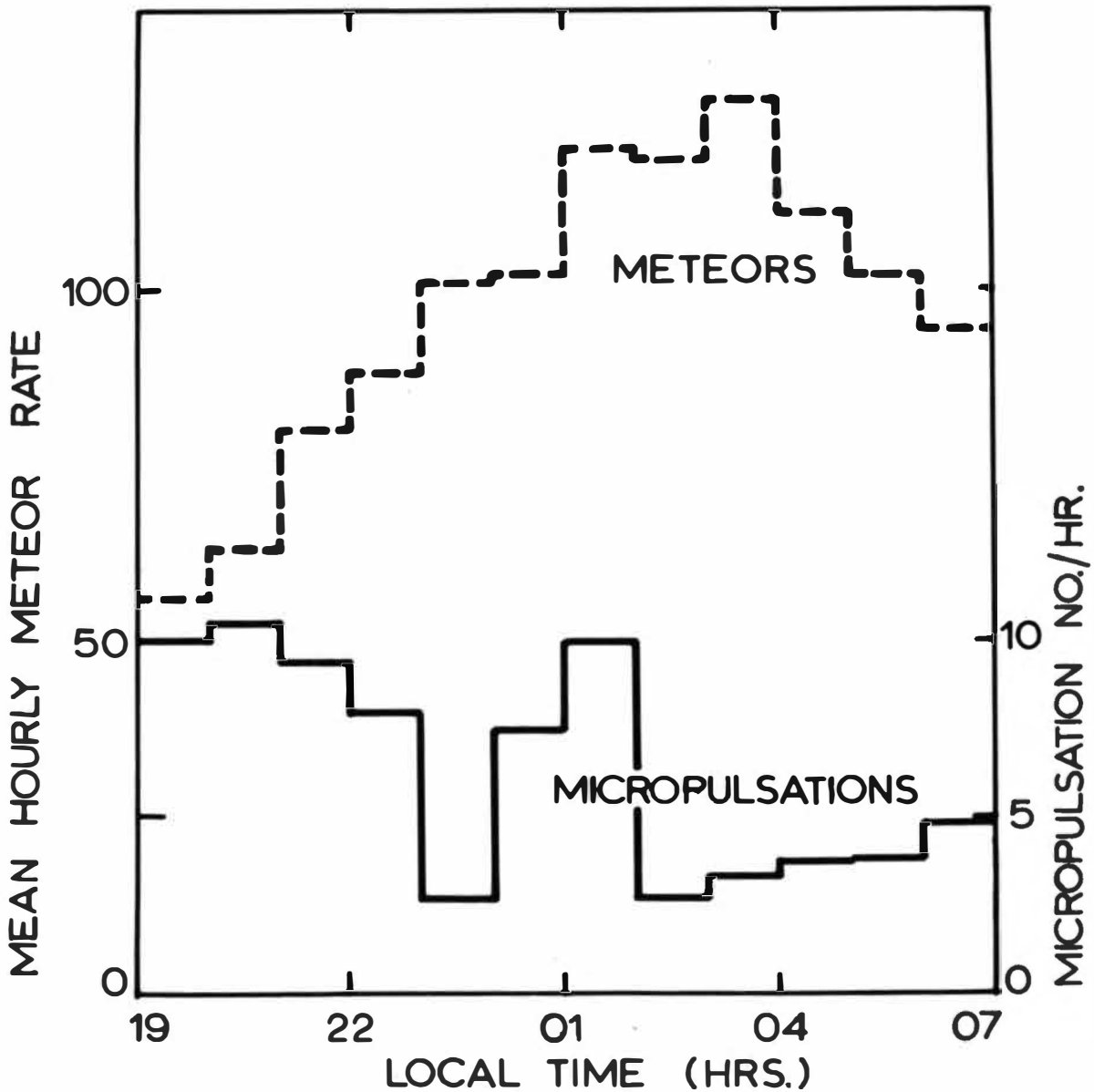
METEORS
MICROPULSATIONS
MEAN HOURLY METEOR RATE
MICROPULSATION NO./HR.
100
50
0
10
5
0
19
22
01
04
07
LOCAL TIME (HRS.)

Figure 2.6. Mean hourly localized meteor rates for the period March 23 through April 6, 1962.

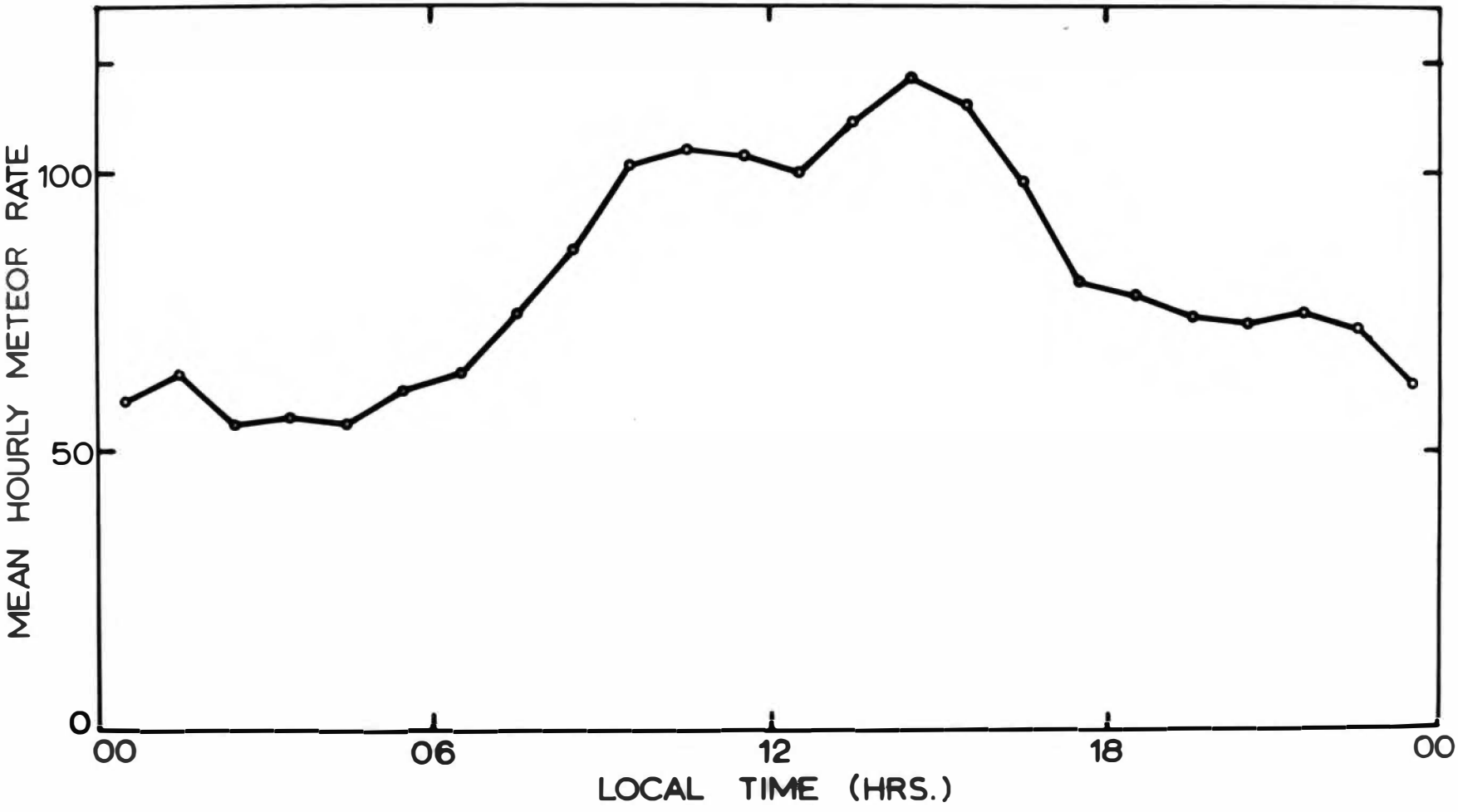
MEAN HOURLY METEOR RATE
100
50
0
00
06
12
18
00
LOCAL TIME (HRS.)

Figure 2.7. Comparison of mean hourly localized meteor rates and mean 1.5 cps micropulsation occurrence rates over the period March 23 through April 6, 1962.

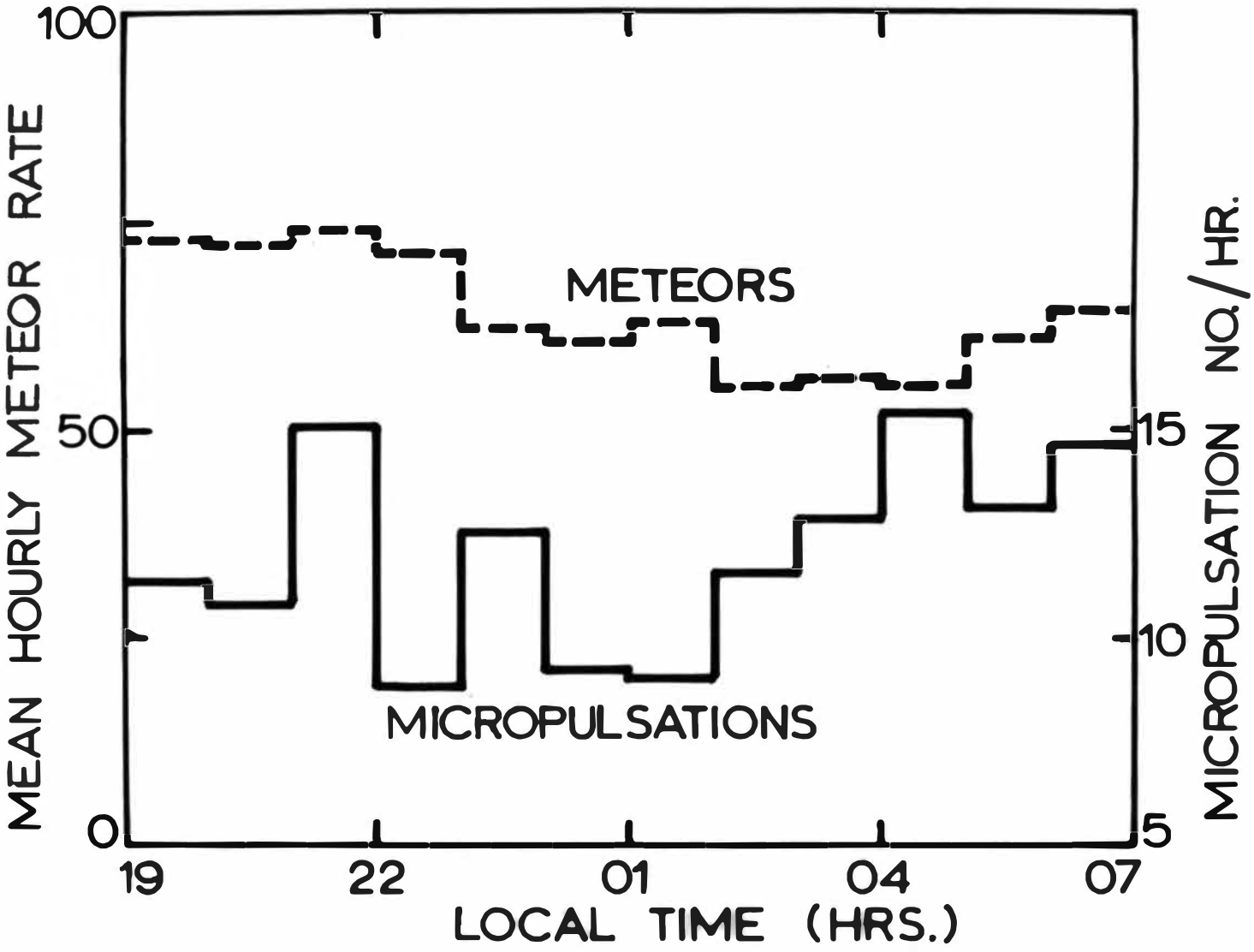
100
50
0
MEAN HOURLY METEOR RATE
METEORS
MICROPULSATIONS
15
10
5
MICROPULSATION NO./HR.
19
22
01
04
07
LOCAL TIME (HRS.)

Figure 2.8. Hourly localized meteor and micropulsation rates for three representative hours in the period March 23 through April 10, 1962.

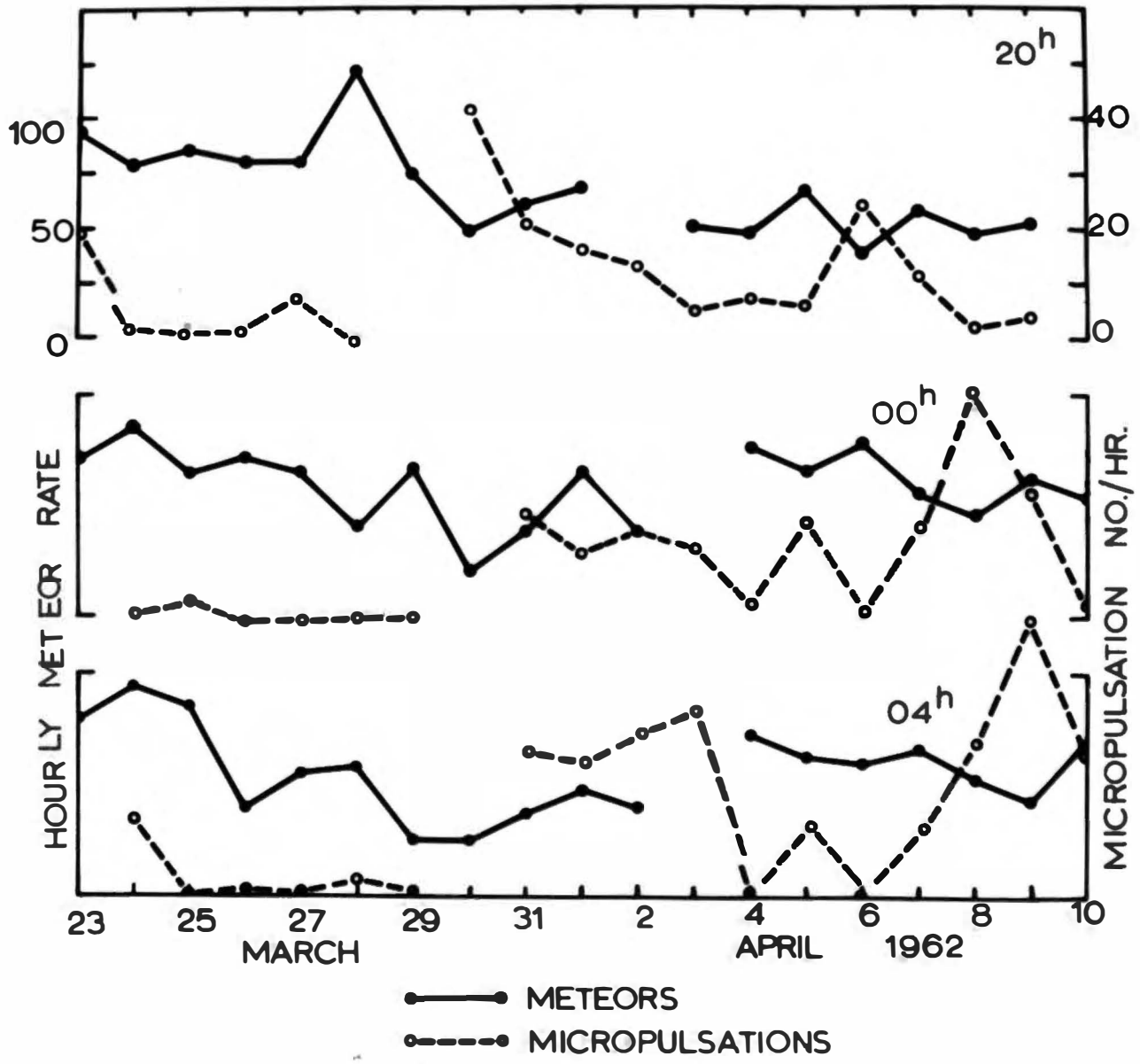
20h
00h
04h
100
50
0
40
20
0
HOURLY METEOR RATE
MICROPULSATION NO./HR.
23
25
27
29
31
2
4
6
8
10
MARCH
APRIL
1962
METEORS
MICROPULSATIONS

Figure 2.9. Mean hourly 1.5 cps micropulsation rates for September 14 through October 6 and October 9 through November 6, 1962.

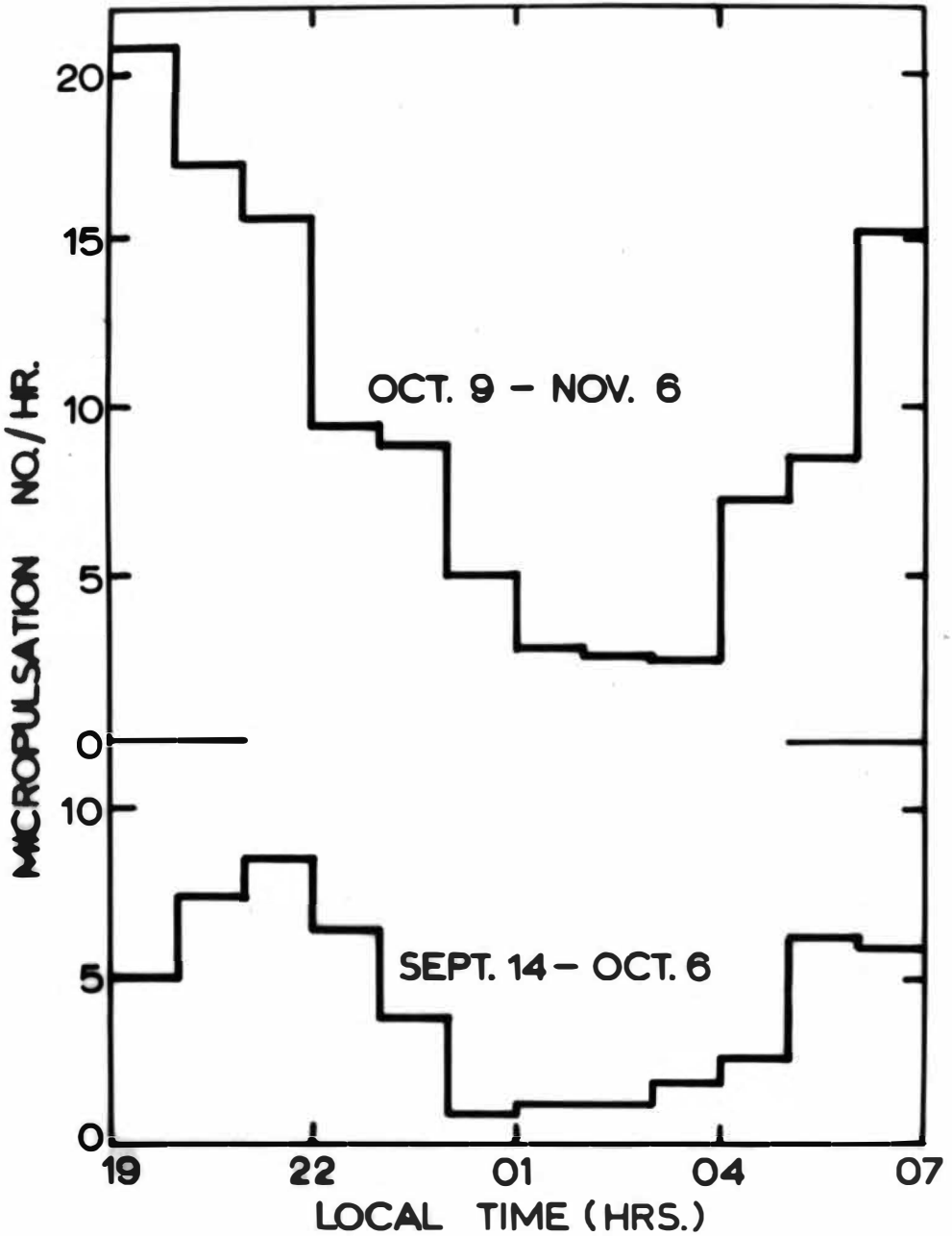
MICROPULSATION NO./HR.
20
15
10
5
0
10
5
0
OCT. 9 – NOV. 6
SEPT. 14 – OCT. 6
19
22
01
04
07
LOCAL TIME (HRS.)

Figure 2.10. Sample of chart obtained on May 27, 1962, giving simultaneous presentation of meteors and micropulsations. The time markers on the bottom trace are at 1 minute intervals.


METEORS
MICROPULSATIONS
1·0 mγ
·3 mγ
·1 mγ
·05 mγ
·3 mγ
1·0 mγ
·1 mγ
·05 mγ

Figure 3.1. Z component record of the magnetic disturbance produced by the July 9, 1962 high-altitude nuclear explosion. Full-scale deflection is 0.5 γ/ sec peak-to-peak.

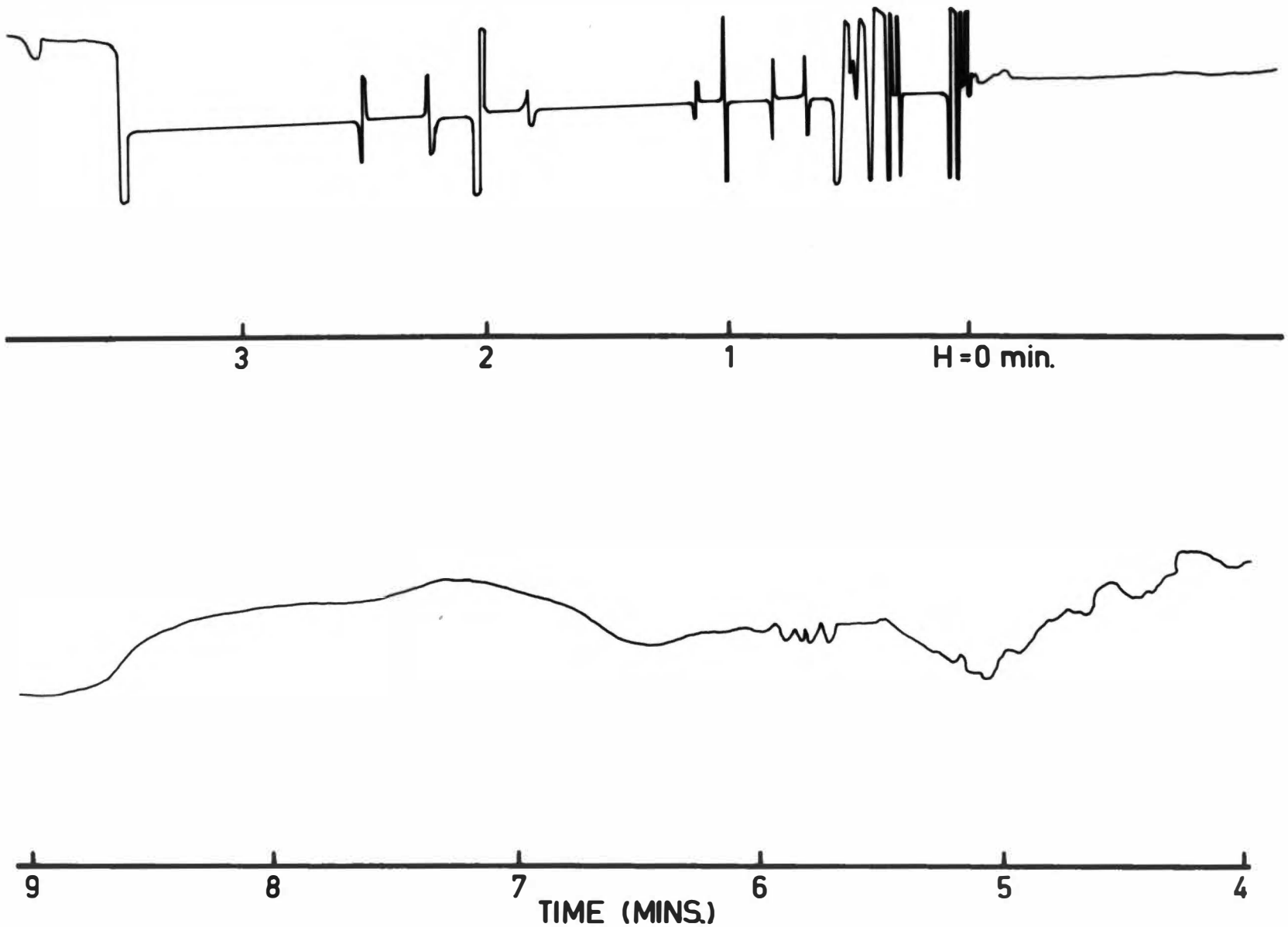
3
2
1
H=0 min.
9
8
7
6
5
4
TIME (MINS.)

Figure 3.2. Reconstructed record of the magnetic disturbance from the July 9, 1962 nuclear explosion. The dotted and dashed lines indicate off-scale peak-to-peak signal levels greater than 0.95 γ / sec, and between 0.5 γ / sec and 0.95 γ / sec respectively.

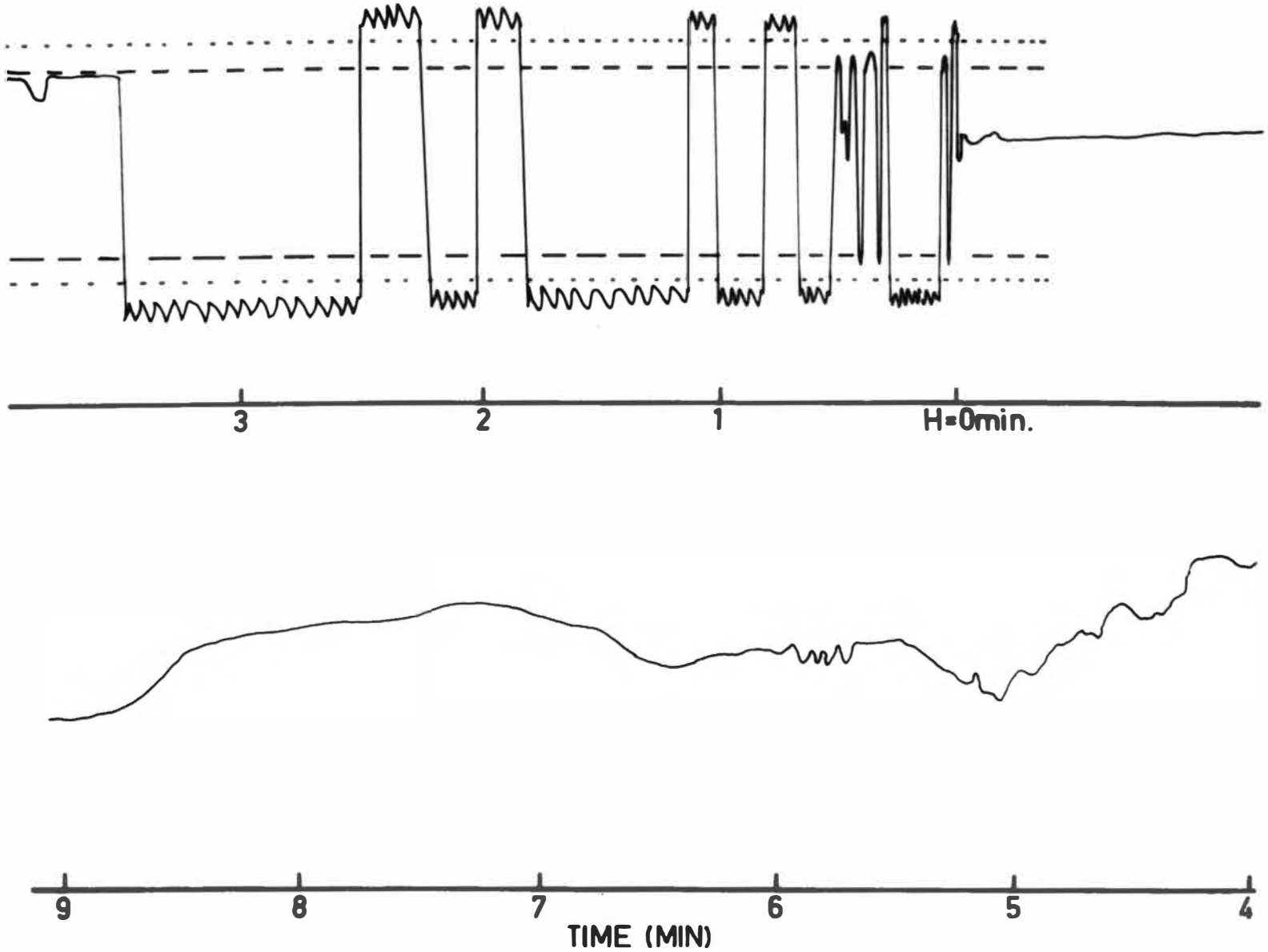
3
2
1
H=0min.
9
8
7
6
5
4
TIME (MIN)

Figure 4.1. Five-day averages of magnetic activity at 1.5 cps recorded within the period September 15 to November 6, 1962.

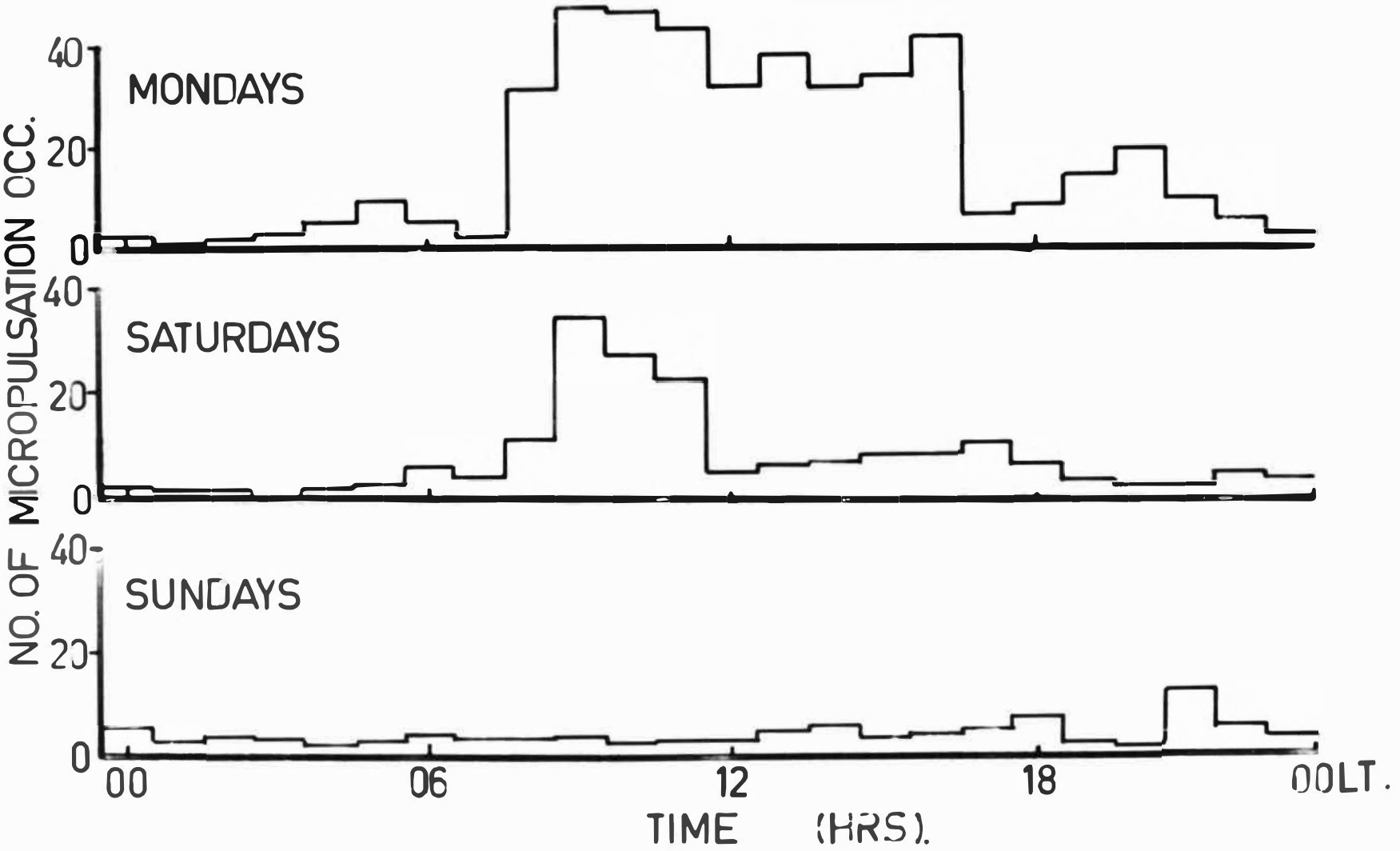
MONDAYS
SATURDAYS
SUNDAYS
40
20
0
NO. OF MICROPULSATION OCC.
00
06
12
18
00LT.
TIME (HRS).

Figure 4.2. Magnetic effects due to power grid supplying electric trains. Top: f = 1.5 cps magnetic record. Middle: f = 0.008 - 1.6 cps magnetic record showing impulsive interference with maximum peak-to-peak amplitudes of 0.05 γ / sec. Bottom: 1 minute time marks. (Time moves from right to left.)

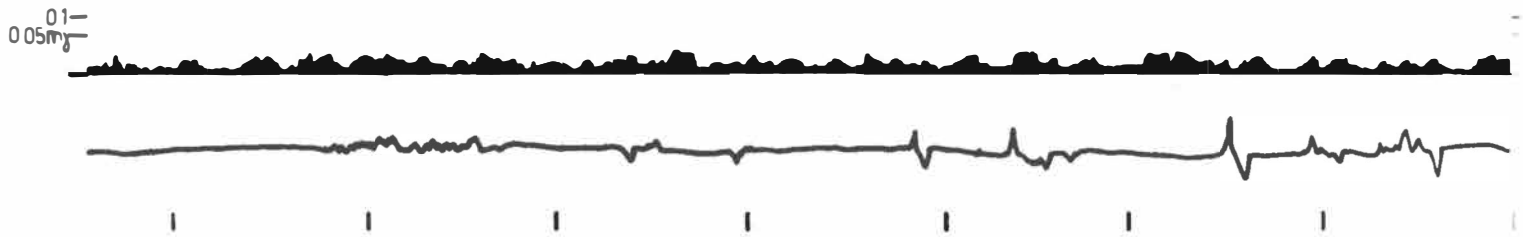
0 1—
0 05mV

Figure 4.3. Correlation of electric train fluctuations due to train movements, and resulting magnetic effects. Time moves from right to left, and the length LC = 17 minutes. Top: electric-power-factor variations (arrows indicate scheduled stopping times at intermediate stations). Middle: simultaneous magnetic effects in the frequency band 0.008-0.25 cps. Bottom: train movements. L = Lyttelton; C = Christchurch.

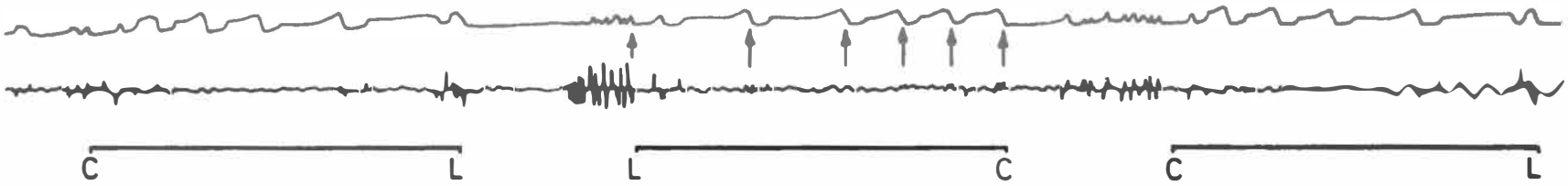
C
L
L
C
C
L

Figure 5.1. Equivalent circuit of the detector coil galvanometer-photocell amplifier system.

The symbols used are:

e_s - voltage generated by the detector coil

N - number of turns on the detector coil

a - cross-sectional area of the detector coil core

B_o - component of the geomagnetic field along the axis of the coil

ω - angular frequency of the oscillations of B_o.

μ' - effective permeability of the detector coil core

θ - angular deflection of the galvanometer mirror

G - galvanometer constant

V_G - back e.m.f. induced in the galvanometer coil

A - gain of the optical-transistor amplifier

R_L - resistance of the detector coil

L - inductance of the detector coil

R_g - galvanometer resistance

R_o - output impedance of the optical-transistor amplifier

R_f - feedback resistance.

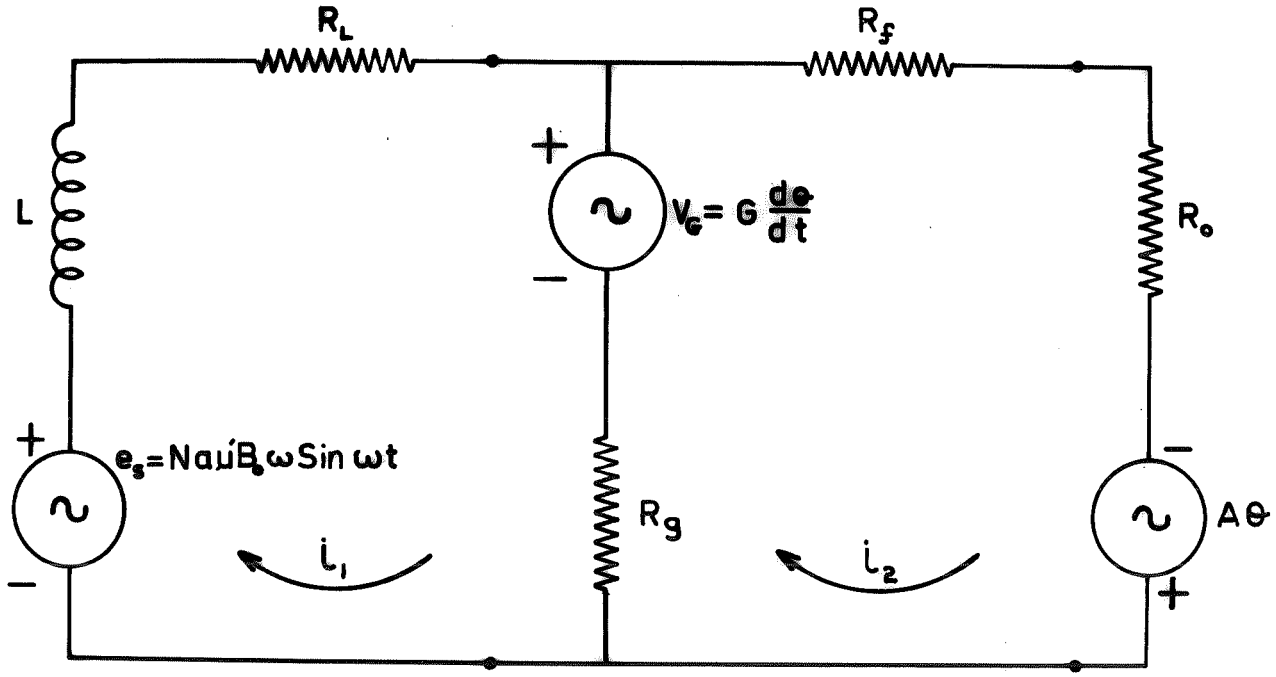
R_L
R_f
L
$V_c = G\frac{de}{dt}$
R_o
$e_s = N a \mu B_0 \omega \sin \omega t$
R_g
i_1
i_2
$A\theta$

Figure 5.2. A family of theoretical frequency response curves for the galvanometer photocell amplifier. The corresponding values of feedback resistance (R_f) are also indicated.

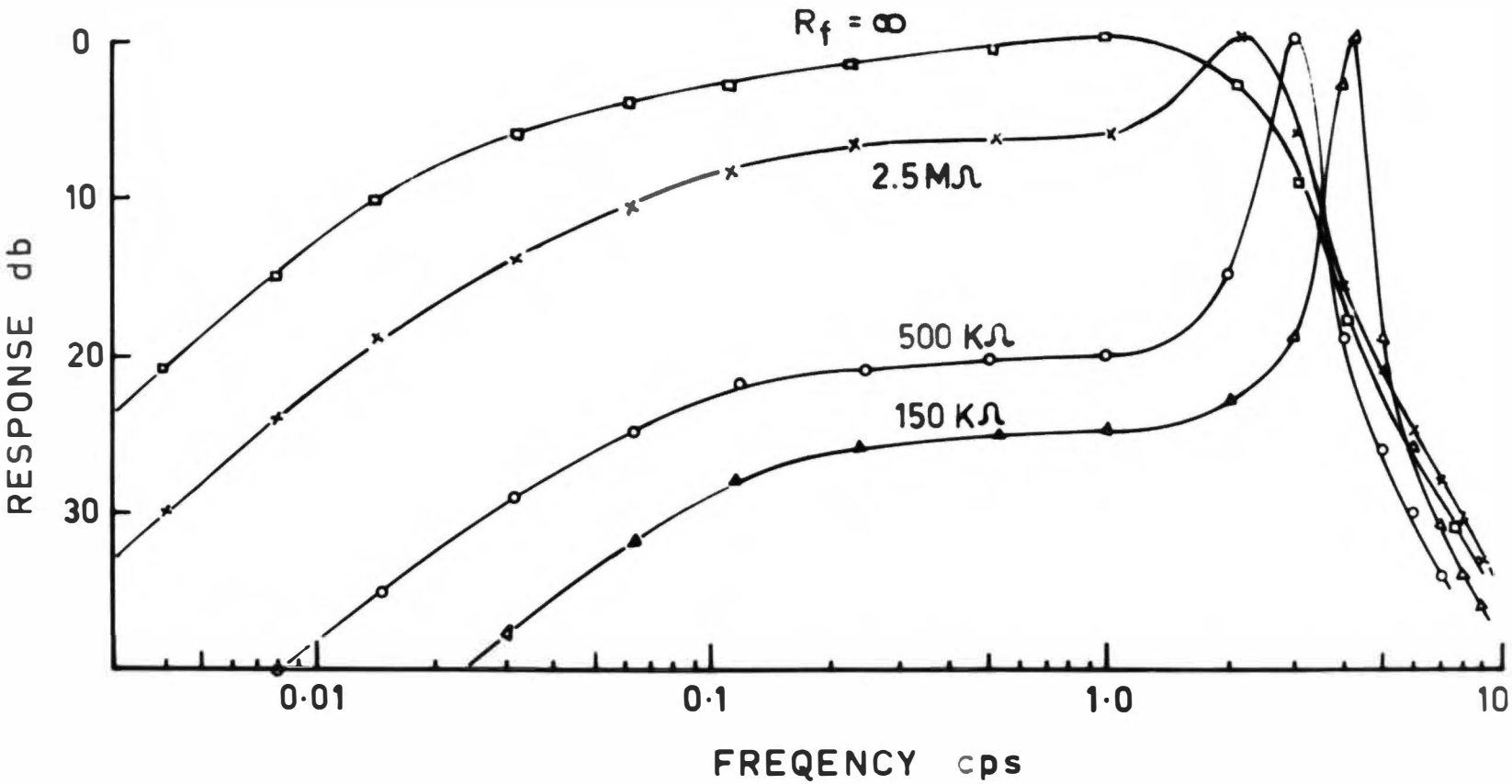
$R_f = \infty$
2.5 MΩ
500 KΩ
150 KΩ
0
10
20
30
RESPONSE db
0·01
0·1
1·0
10
FREQENCY cps

Figure 5.3 A comparison of theoretical and experimental galvanometer photocell amplifier frequency response curves. The theoretical curve was calculated for R_f = 1.2MΩ and the experimental curve (dashed) was obtained for R_f = 1.17MΩ.

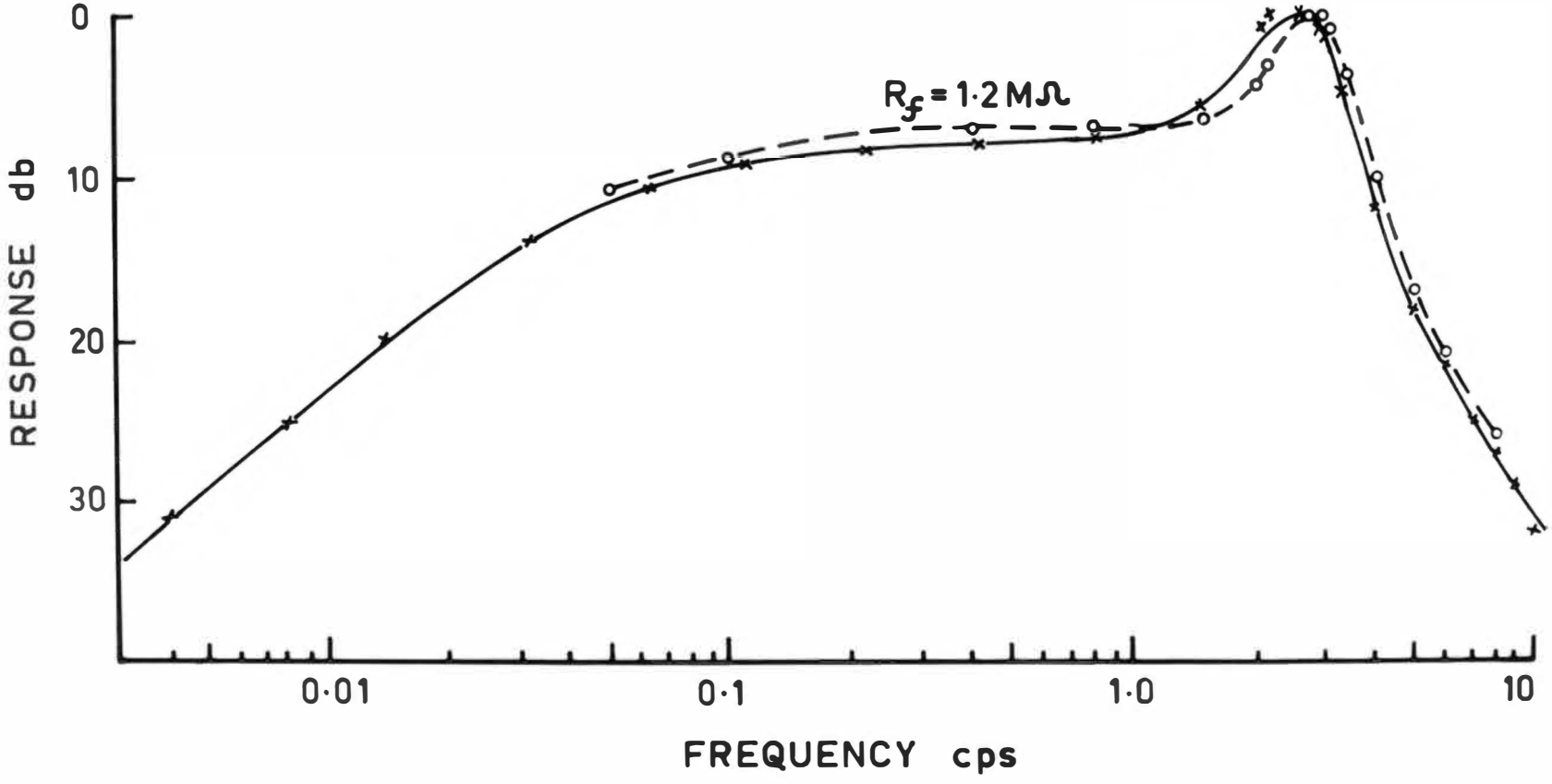
0
10
20
30
RESPONSE db
$R_f = 1{\cdot}2\,M\Omega$
0·01
0·1
1·0
10
FREQUENCY cps

Figure 6.1 (a). The portable transistorized micropulsation recording equipment. From left to right; galvanometer-photocell amplifier, slow-speed tape recorder, batteries, and voltage regulator.

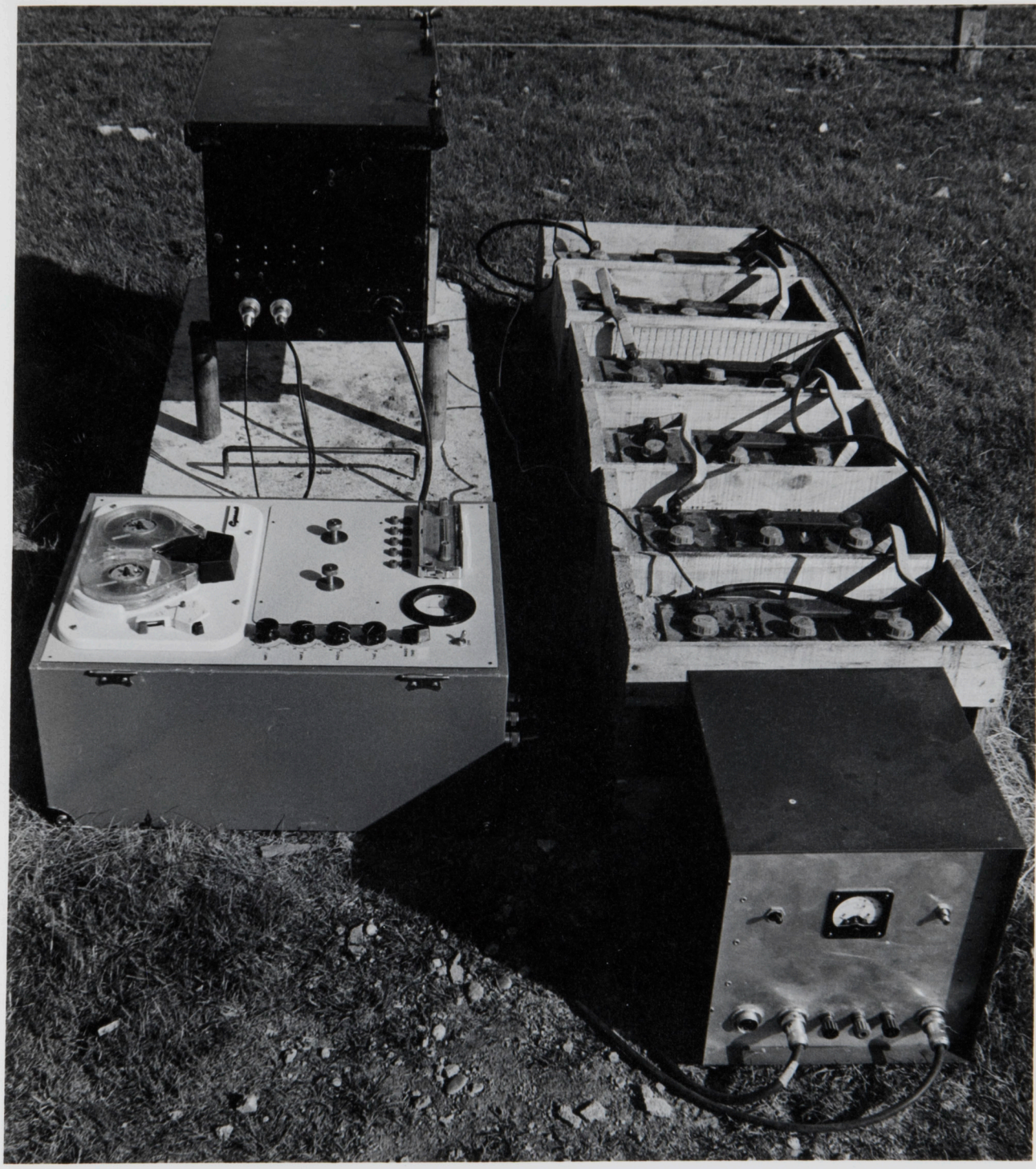

Figure 6.1 (b). The slow-speed tape deck showing the "Vero-board" circuitry.

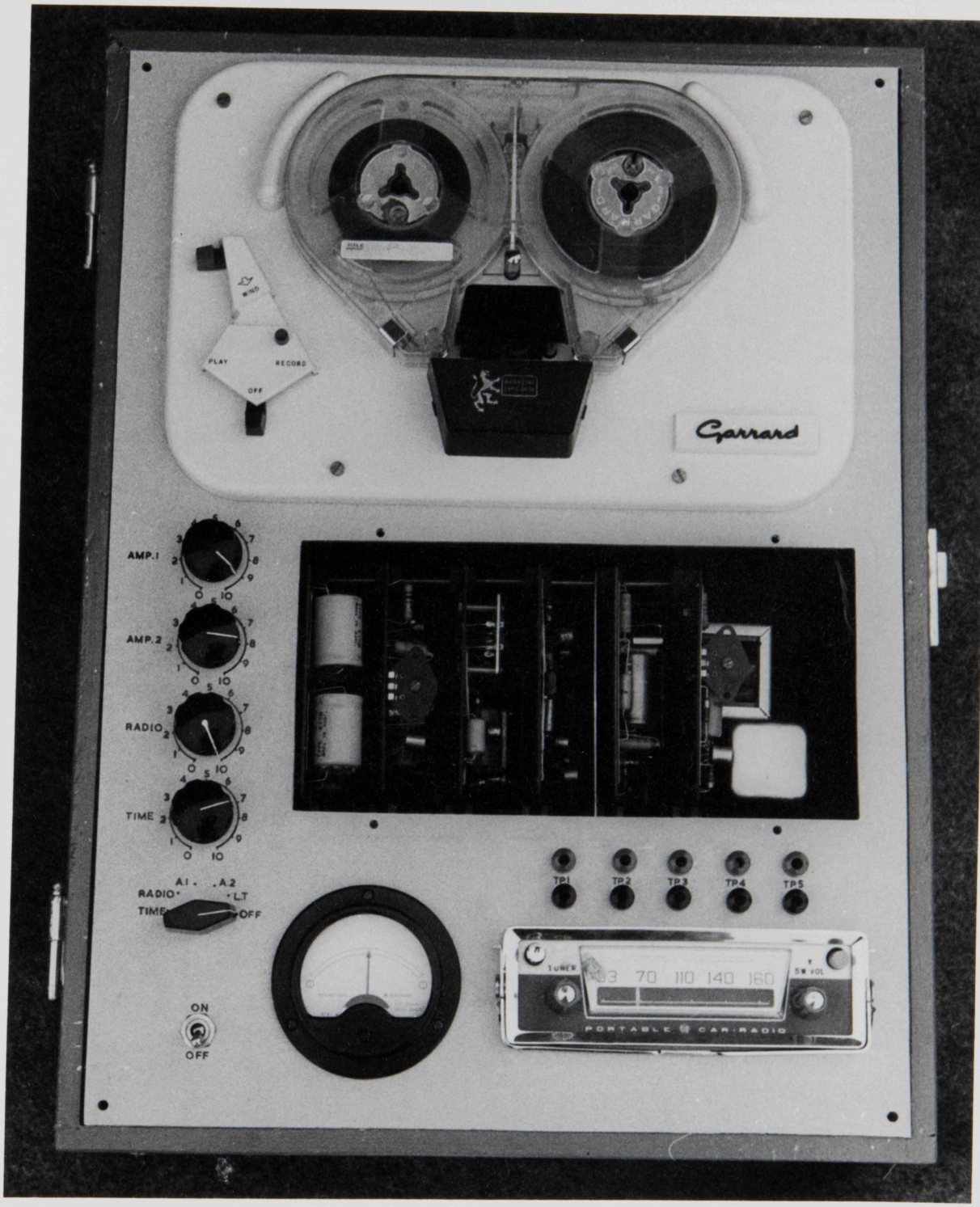
WIND
PLAY
RECORD
OFF
Garrard
AMP.1
AMP.2
RADIO
TIME
A1 . . A2
RADIO
LT
TIME
OFF
ON
OFF
TP1
TP2
TP3
TP4
TP5
TUNER
SW VOL
70 110 140 160
PORTABLE CAR-RADIO

Figure 6.2. Block diagram of the portable transistorized recording system.

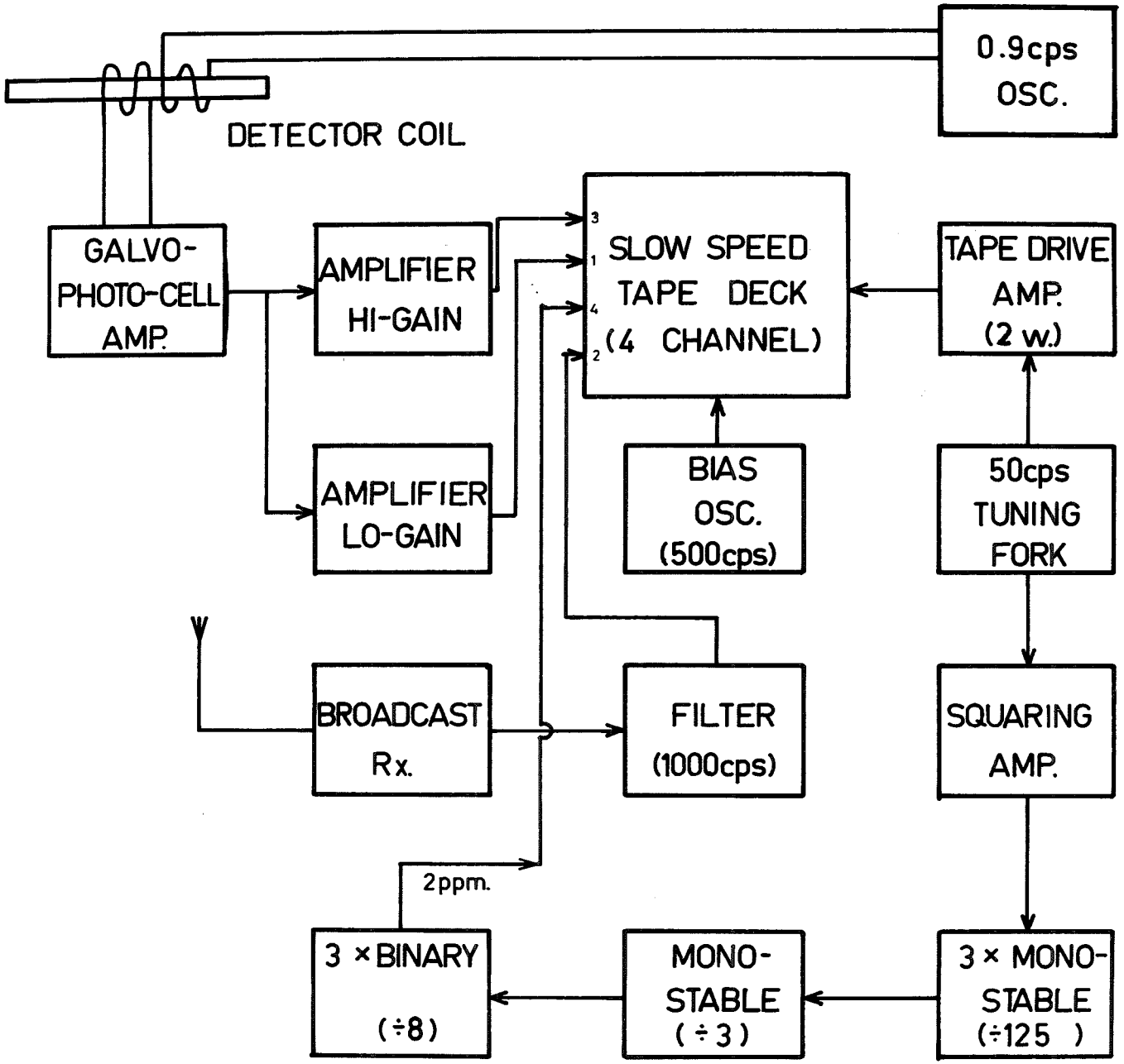
0.9cps
OSC.
DETECTOR COIL
GALVO-
PHOTO-CELL
AMP.
AMPLIFIER
HI-GAIN
3
1
4
2
SLOW SPEED
TAPE DECK
(4 CHANNEL)
TAPE DRIVE
AMP.
(2 w.)
AMPLIFIER
LO-GAIN
BIAS
OSC.
(500cps)
50cps
TUNING
FORK
BROADCAST
Rx.
FILTER
(1000cps)
SQUARING
AMP.
2ppm.
3 × BINARY
(÷8)
MONO-
STABLE
(÷3)
3 × MONO-
STABLE
(÷125)

Figure 7.1. Data analysis equipment. From left to right; pulse counter, playback tape recorder (containing the AF and pulse amplifiers), Sonagraph amplifier-analyser, and Sonagraph display unit.

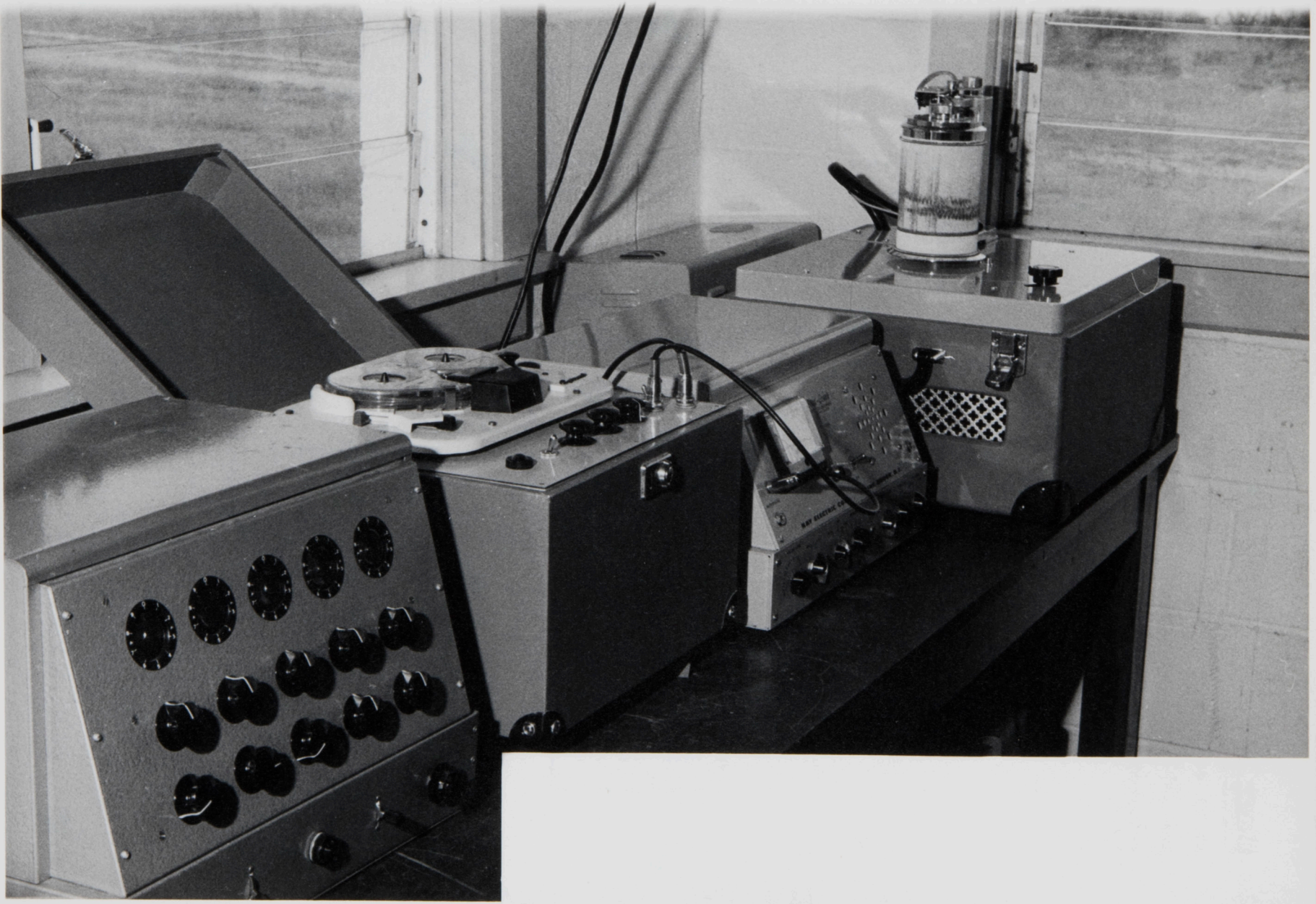

Figure 7.2. Block diagram of the data analysis system.

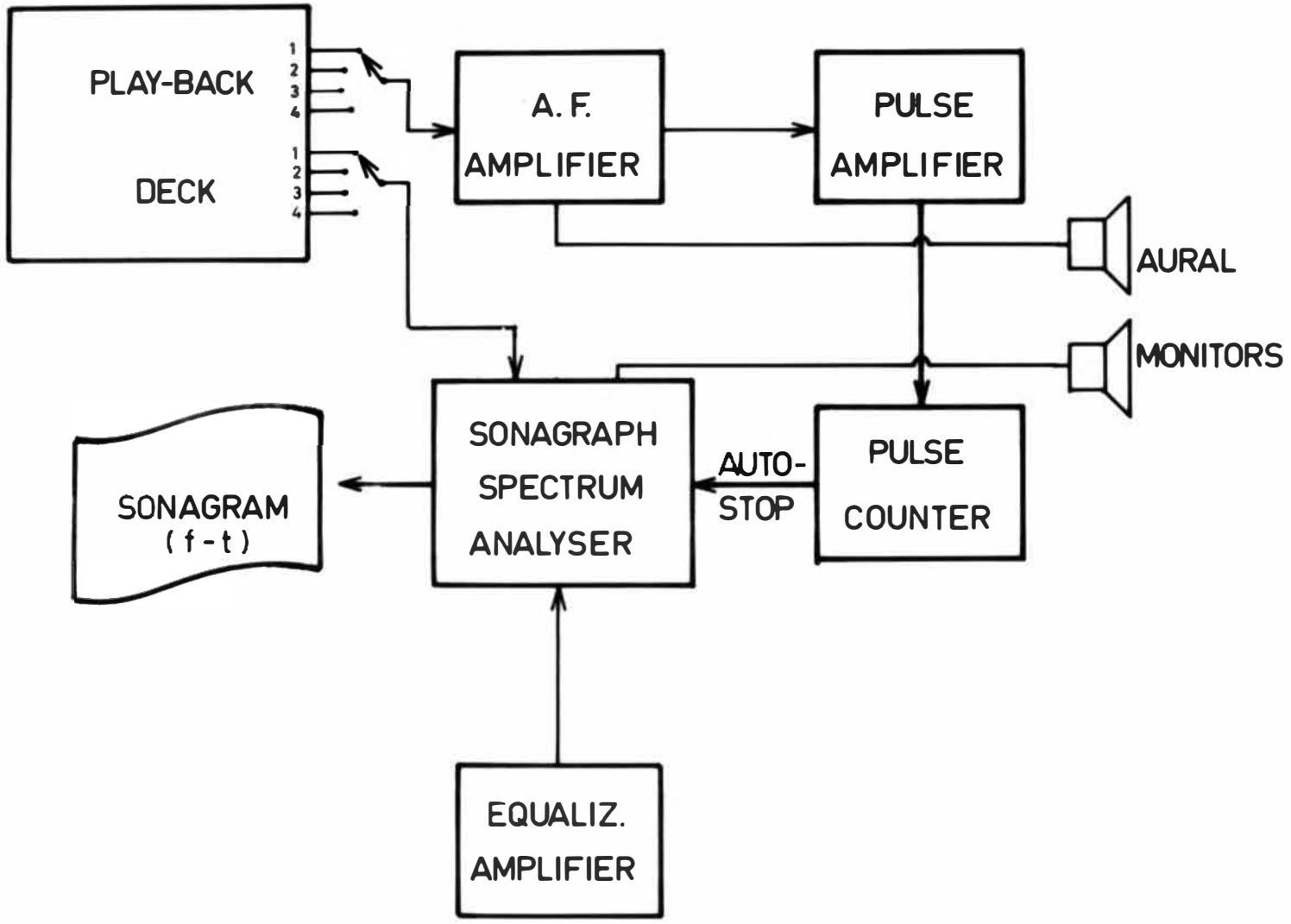

DATA ANALYSIS SYSTEM.

Figure 7.3. Frequency response curves for the record-playback system. The solid curves indicate the response with equalization applied and the dotted curves give the unequalized record-playback characteristics.

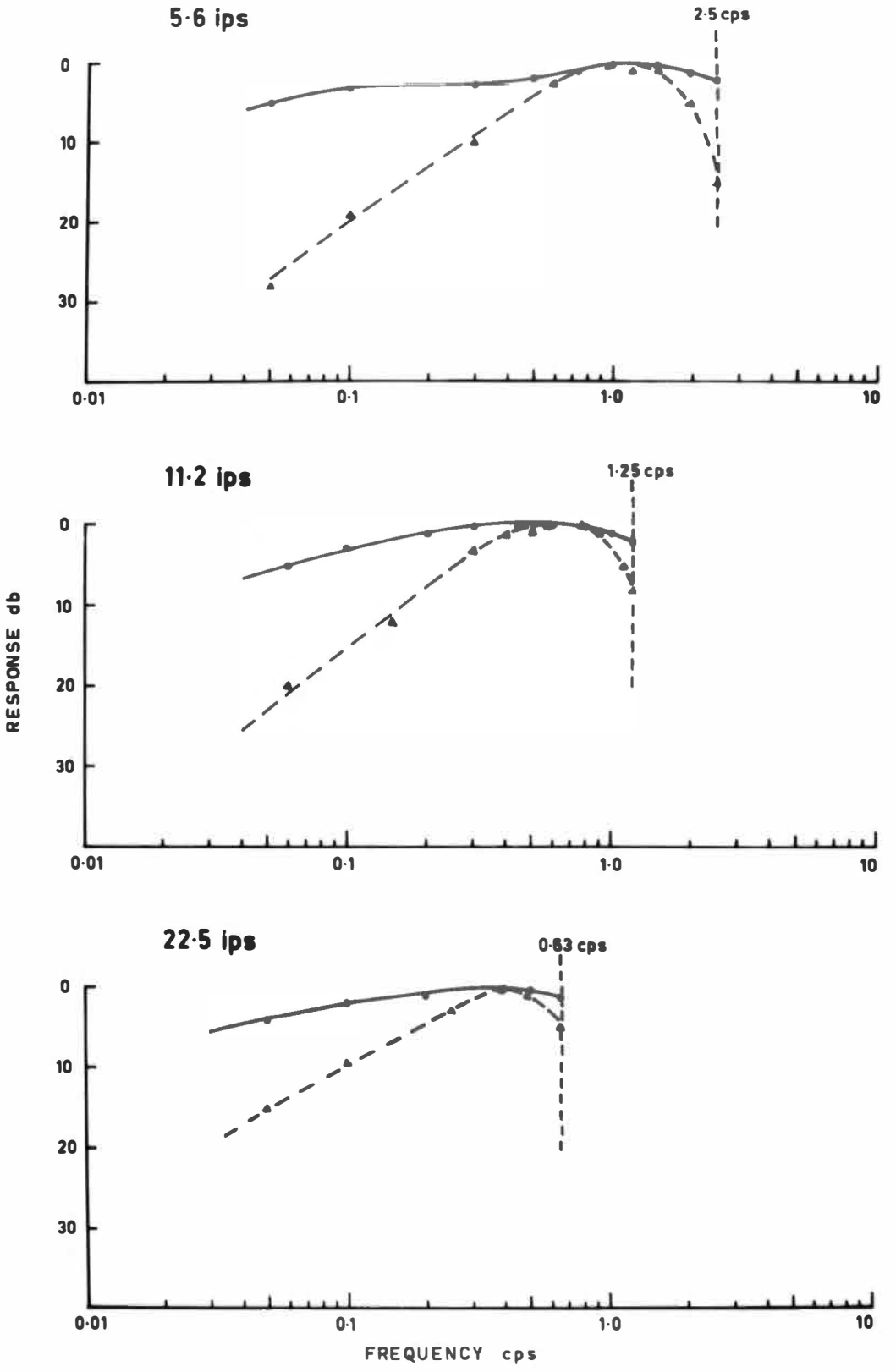
5·6 ips
2·5 cps
11·2 ips
1·25 cps
22·5 ips
0·63 cps
0
10
20
30
0·01
0·1
1·0
10
RESPONSE db
FREQUENCY cps

Figure 7.4. Calibration signals.

(a) Frequency calibration signals with amplitudes of 25m γ .

(b) Sensitivity calibration with a 1 cps constant frequency signal. The minimum detectable signal is 3m γ .

(c) and (d) Sweep frequency calibrations with ramp signals increasing with frequency at rates of 0.02 cps/min and 0.18 cps/min.

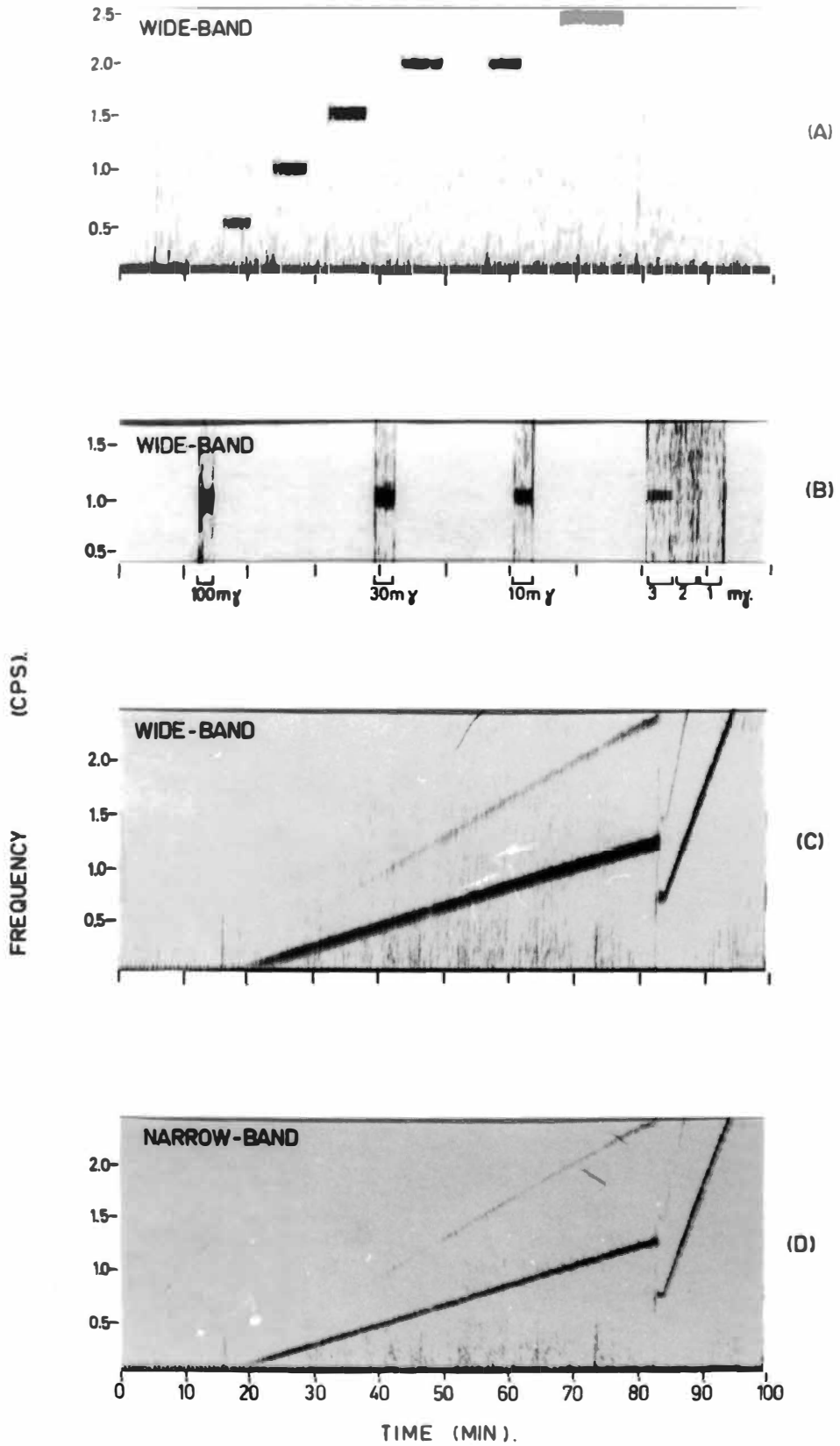
WIDE-BAND
2.5
2.0
1.5
1.0
0.5
(A)
WIDE-BAND
1.5
1.0
0.5
100mγ
30mγ
10mγ
3 2 1 mγ.
(B)
FREQUENCY (CPS).
WIDE-BAND
2.0
1.5
1.0
0.5
(C)
NARROW-BAND
2.0
1.5
1.0
0.5
(D)
0 10 20 30 40 50 60 70 80 90 100
TIME (MIN).

Figure 8.1. Amplitude-time record of a hydromagnetic emission recorded on the Z component at Christchurch. The mean oscillation frequency is approximately 0.6 cps and the maximum peak-to-peak amplitude is 0.1 γ .

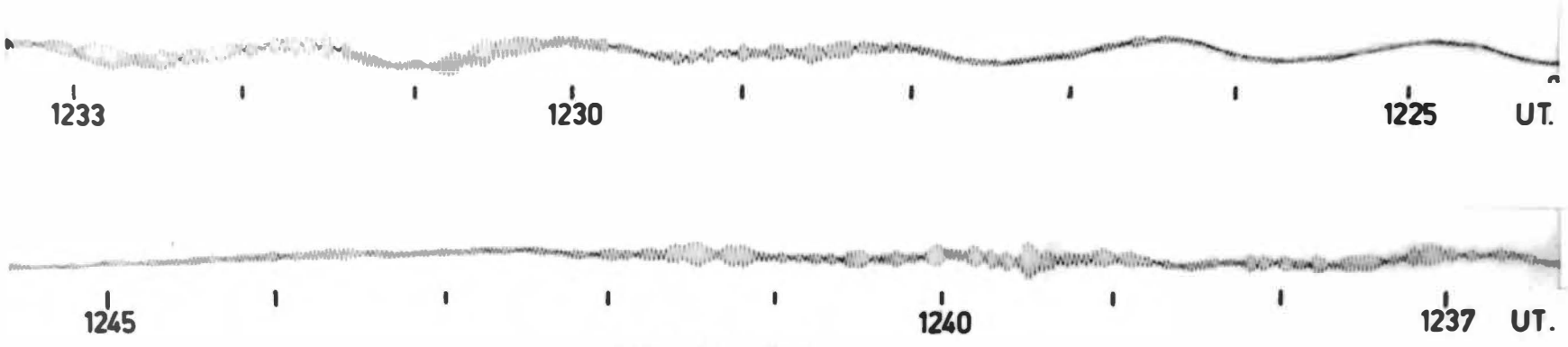

MAR 15, 1963.

Figure 8.2. Frequency-time display of a long duration hydromagnetic emission event exhibiting fine structure. (The activity occurring between 1840 and 1845 hr UT is broadband interference.)

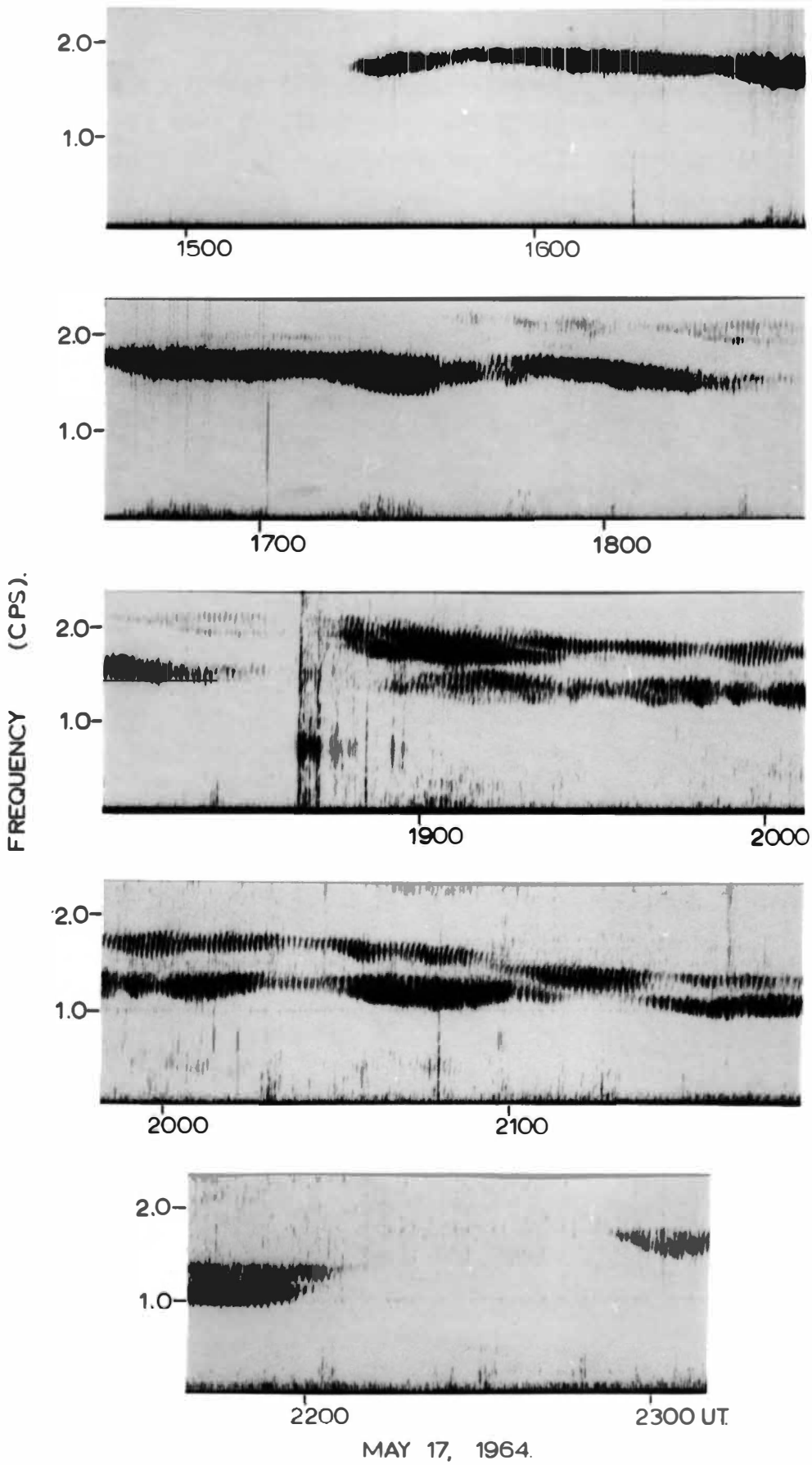
2.0
1.0
1500
1600
2.0
1.0
1700
1800
FREQUENCY (CPS).
2.0
1.0
1900
2000
2.0
1.0
2000
2100
2.0
1.0
2200
2300 UT.
MAY 17, 1964.

Figure 9.1. Theoretical frequency-time displays of hydromagnetic emissions resulting from ion cyclotion wave packets propagating along field aligned paths at L = 4 ($\phi_0 = 60^\circ$) and L = 5.6 ($\phi_0 = 65^\circ$). The horizontal dotted line at 2.7 cps indicates the equatorial ion cyclotron frequency at L = 5.6. (Diagram after Obayashi, 1964).

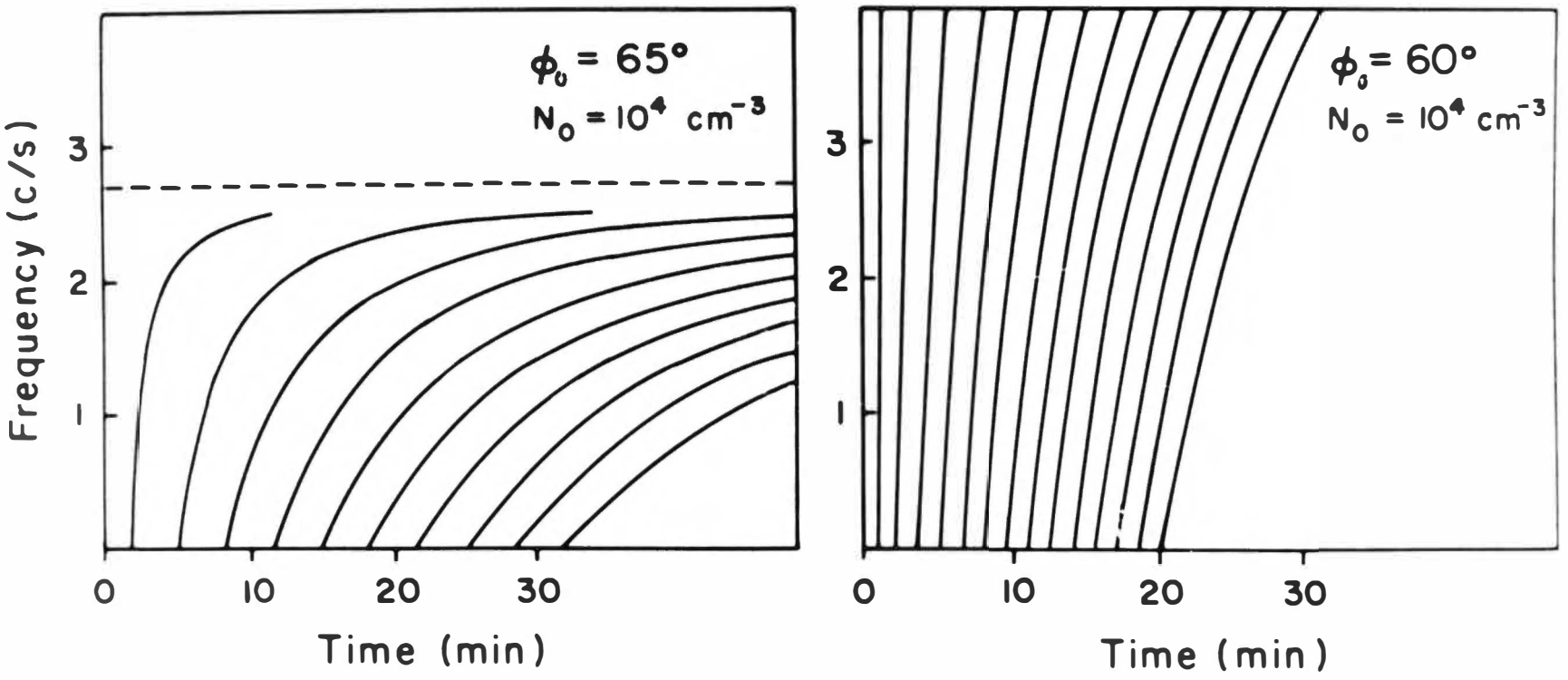
$\phi_0 = 65°$
$N_0 = 10^4\ cm^{-3}$
Frequency (c/s)
3
2
1
0
10
20
30
Time (min)
$\phi_0 = 60°$
$N_0 = 10^4\ cm^{-3}$
3
2
1
0
10
20
30
Time (min)

Figure 9.2 Hydromagnetic wave attenuation processes. Curve (a) Ionospheric attenuation characteristic for hydromagnetic waves propagating downwards through the ionosphere under daytime sunspot minimum conditions. The slope is approximately 6db/octave. (From Karplus et al. 1962). Curve (b) Magnetospheric attenuation due to cyclotron damping for ion cyclotron waves propagating along the field aligned path L = 4.8 and f_{Hc} = 4.5 cps. (From Scarf, 1962)

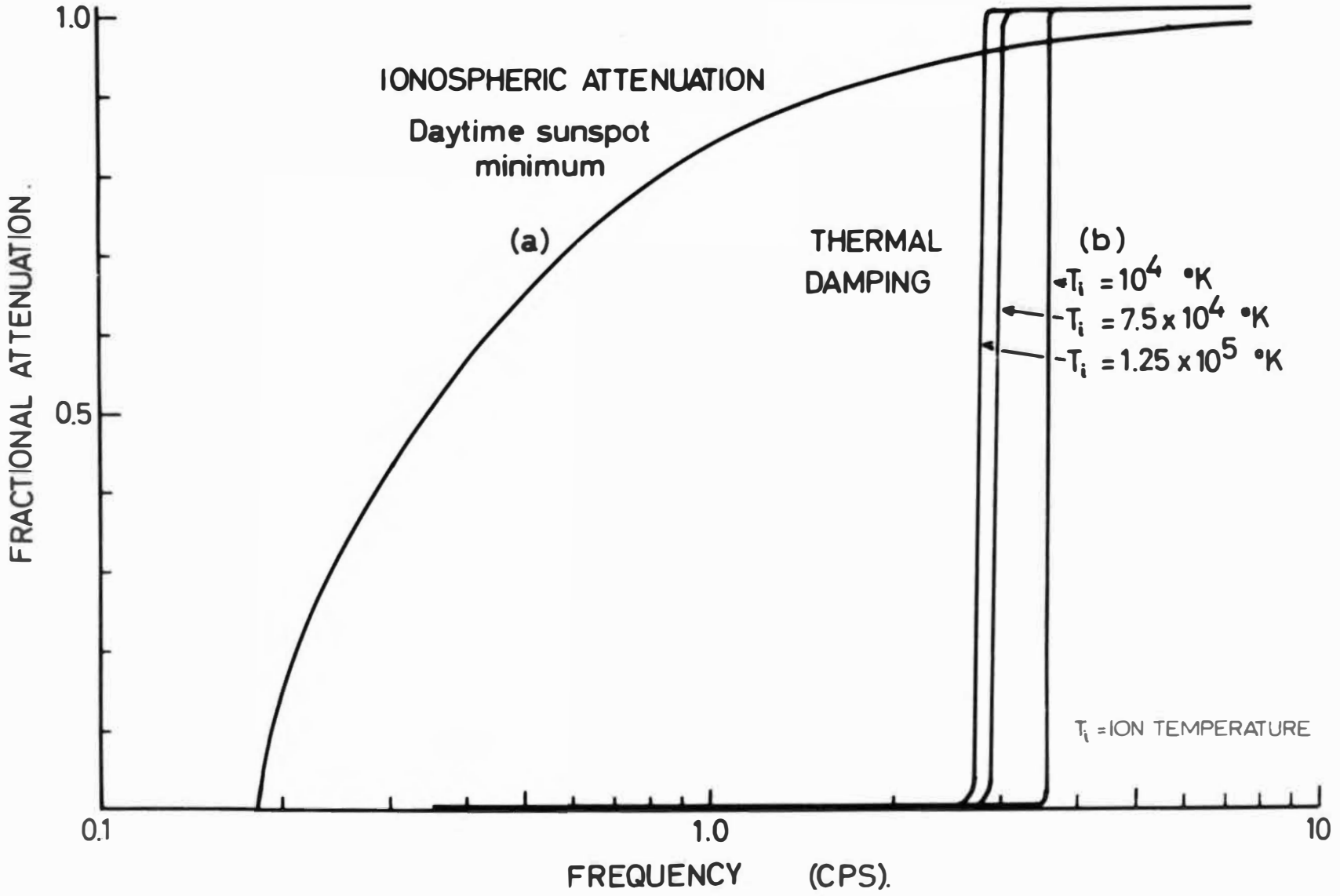
1.0
0.5
FRACTIONAL ATTENUATION.
IONOSPHERIC ATTENUATION
Daytime sunspot
minimum
(a)
THERMAL
DAMPING
(b)
$T_i = 10^4$ °K
$T_i = 7.5 \times 10^4$ °K
$T_i = 1.25 \times 10^5$ °K
T_i = ION TEMPERATURE
0.1
1.0
10
FREQUENCY (CPS).

Figure 10.1 Schematic frequency-time diagram illustrating the hm emission parameters measured from sonagrams. The midband frequency $f_m = (f_1 + f_2) / 2$ and the mean fine structure band spacing $T = (t_n - t_1) / (n - 1)$, where n is the number of coherent bands present. The relative bandwidth is $\Delta f / f_m$ and the mean band slope is $m = (m_1 + m_n) / 2$ where m_1 to m_n express the slope of individual bands.

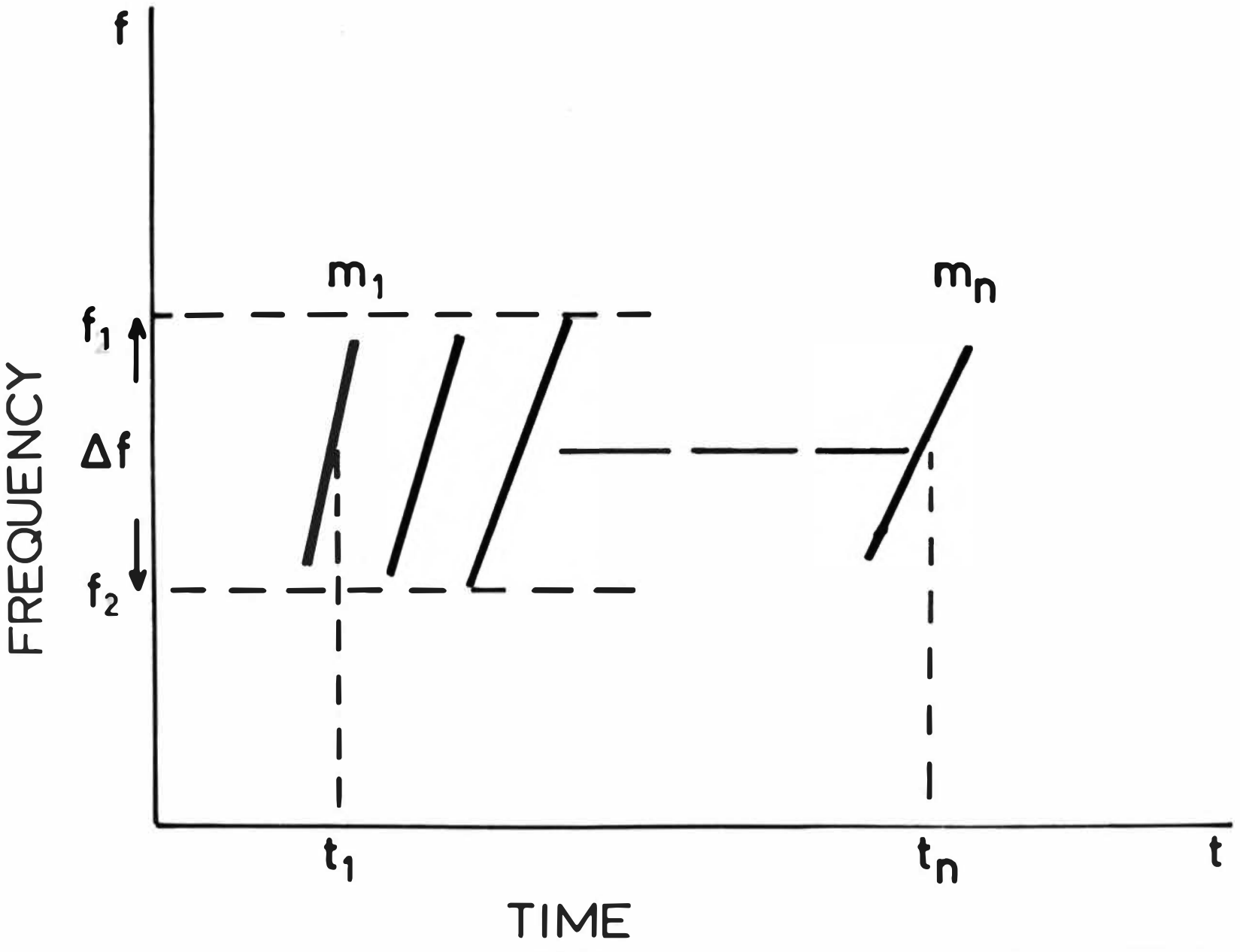
f
m1
mn
f1
Δf
f2
FREQUENCY
t1
tn
t
TIME

Figure 10.2 Typical broad-band and narrow-band emissions. The relative bandwidths $\Delta f/f_m$ are 0.75 and 0.12 respectively. The constant frequency signal at 1 cps in the bottom sonagram is of instrumental origin. This signal also appears on many of the sonagrams in the following Figures

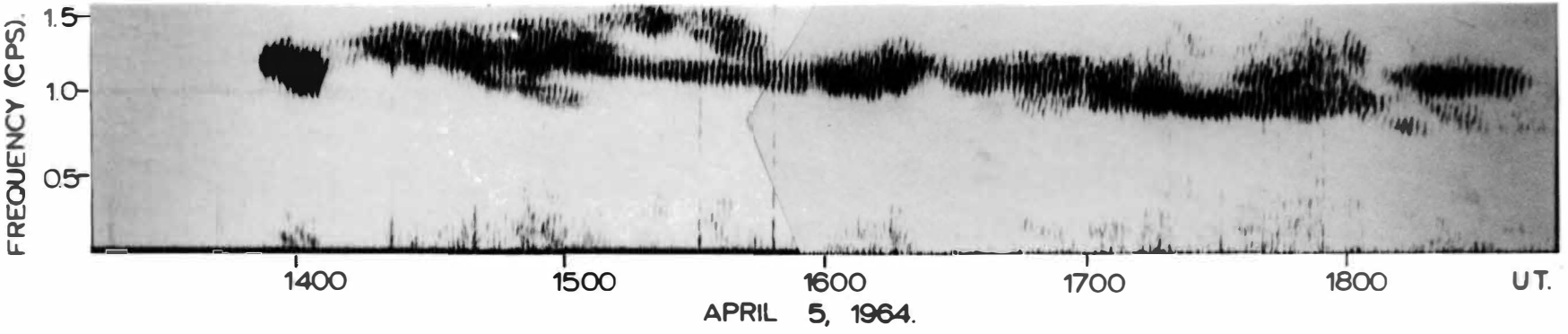
FREQUENCY (CPS).
1.5
1.0
0.5
1400
1500
1600
1700
1800
UT.
APRIL 5, 1964.

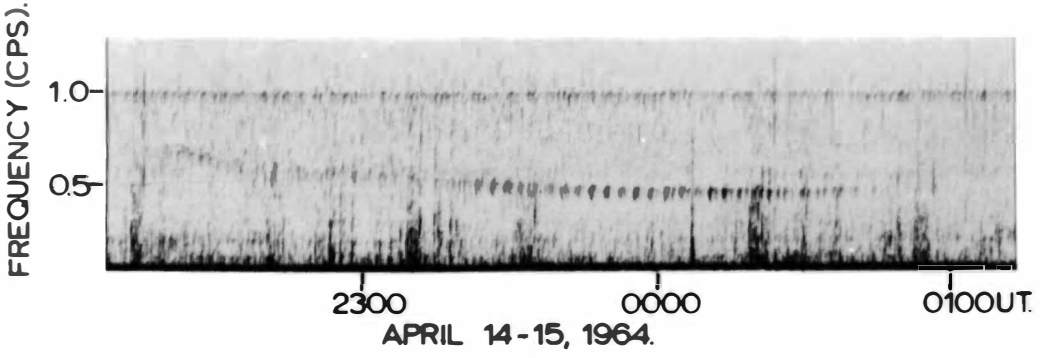
FREQUENCY (CPS).
1.0
0.5
2300
0000
0100UT.
APRIL 14-15, 1964.

Figure 10.3 Narrow-band hm emission in which the fine structure bands do not overlap in time. The individual bands on the sonagram correspond to the envelopes on the amplitude-time chart. The mean band spacing on the sonagram is 2.10 ± 0.05 min and the envelope spacing on the 1.0 cps channel of the amplitude time record is 2.2 ± 0.1 min.

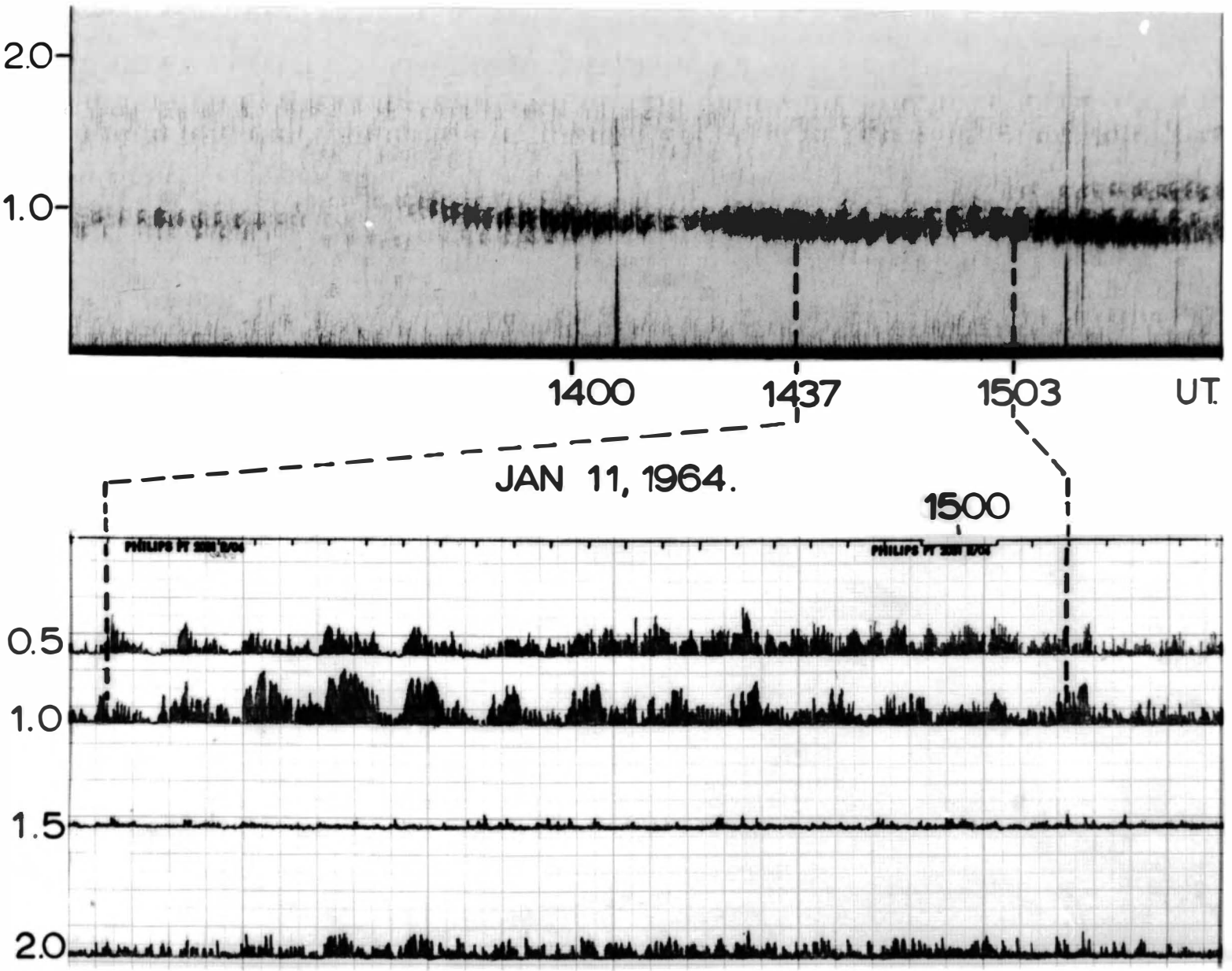
FREQUENCY (CPS).
2.0
1.0
1400
1437
1503
UT.
JAN 11, 1964.
1500
0.5
1.0
1.5
2.0

Figure 10.4 Hm emissions in which the fine structure bands show a regular intensity variation with frequency. The upper emission appears to be composed of three very narrow band emissions. In the lower emission the elementary structure is less regular.

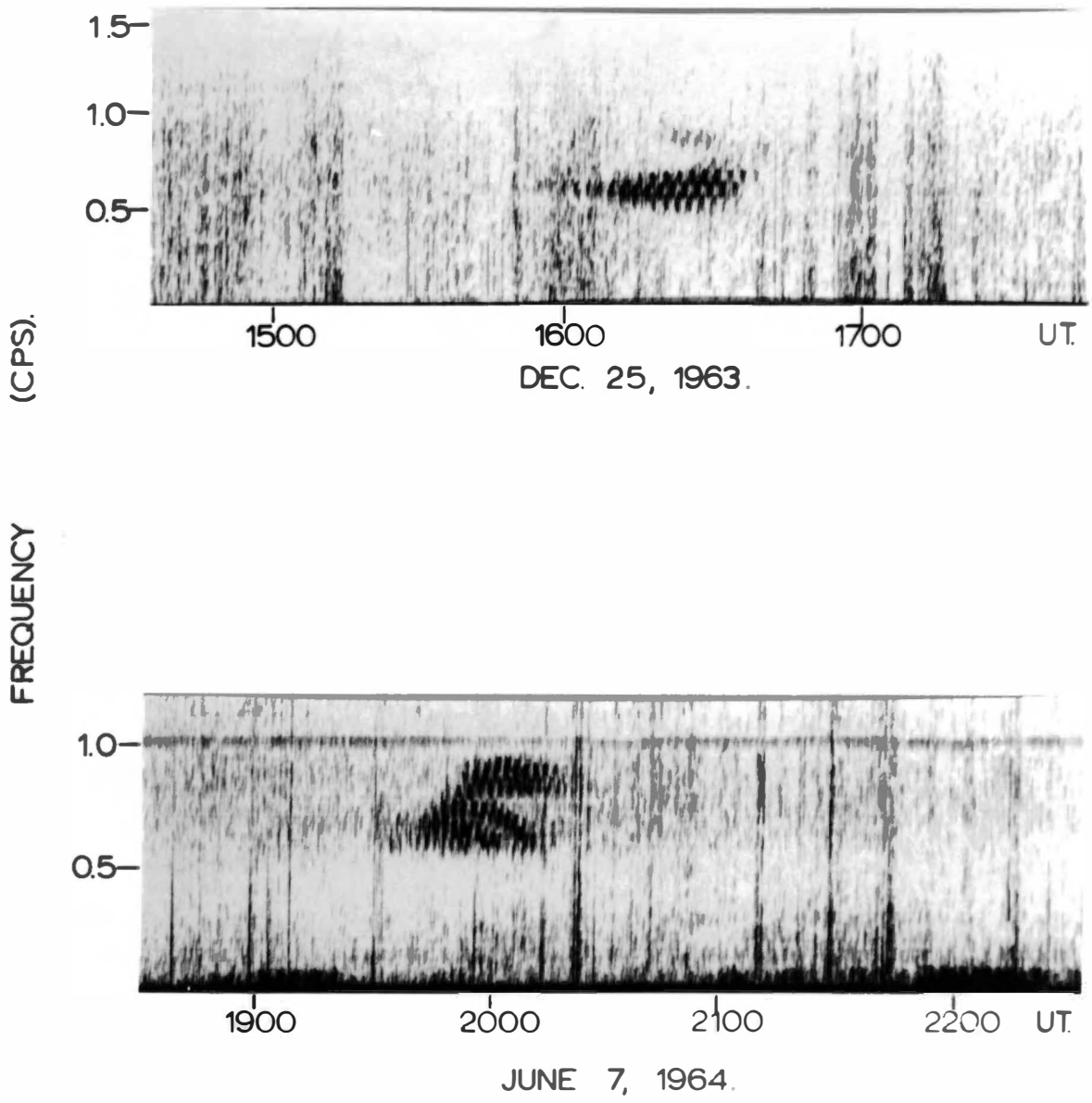
1.5
1.0
0.5
(CPS).
1500
1600
1700
UT.
DEC. 25, 1963.
FREQUENCY
1.0
0.5
1900
2000
2100
2200
UT.
JUNE 7, 1964.

Figure 10.5 (a) Enlargement of a section of the April 5, 1964 emission event shown in Figure 10.2. Note the discontinuities in fine structure band slope at approximately 0.05 - 0.1 cps intervals between 1530 hr. and 1550 hr. UT. (b) Example of individual narrow-band emissions exhibiting an increase in band spacing within a broad-band emission. The mean band spacing for the four numbered narrow-band emissions are listed below.

1. $f = 0.40 - 0.48 \pm 0.05$ cps, $T = 2.52 \pm 0.06$ min
2. $f = 0.45 - 0.55$, $T = 2.65 \pm 0.05$
3. $f = 0.55 - 0.65$, $T - 3.00 \pm 0.05$
4. $f = 0.75 - 0.85$, $T \quad 3.30 \pm 0.05$

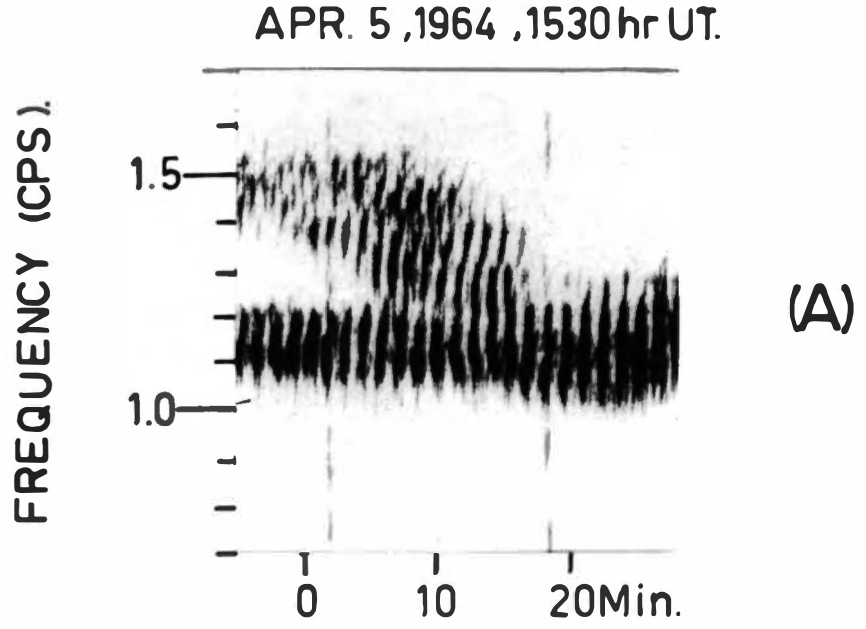
APR. 5, 1964, 1530 hr UT.
FREQUENCY (CPS).
1.5
1.0
0
10
20Min.
(A)

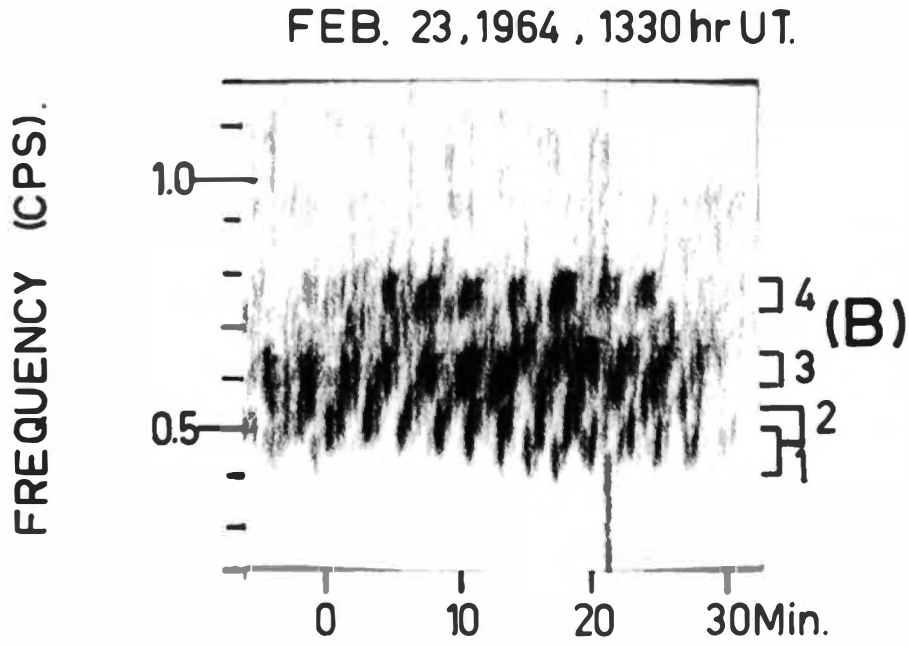
FEB. 23, 1964, 1330 hr UT.
FREQUENCY (CPS).
1.0
0.5
0
10
20
30Min.
4
3
2
(B)

Figure 10.6 Variation in hm emission midband period with mean band spacing. Emissions occurring during the local daytime between 22 - 06 hr. UT (0930 - 1730 hr. LT) and within the three days following the commencement of a geomagnetic storm containing $K_p \geq 6$ are also indicated.

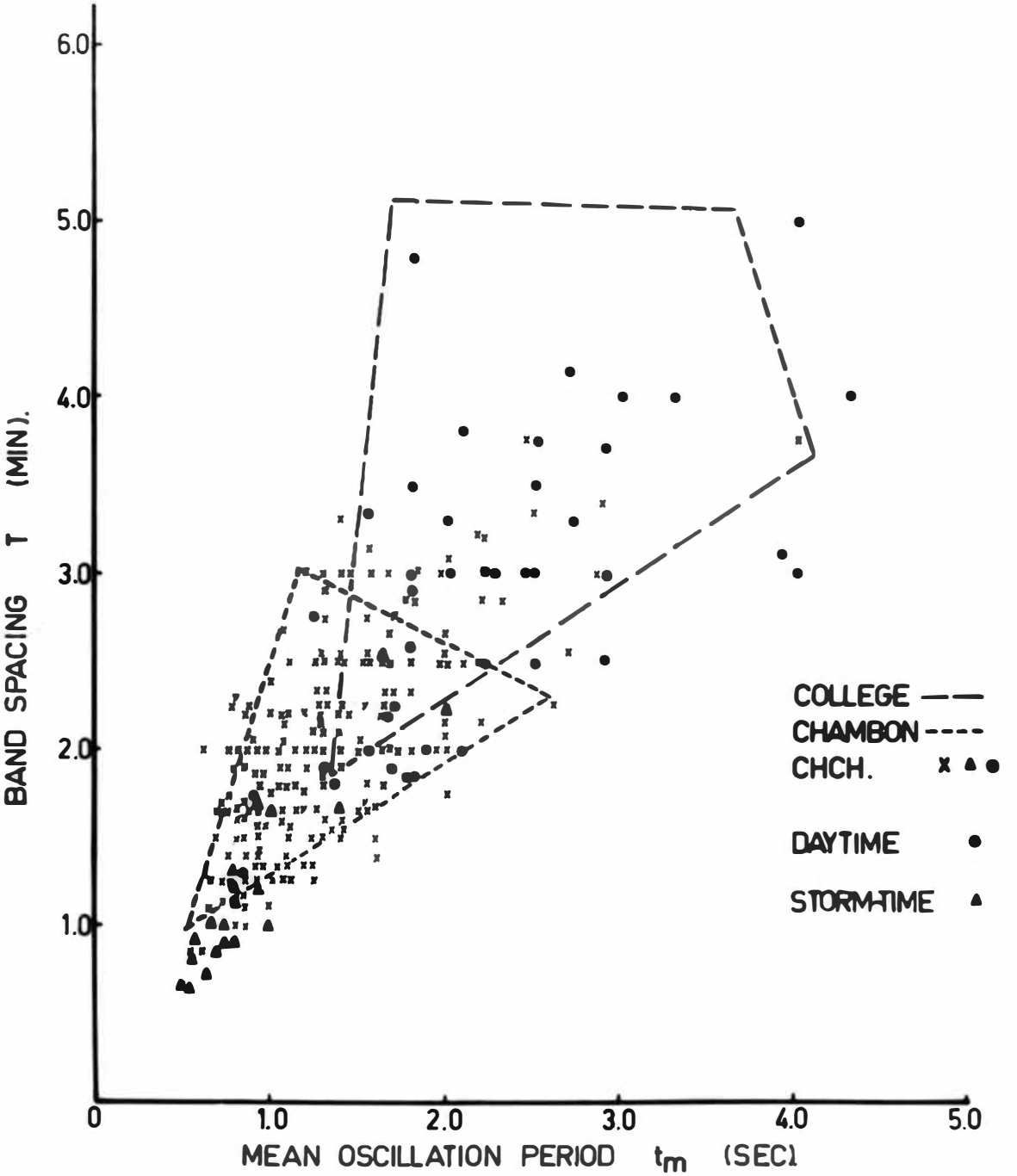
6.0
5.0
4.0
3.0
2.0
1.0
0
1.0
2.0
3.0
4.0
5.0
BAND SPACING T (MIN).
MEAN OSCILLATION PERIOD t_m (SEC)
COLLEGE
CHAMBON
CHCH.
DAYTIME
STORM-TIME

Figure 10.7 Variation in the mean fine structure band slope with mean band spacing for 51 data samples from broadband emissions.

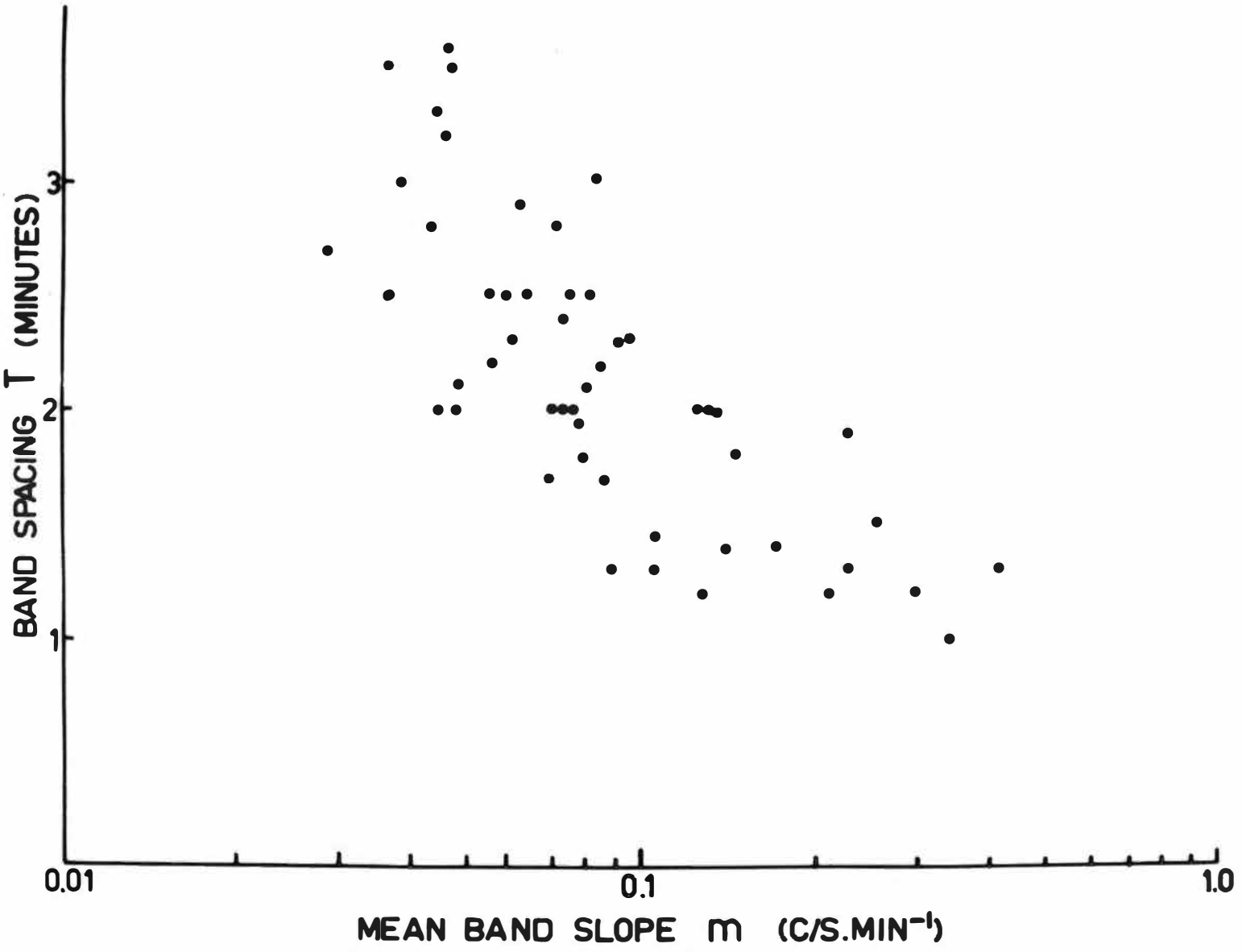
BAND SPACING T (MINUTES)
3
2
1
0.01
0.1
1.0
MEAN BAND SLOPE m (C/S.MIN⁻¹)

Figure 10.8 Occurrence of hm emissions and geomagnetic activity. Top Distributions of twenty minute hm emission occurrences with K_{AM} and K_p over the period November 27, 1963 to July, 20, 1964 Middle Distributions of K_p and K_{AM} over the same period. Bottom Normalized hm emission occurrence distributions.

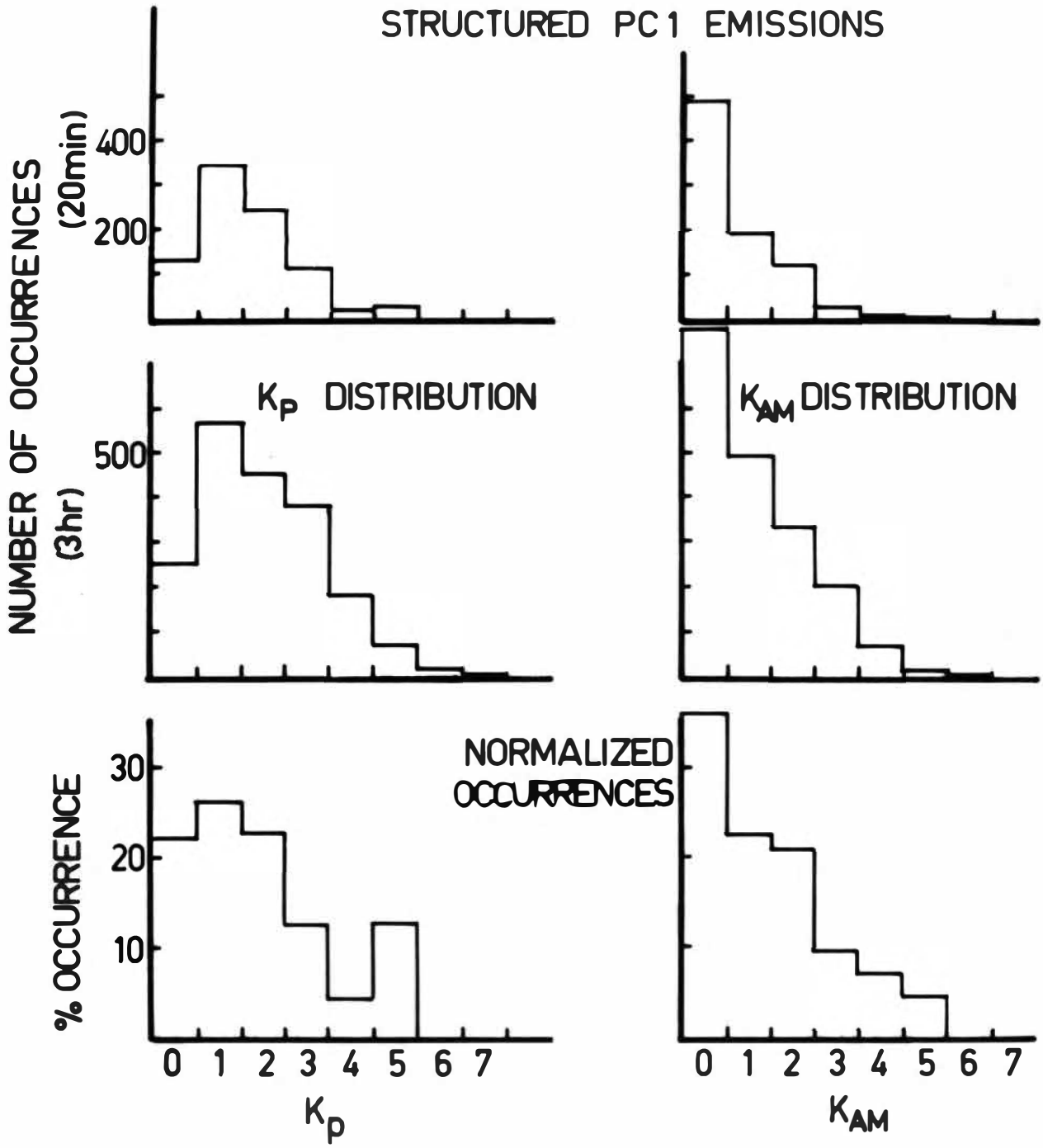
STRUCTURED PC 1 EMISSIONS
NUMBER OF OCCURRENCES
(20min)
400
200
K_P DISTRIBUTION
K_{AM} DISTRIBUTION
(3hr)
500
NORMALIZED
OCCURRENCES
% OCCURRENCE
30
20
10
0 1 2 3 4 5 6 7
K_P
0 1 2 3 4 5 6 7
K_{AM}

Figure 10.9 Hm emission event recorded simultaneously at four middle and high latitude stations.

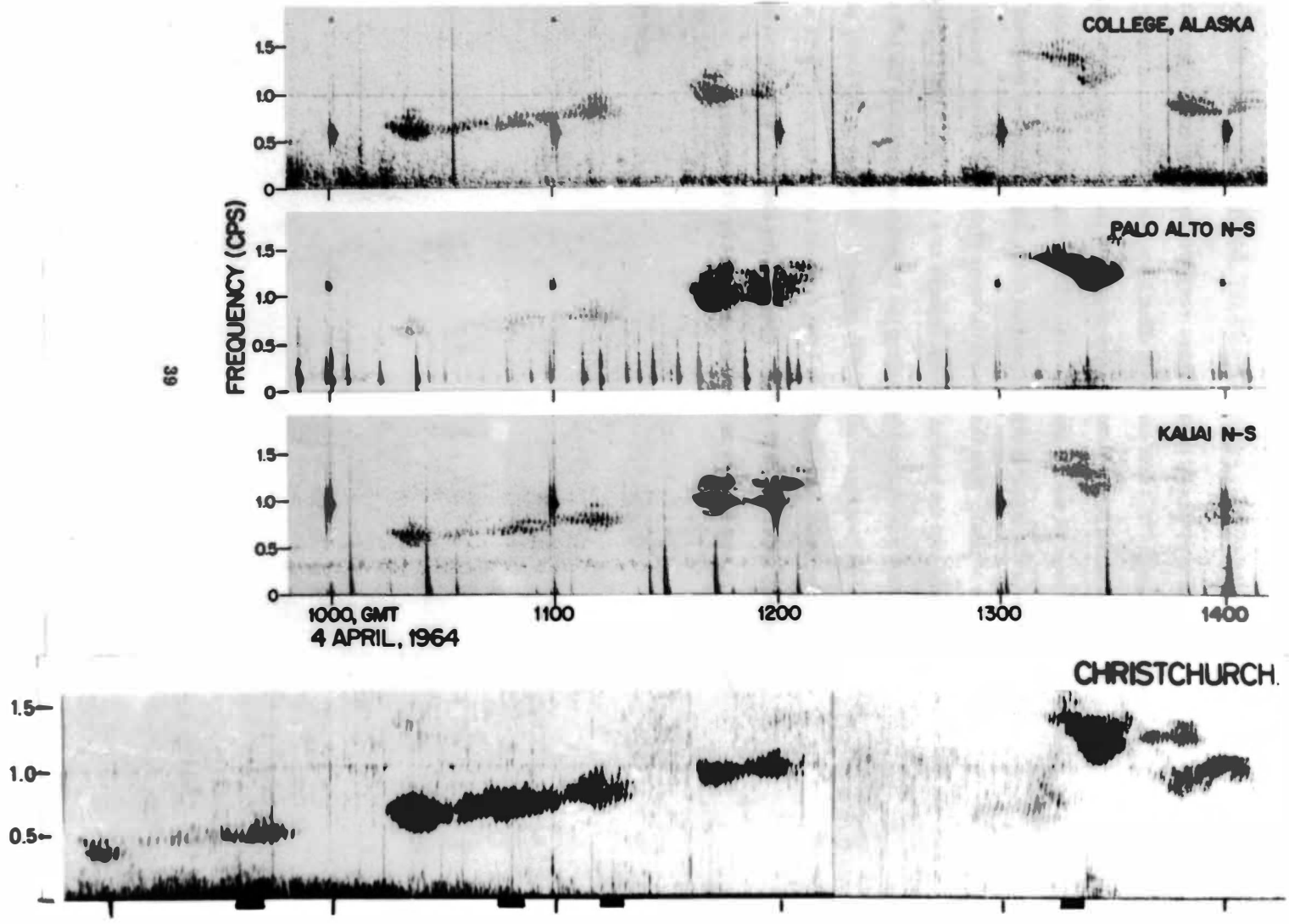
COLLEGE, ALASKA
PALO ALTO N-S
KAUAI N-S
CHRISTCHURCH
FREQUENCY (CPS)
1.5
1.0
0.5
0
1000, GMT
4 APRIL, 1964
1100
1200
1300
1400

Figure 10.10 Three examples of narrow-band storm-time Pc1 emissions.

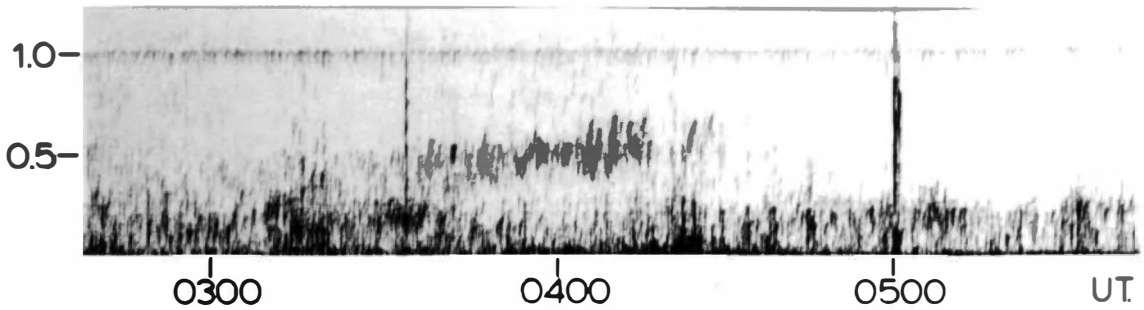

APRIL 17, 1964.

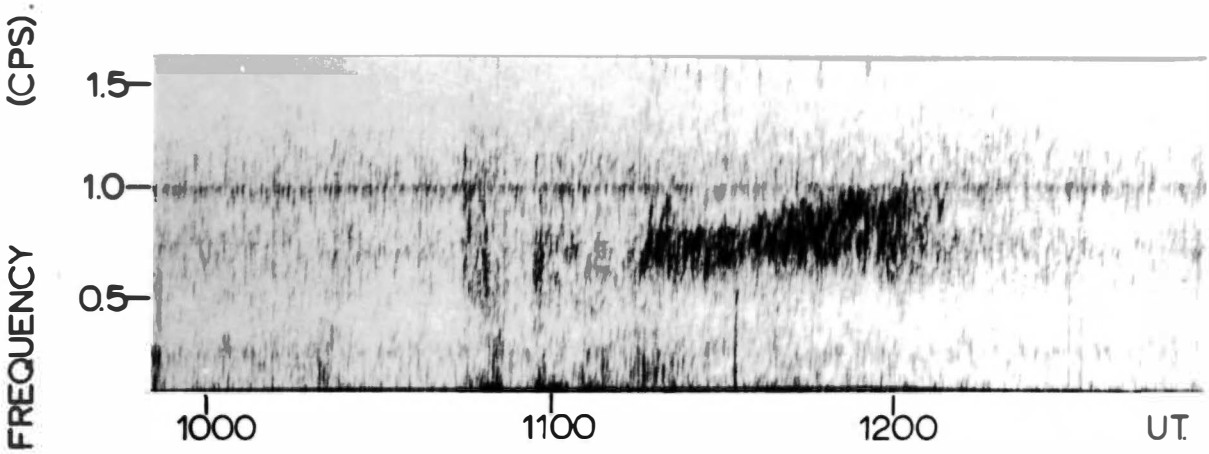

APRIL 25, 1964.

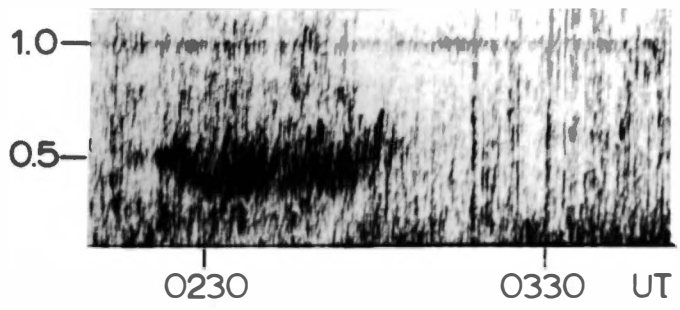

APRIL 2, 1964.

Figure 10.11 The occurrence of narrow-band irregular and non-structural Pc1 emissions and geomagnetic activity. Top Distributions of twenty minute emission occurrences with K_{AM} and K_p over the period November 27, 1963 to July 20, 1964. Middle Distributions of K_{AM} and K_p over the same period. Bottom Normalized emission occurrence distributions.

NON-STRUCTURED AND IRREGULAR-STRUCTURED PC1 EMISSIONS

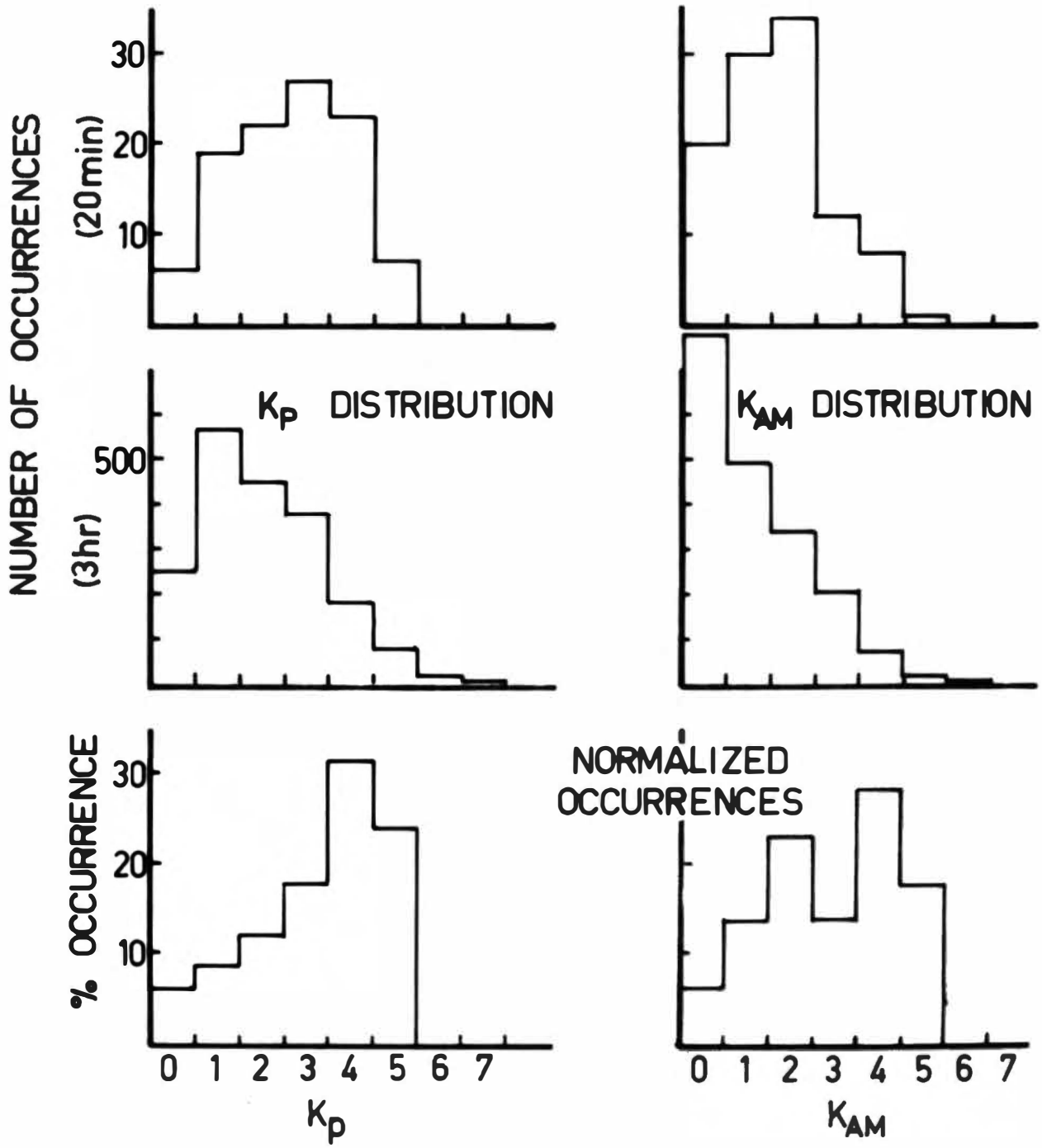

Figure 10.12 Diurnal variation in the twenty minute occurrence rates of narrow-band storm-time emissions. The full line indicates rates smoothed in sliding groups of three.

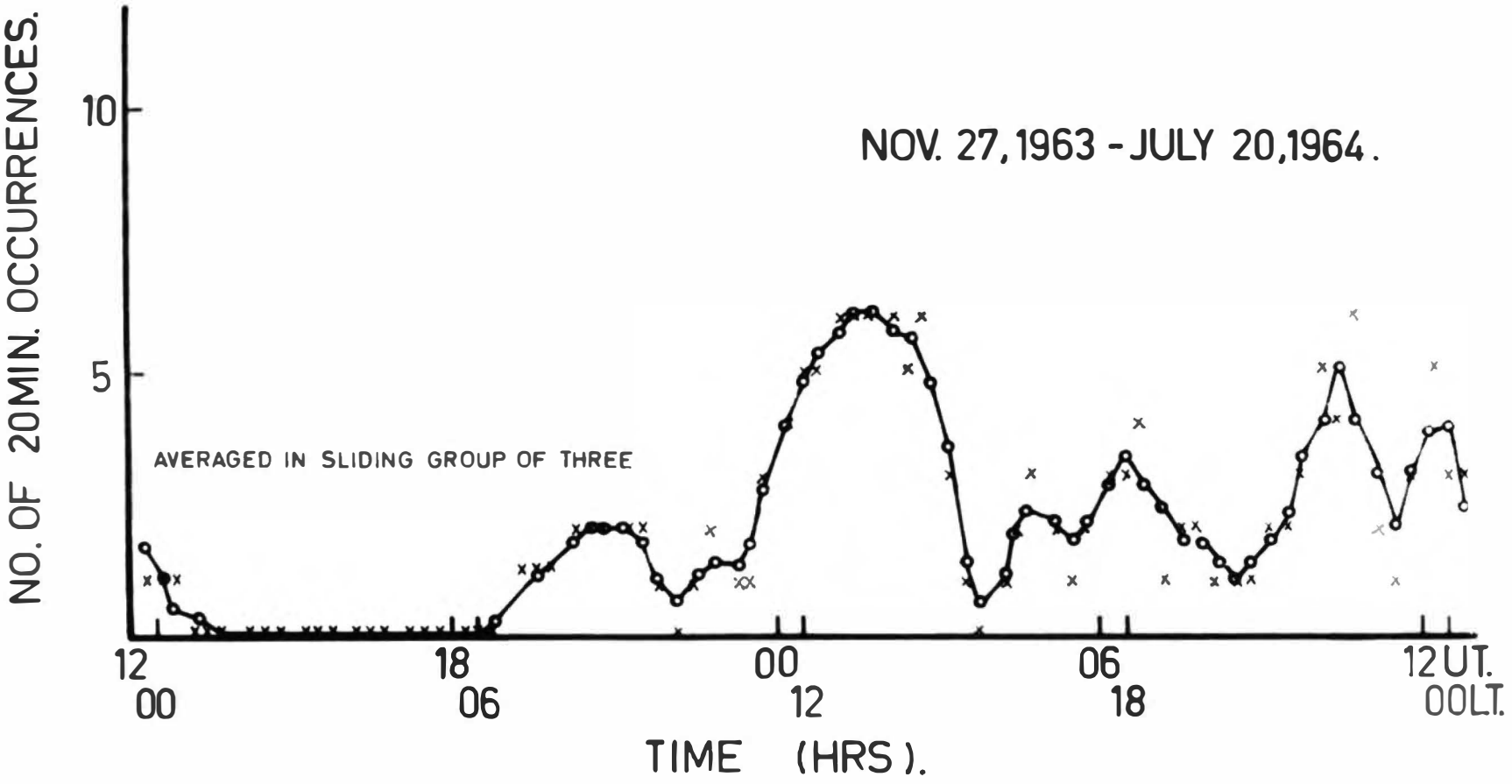
NO. OF 20MIN. OCCURRENCES.
10
5
NOV. 27, 1963 - JULY 20, 1964.
AVERAGED IN SLIDING GROUP OF THREE
12
00
18
06
00
12
06
18
12 UT.
00 LT.
TIME (HRS).

Figure 10.13 Irregular structured and non-structured broad-band storm-time emissions.

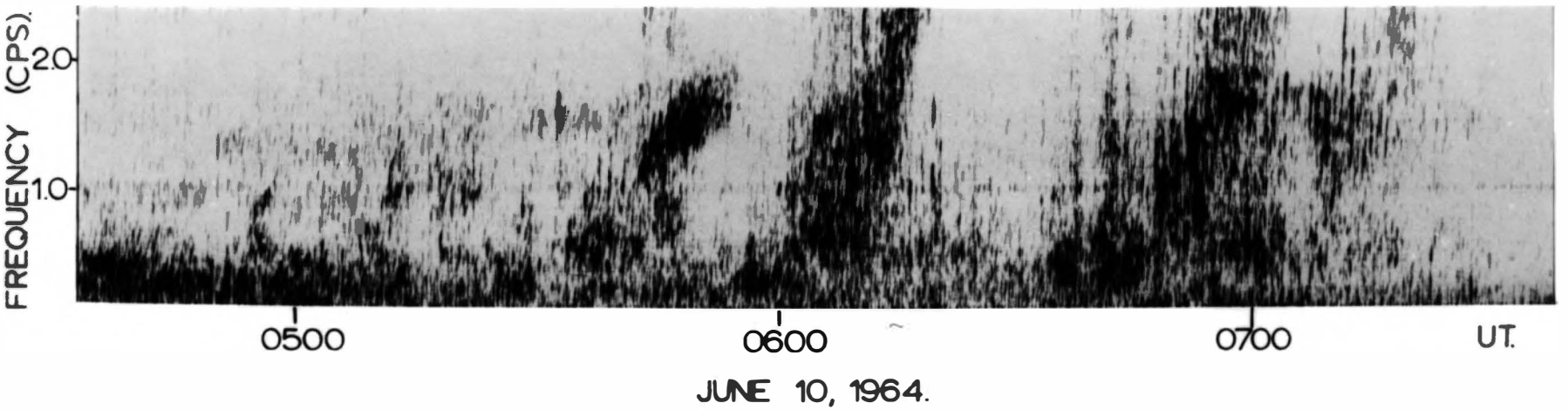

JUNE 10, 1964.

Figure 11.1 Diurnal variation in the twenty minute occurrence rates of hm emissions. The full line represents rates smoothed in sliding groups of three

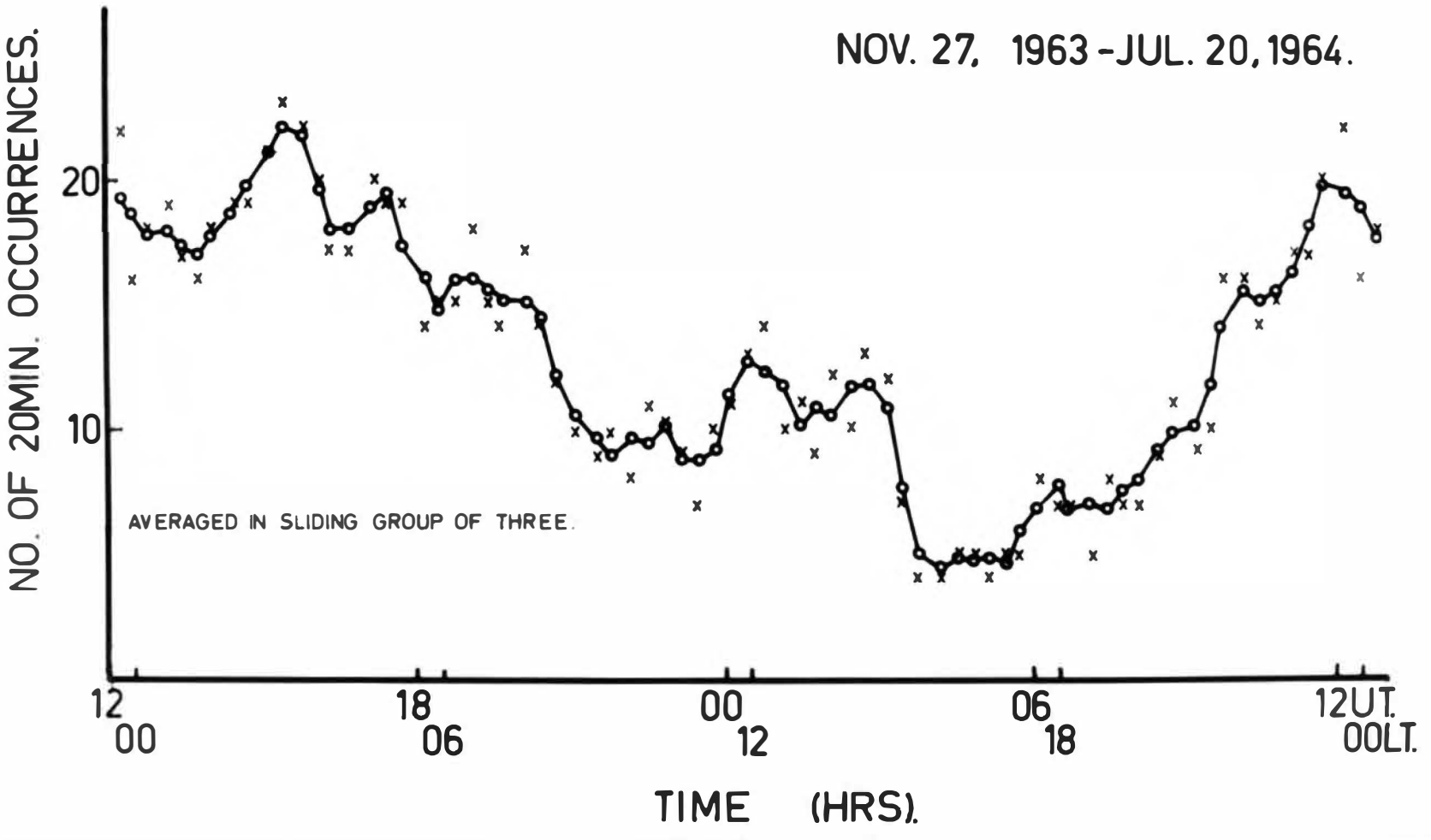
NOV. 27, 1963 - JUL. 20, 1964.
NO. OF 20MIN. OCCURRENCES.
20
10
AVERAGED IN SLIDING GROUP OF THREE.
12
00
18
06
00
12
06
18
12UT.
00LT.
TIME (HRS).

Figure 11.2 Diurnal variation in midband frequency for hm emissions recorded over the period November 27, 1963 to July 20, 1964. Each point is the mean of the indicated number and the error bars indicate the standard deviation.

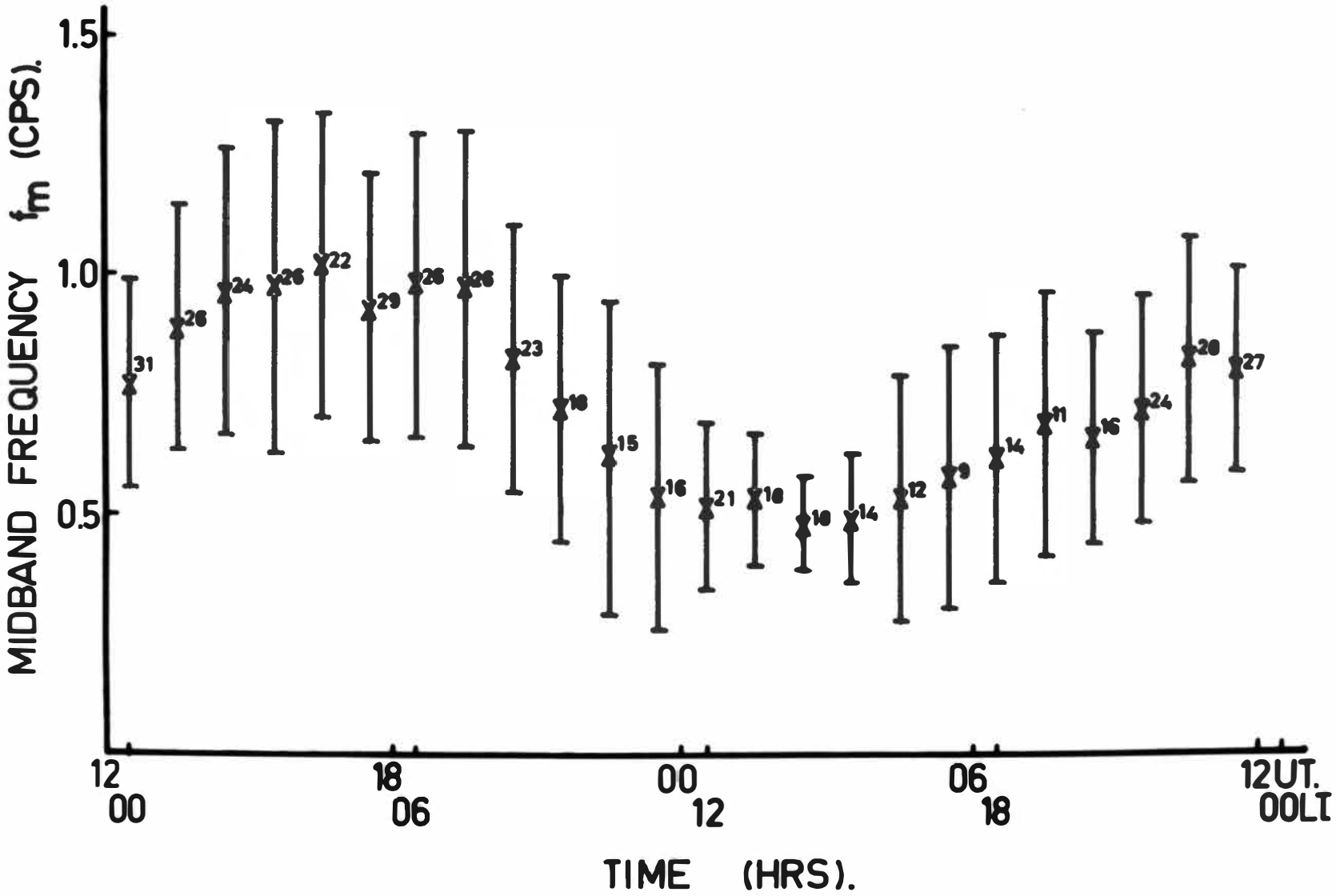
MIDBAND FREQUENCY f_m (CPS).
1.5
1.0
0.5
31
26
24
26
22
29
26
26
23
18
15
16
21
18
18
14
12
9
14
11
16
24
28
27
12
00
18
06
00
12
06
18
12UT.
00LT
TIME (HRS).

Figure 11.3 Five individual days showing the diurnal variation in midband frequency. The data for May 17 - 18 and June 10 - 11, 1964 indicate enhanced values of midband frequency which typify emissions observed following geomagnetic storms.

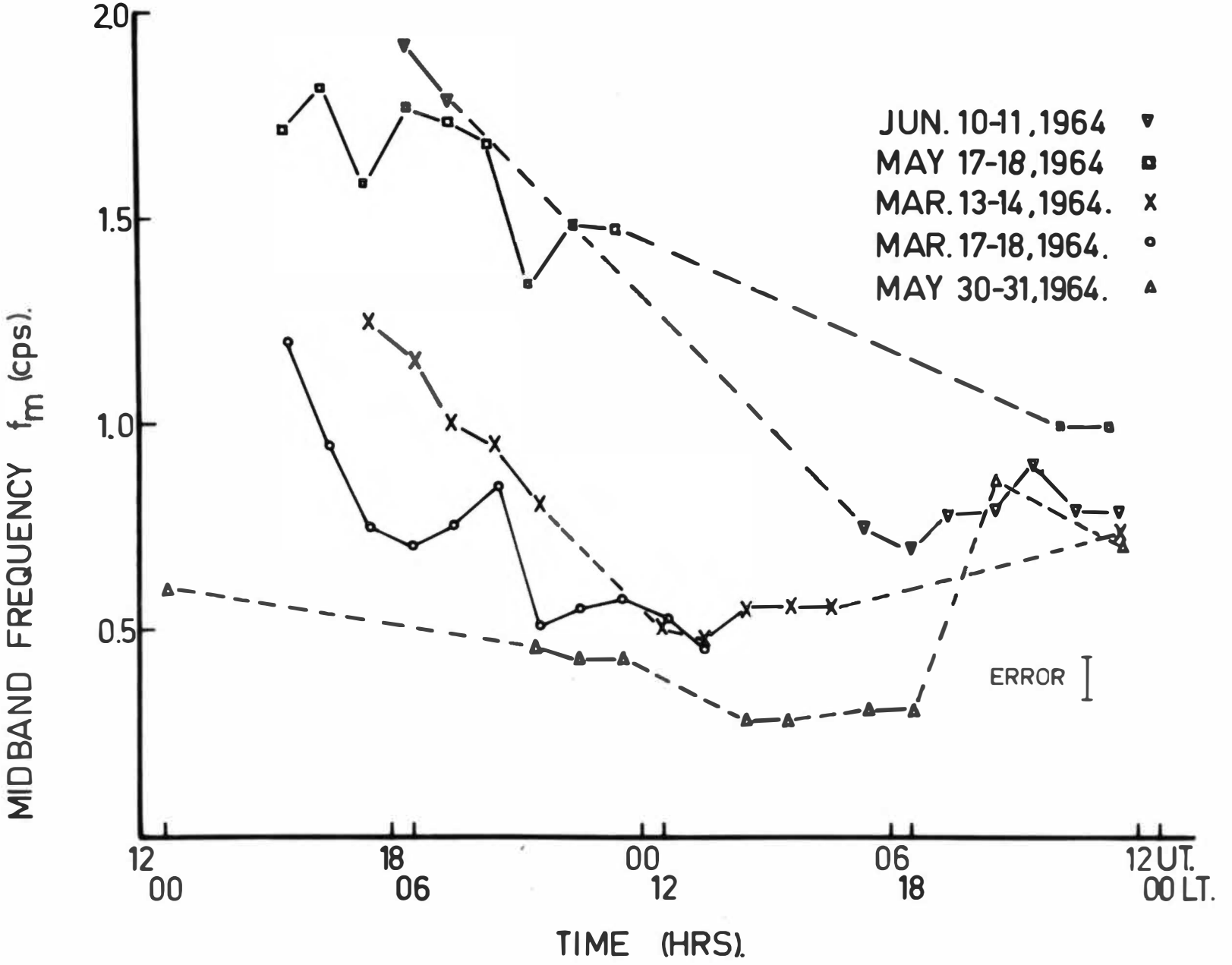
2.0
1.5
1.0
0.5
MIDBAND FREQUENCY f_m (cps).
JUN. 10-11, 1964
MAY 17-18, 1964
MAR. 13-14, 1964.
MAR. 17-18, 1964.
MAY 30-31, 1964.
ERROR
12 00
18 06
00 12
06 18
12 UT. 00 LT.
TIME (HRS).

Figure 11.4 Three hm emission events exhibiting gradually increasing midband frequencies with time.

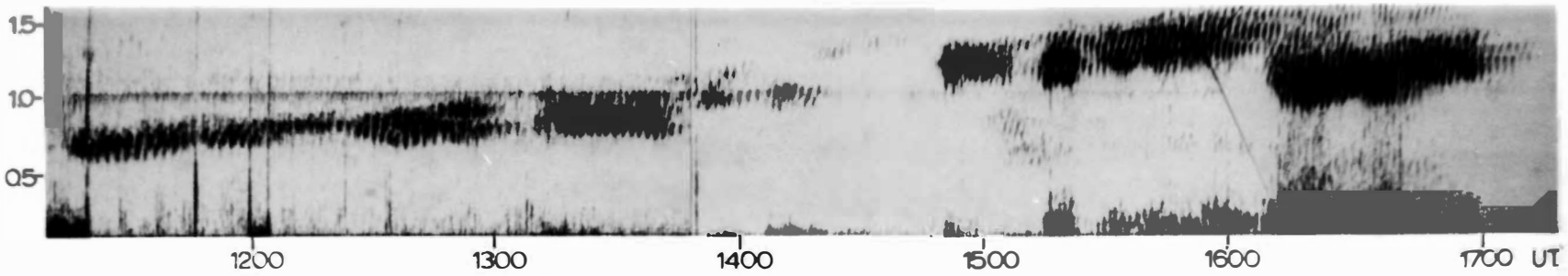

APRIL 6, 1964.

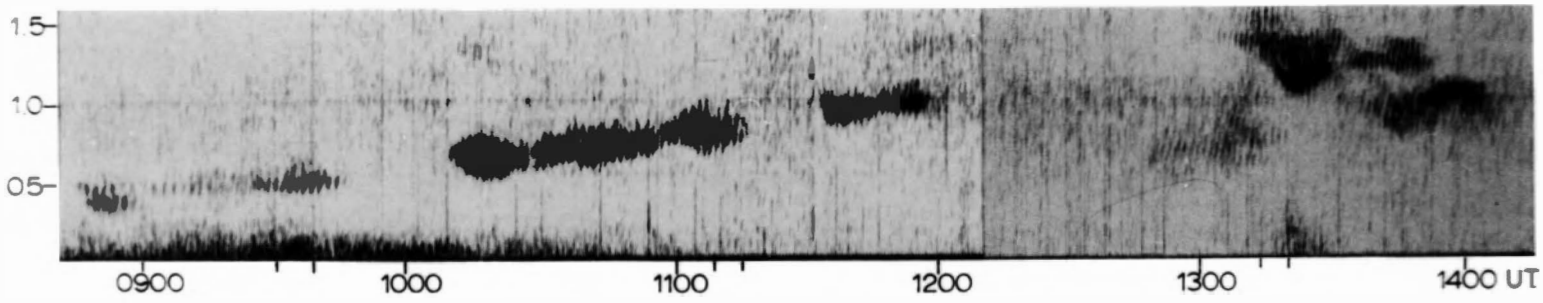

APRIL 4, 1964.

FREQUENCY (CPS)

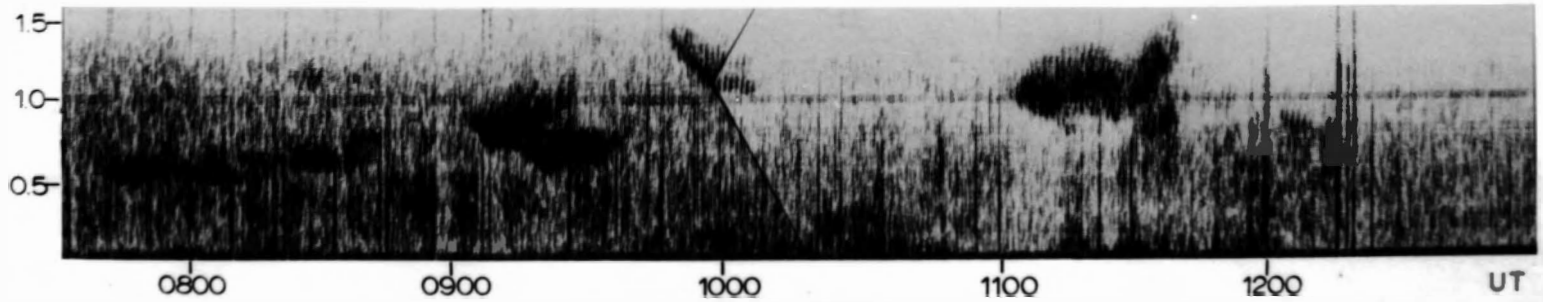

APRIL 3, 1964.

Figure 11.5 Diurnal variation in hm emission fine structure band spacing over the period November 27, 1963 to July 20, 1964. Each point is the mean of the indicated number and the error bars indicate the standard deviation.

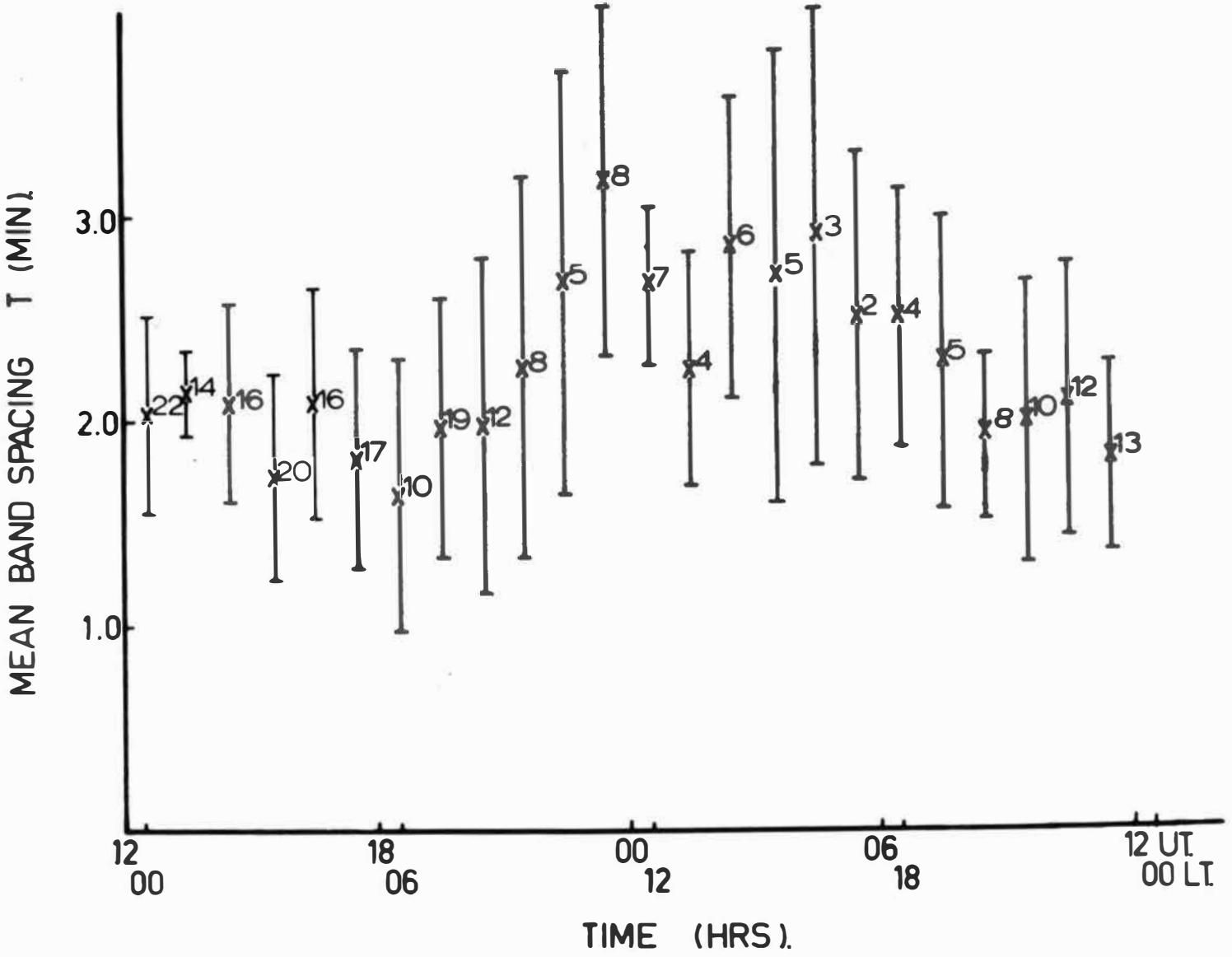
MEAN BAND SPACING T (MIN).
3.0
2.0
1.0
22
14
16
20
16
17
10
19
12
8
5
8
7
4
6
5
3
2
4
5
8
10
12
13
12
00
18
06
00
12
06
18
12 UT.
00 LT.
TIME (HRS).

Figure 11.6 Day and night hm emission frequency spectra for the period December 1, 1963 to July 20, 1964 and the two four month periods December - March and April - July.

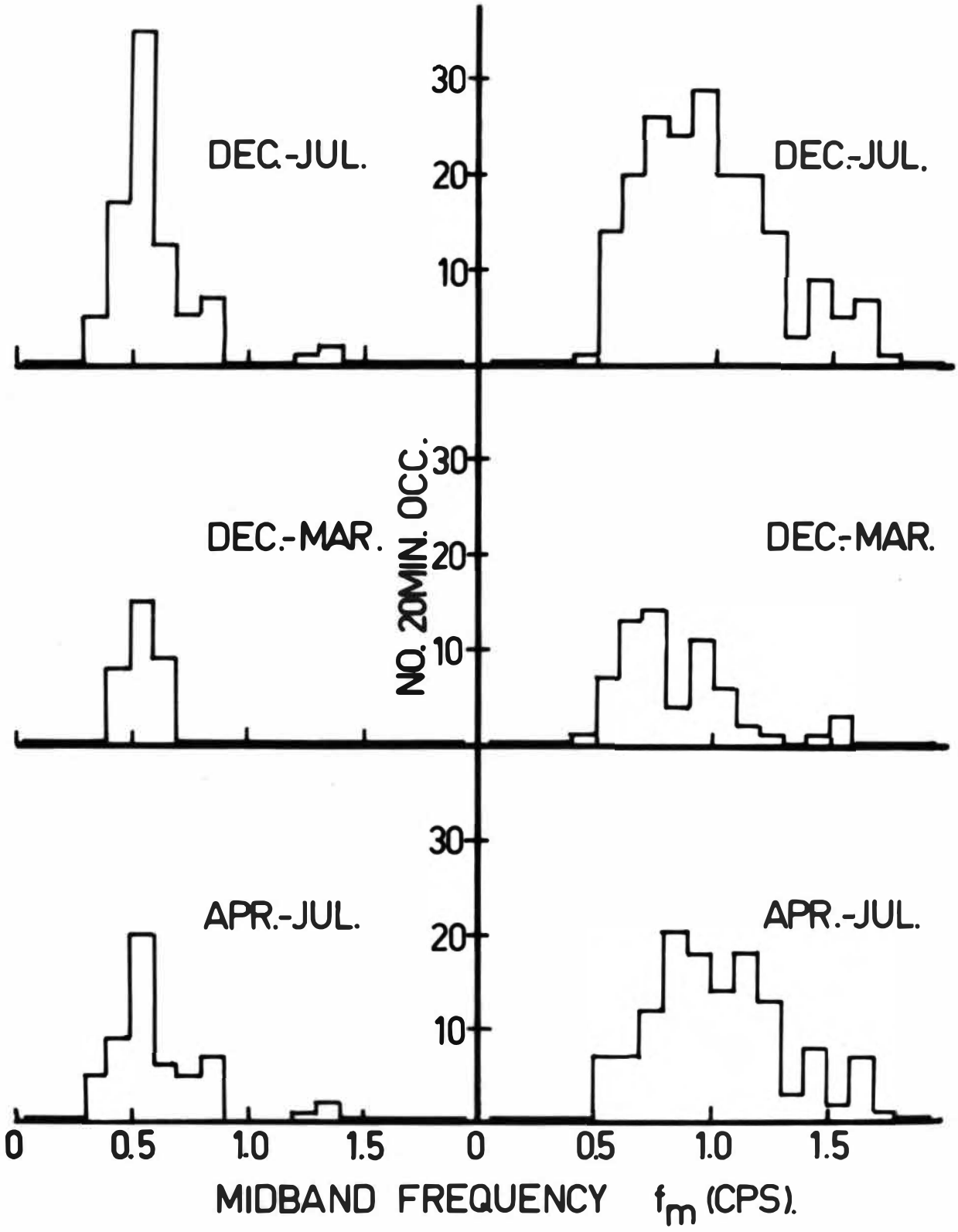
DAY 2200-0600UT.
NIGHT 1000-1800UT.
DEC.-JUL.
DEC.-JUL.
DEC.-MAR.
DEC.-MAR.
APR.-JUL.
APR.-JUL.
NO. 20MIN. OCC.
30
20
10
0
0.5
1.0
1.5
MIDBAND FREQUENCY f_m (CPS).

Figure 11.7 Low frequency daytime hm emissions.
Top. An unusually intense low frequency daytime emission. Note also the very narrow-band emissions occurring between 0420 - 0440 hr and 0455 - 0530 hr. UT. (The activity in the range 0.7 - 1.2 cps between 0600 - 0645 hr. represents the second harmonics of this event)
Bottom A more typical low amplitude daytime emission.

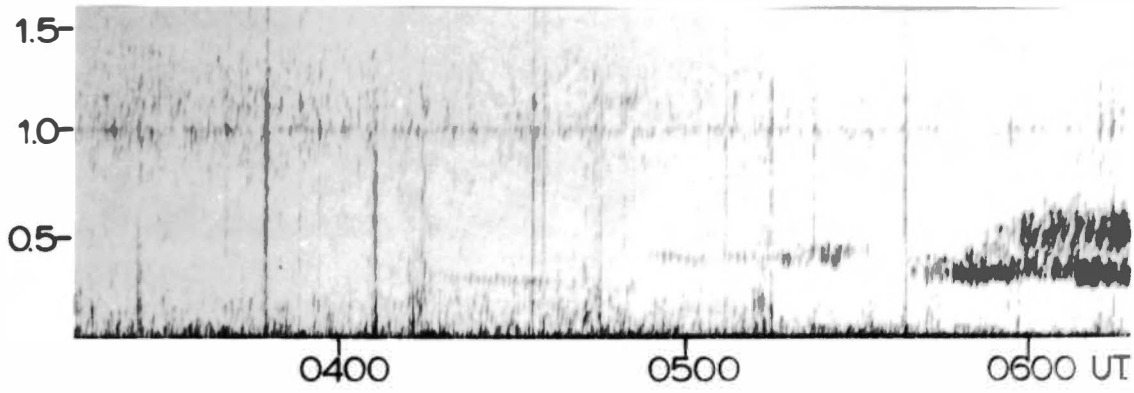

APRIL 5, 1964.

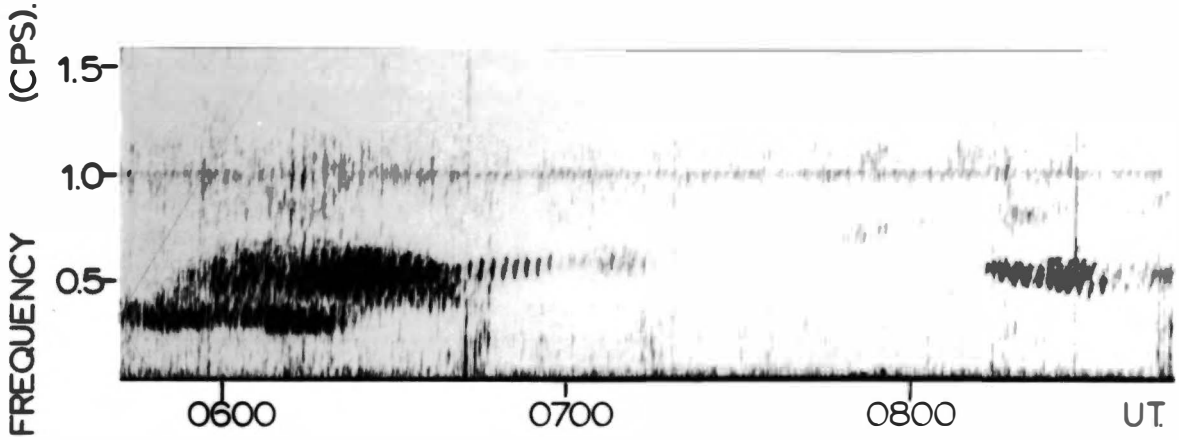

APRIL 5, 1964.

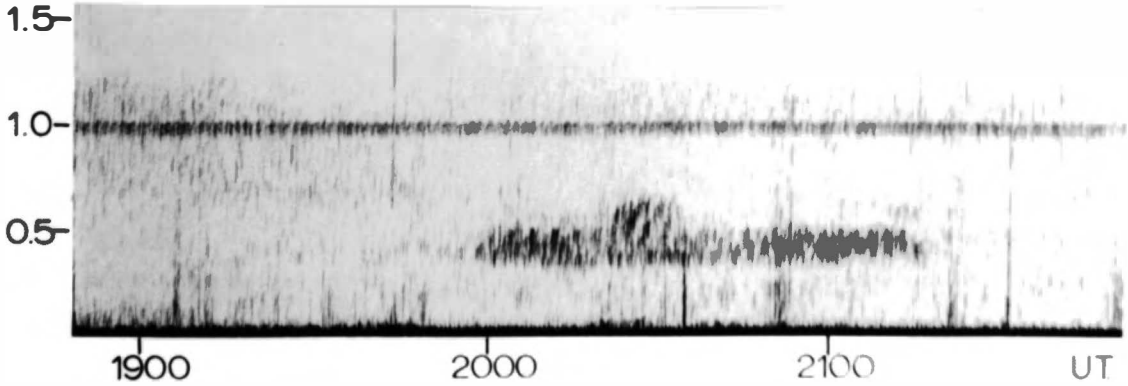

APRIL 24, 1964

Figure 11.8 Relationships between the hourly values of hm emission upper frequency cutoff for daytime emissions occurring between 10-18 hr UT (0930 - 1730 hr LT) and the ion densities of the E, F1 and F2 regions. The ion densities were calculated from the critical frequencies f_oEs, f_oF1 and f_oF2.

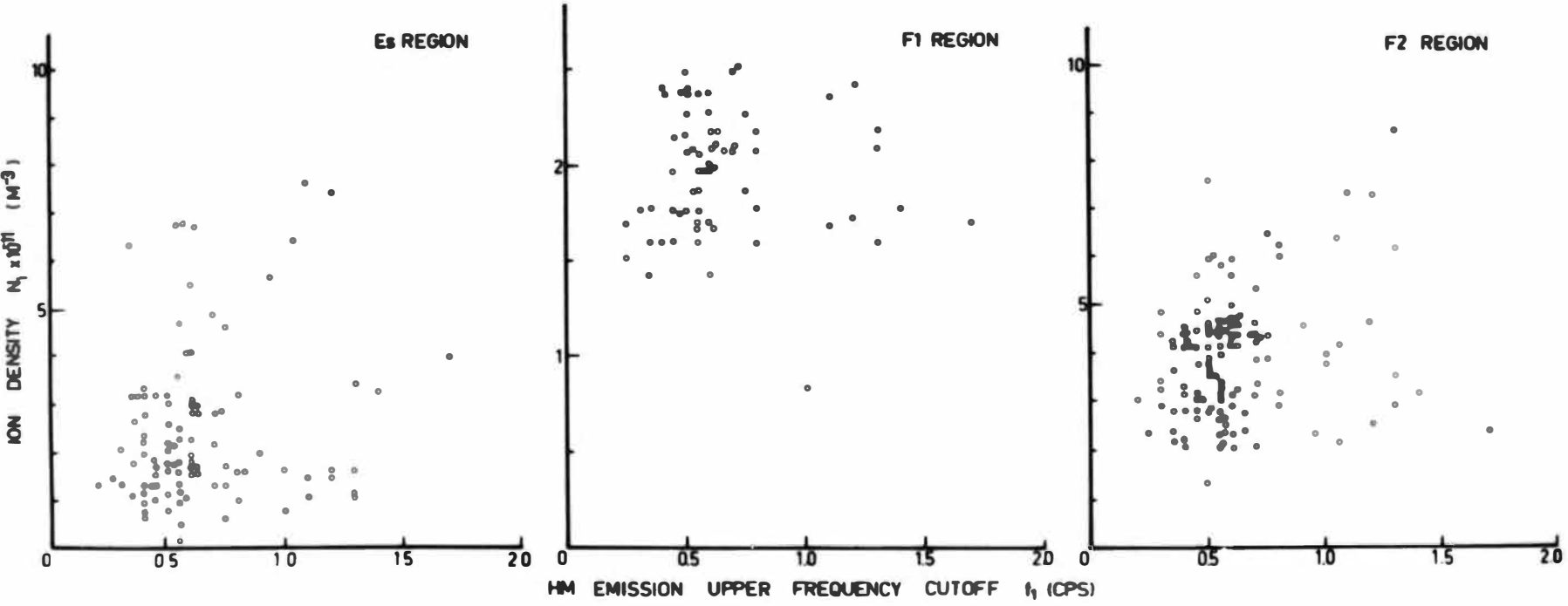
Es REGION
F1 REGION
F2 REGION
ION DENSITY $N_i \times 10^{11}$ (M^{-3})
HM EMISSION UPPER FREQUENCY CUTOFF f_1 (CPS)
0
0.5
1.0
1.5
2.0
5
10
1
2

Figure 12.1 Variation in the nighttime hourly values of fine structure band spacing with daily magnetic activity as indicated by ΣK_p.

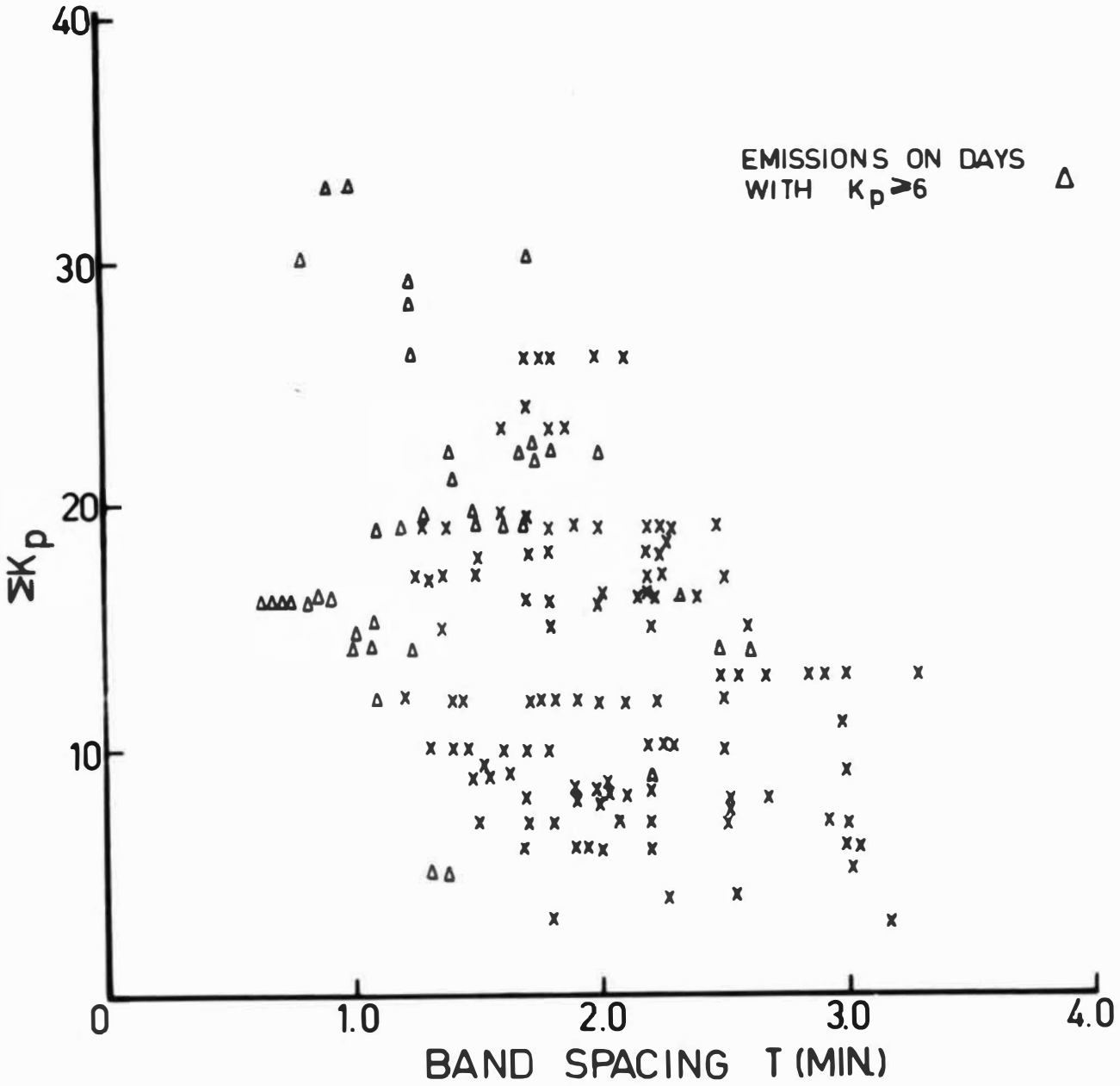
EMISSIONS ON DAYS
WITH $K_p \geq 6$
ΣK_p
40
30
20
10
0
1.0
2.0
3.0
4.0
BAND SPACING T (MIN.)

Figure 12.2 (a) The mean hourly values of midband frequency for nighttime data plotted as a function of ΣK_p values taken in groups of five

(b) The mean hourly values of band spacing plotted in a similar manner. In both graphs each point is the mean of the indicated number and the vertical line segment centred on each point indicates the standard deviation.

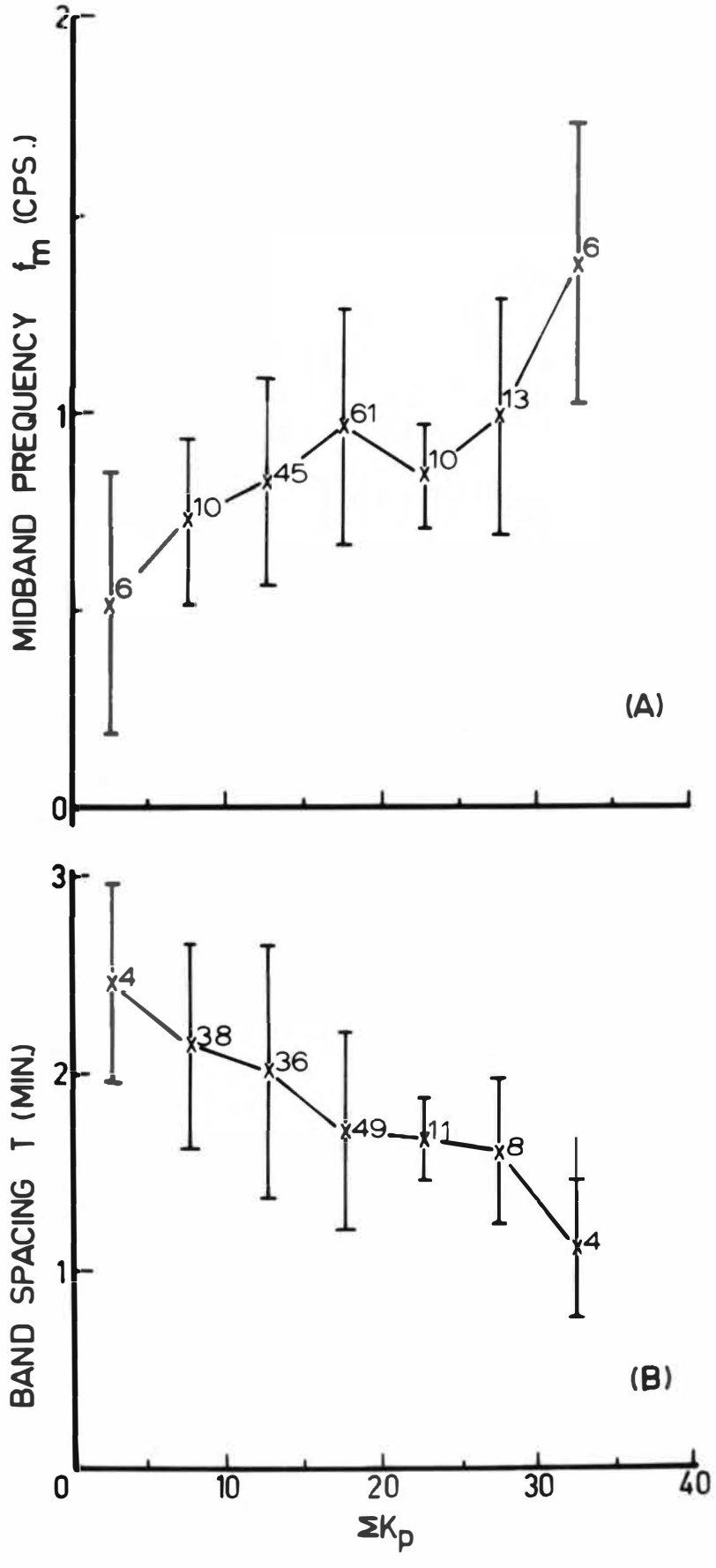
MIDBAND PREQUENCY f_m (CPS.)
2
1
0
6
10
45
61
10
13
6
(A)
BAND SPACING T (MIN.)
3
2
1
0
4
38
36
49
11
8
4
(B)
10
20
30
40
ΣK_p

Figure 13.1 Latitude variations of the hm wave packet bounce period calculated using equation 13.1. The propagation velocity is assumed to be the Alfven velocity. An inverse cube law plasma density distribution is assumed with $N_o = 1.41 \times 10^{10}$ / m^3 for the normal curve. The knee curve assumes a plasma density one-sixth of that of the normal curve.

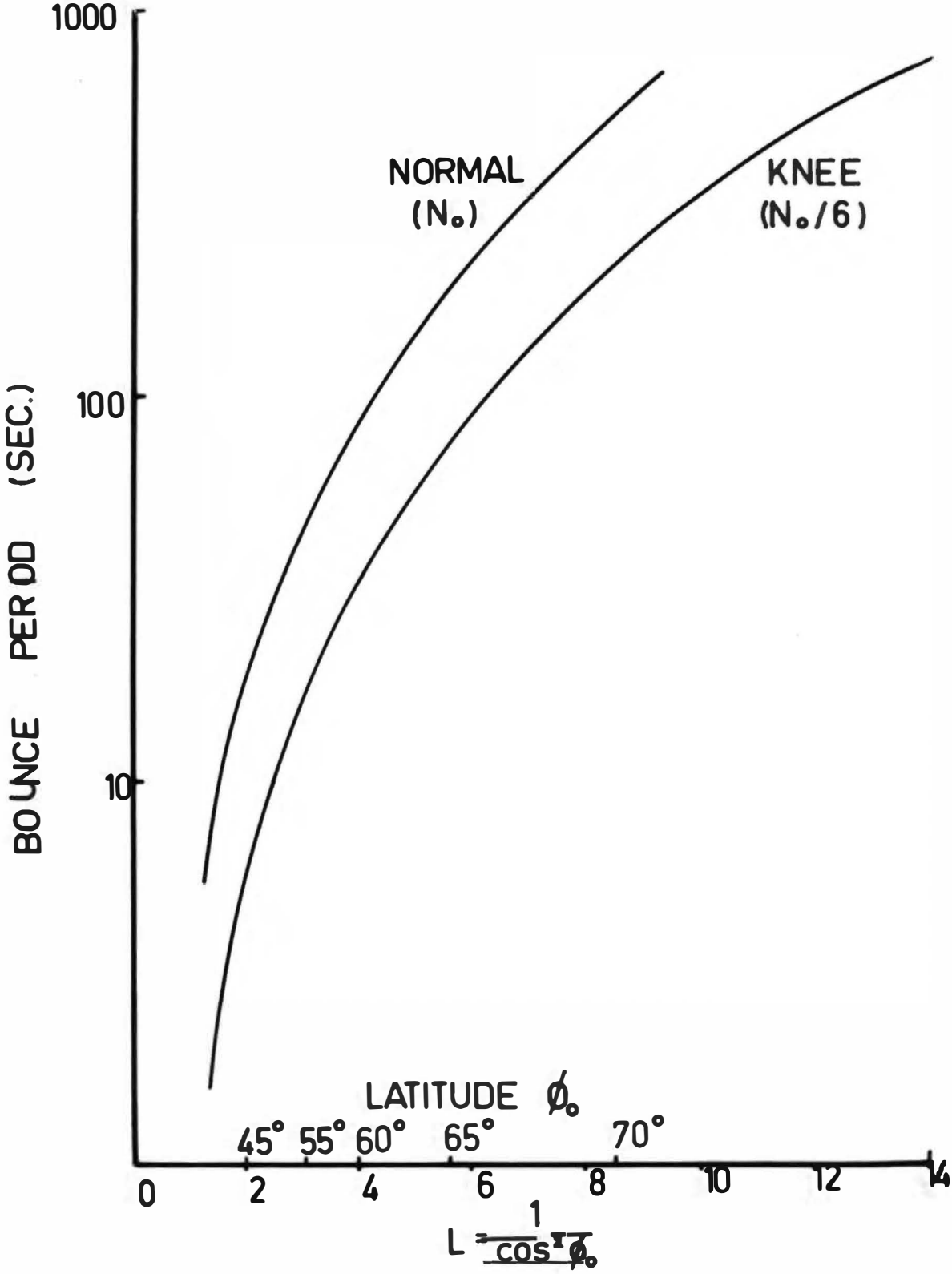
1000
100
10
BOUNCE PERIOD (SEC.)
NORMAL
(N₀)
KNEE
(N₀/6)
LATITUDE ∅₀
45°
55°
60°
65°
70°
0
2
4
6
8
10
12
14
L = 1 / cos³∅₀

Figure 13.2 Locus of the emission source as deduced from the diurnal variation in fine structure band spacing. The full curve corresponds to the average T values plotted in Figure 11.5 and the dashed curves correspond to the maximum and minimum hourly T values. The minimum curve represents the location of the emission source at disturbed periods. The dotted curve is the average position of the source for a magnetospheric plasma density distribution with a knee at L=5.

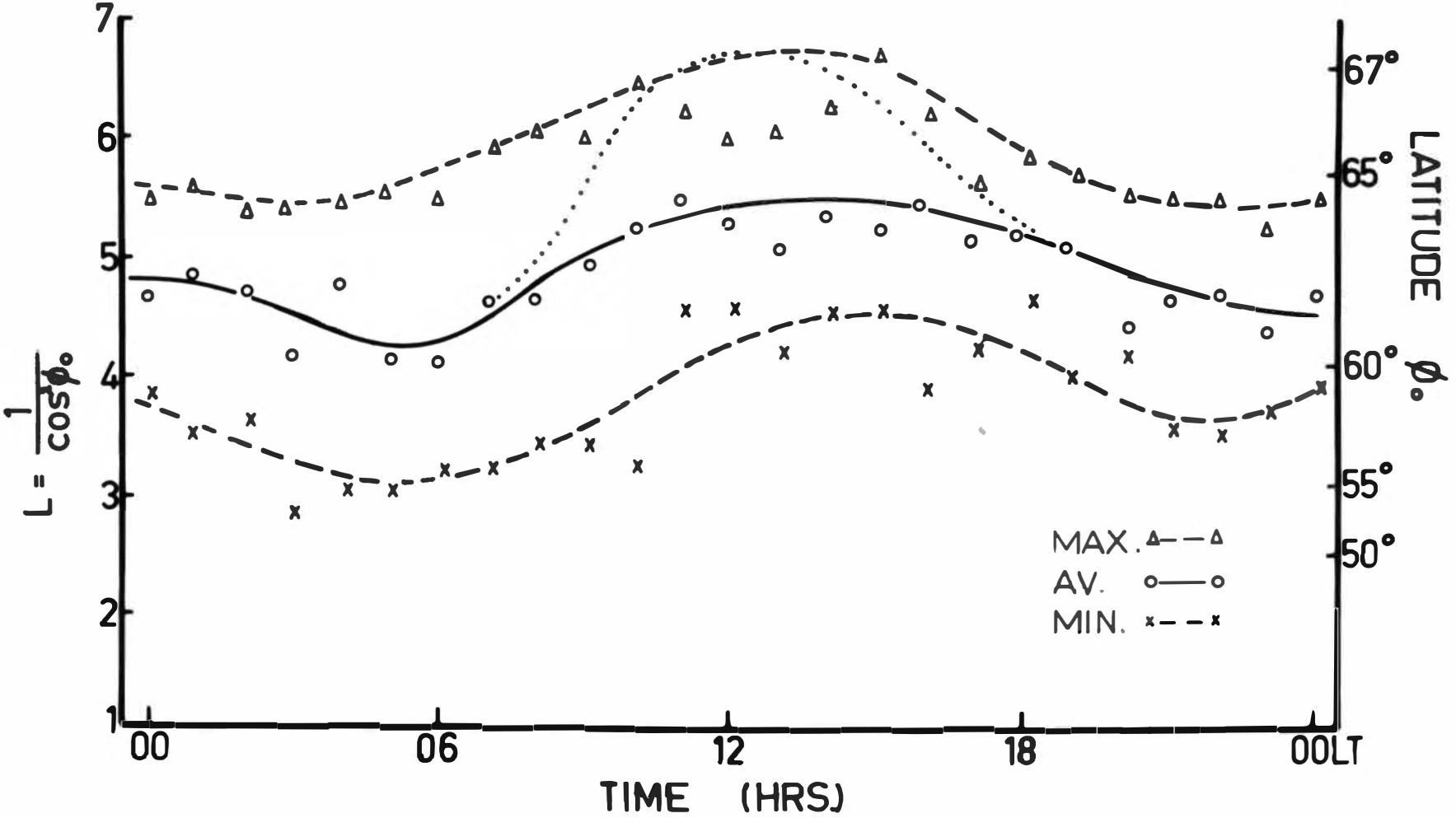
7
6
5
4
3
2
1
$L = \frac{1}{\cos^3\phi_o}$
67°
65°
60°
55°
50°
LATITUDE ϕ_o
MAX.
AV.
MIN.
00
06
12
18
00LT
TIME (HRS)

Figure 13.3. Variation in hm emission occurrence at fourteen stations.

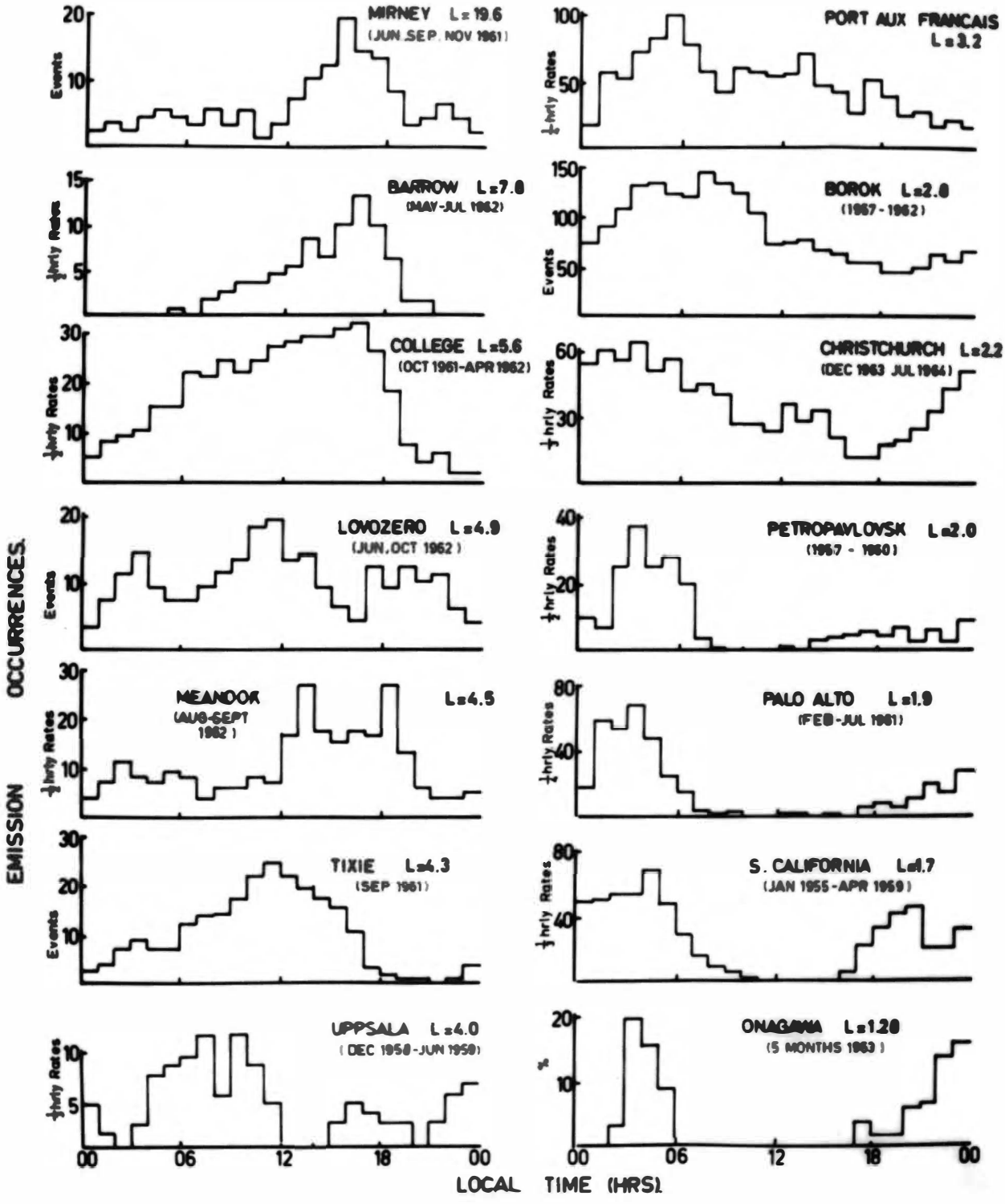
MIRNEY L = 19.6
(JUN.SEP. NOV 1961)
PORT AUX FRANCAIS
L = 3.2
BARROW L = 7.8
(MAY-JUL 1962)
BOROK L = 2.8
(1957 - 1962)
COLLEGE L = 5.6
(OCT 1961-APR 1962)
CHRISTCHURCH L = 2.2
(DEC 1963 JUL 1964)
LOVOZERO L = 4.9
(JUN.OCT 1962)
PETROPAVLOVSK L = 2.0
(1957 - 1960)
MEANOOK
(AUG-SEPT
1962)
L = 4.5
PALO ALTO L = 1.9
(FEB-JUL 1961)
TIXIE L = 4.3
(SEP 1961)
S. CALIFORNIA L = 1.7
(JAN 1955-APR 1959)
UPPSALA L = 4.0
(DEC 1958-JUN 1959)
ONAGAWA L = 1.28
(5 MONTHS 1963)
Events
Hrly Rates
%
EMISSION OCCURRENCES.
00
06
12
18
00
LOCAL TIME (HRS)

Figure 13.4 Variation in the time of diurnal peak occurrence of hm emission activity with latitude for the fifteen stations listed in Table 13.1.

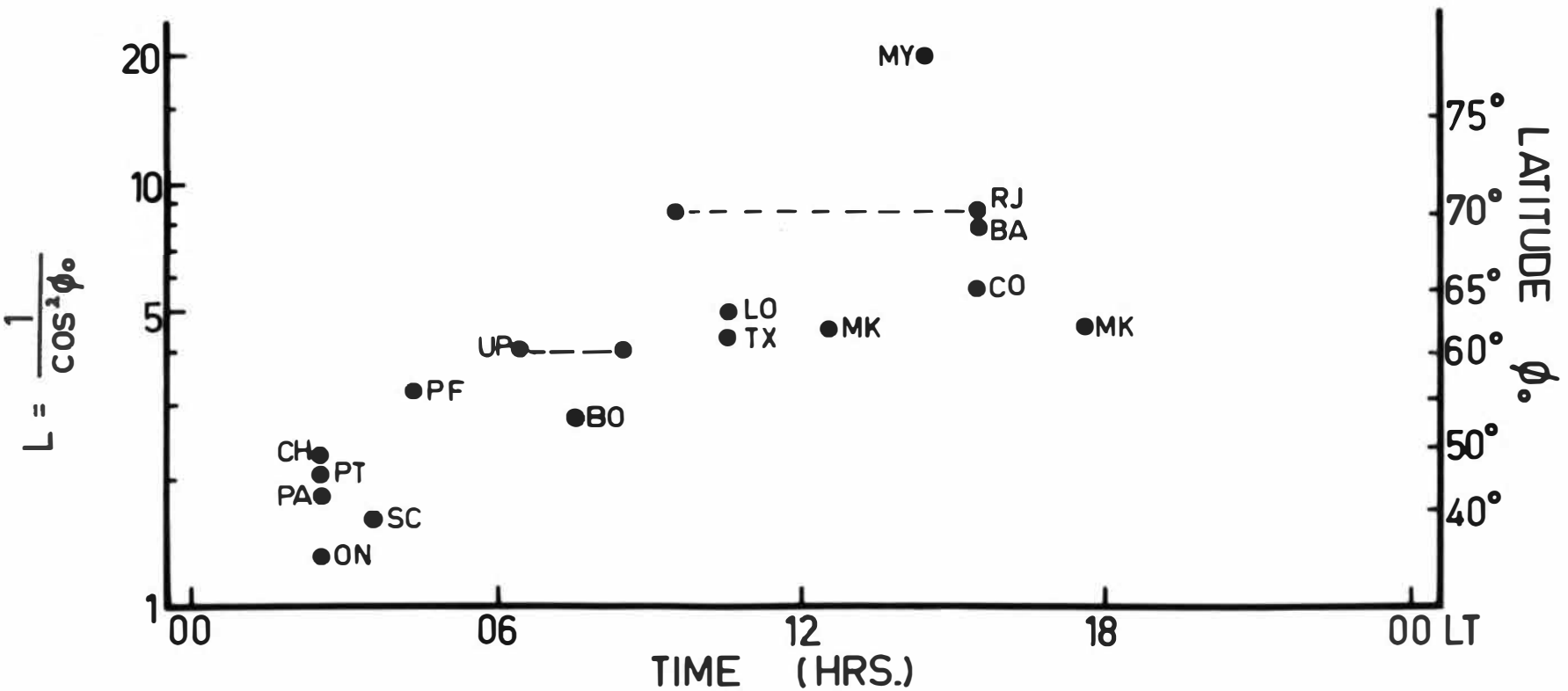
20
10
5
1
$L = \frac{1}{\cos^2 \phi_o}$
MY
RJ
BA
CO
LO
TX
MK
MK
UP
PF
BO
CH
PT
PA
SC
ON
00
06
12
18
00 LT
TIME (HRS.)
75°
70°
65°
60°
50°
40°
LATITUDE ϕ_o

Figure 13.5 Variation in the nighttime location of the hm emission source with daily magnetic activity as indicated by ΣK_p. The full curve corresponds to the average T values plotted in Figure 12.2, and the triangular and crossed data points represent the maximum and minimum hourly T values respectively.

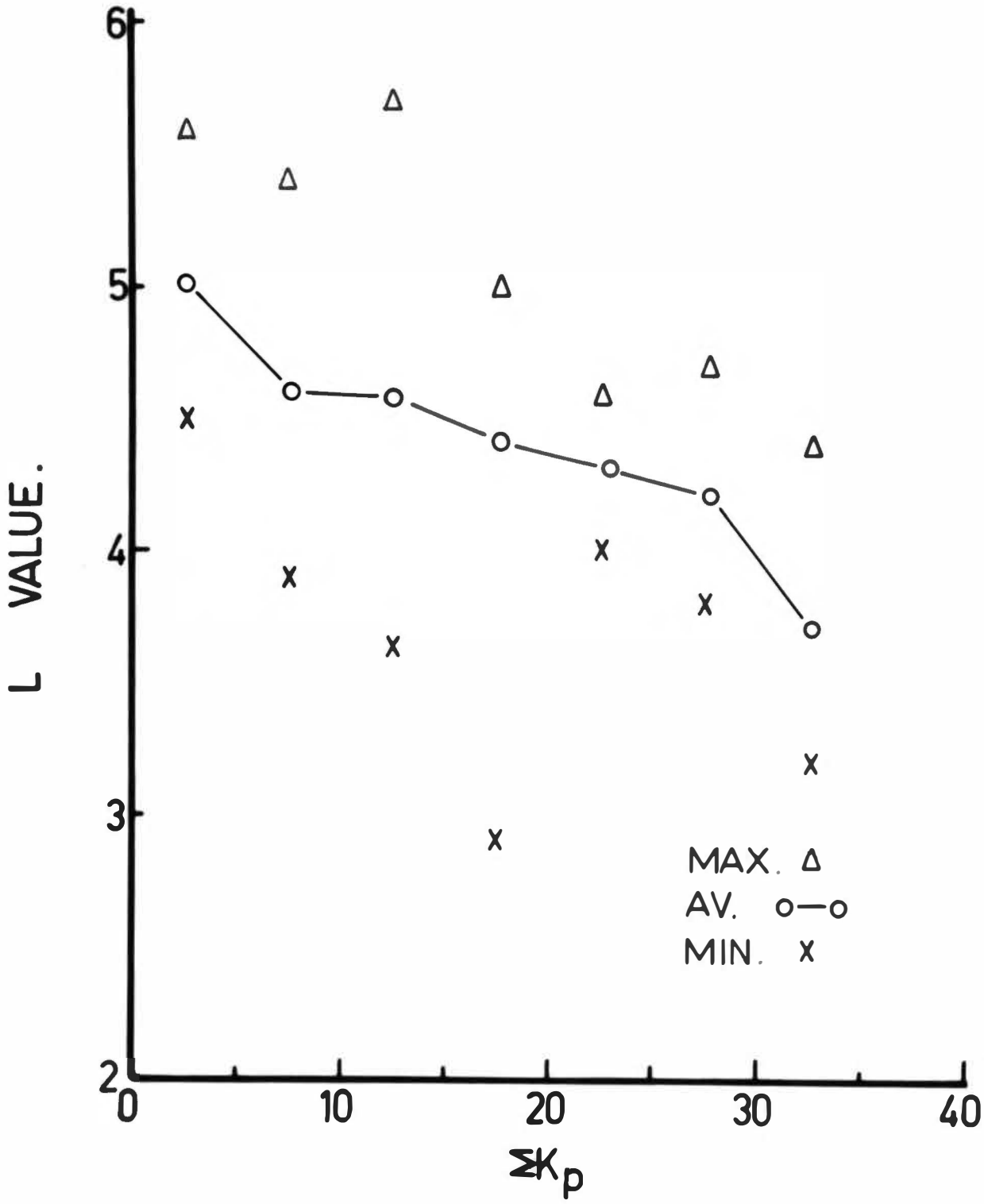
6
5
4
3
2
L VALUE.
0
10
20
30
40
ΣKp
MAX. Δ
AV. o—o
MIN. x

Figure A2.1 Detector coil. The calibration coil is wound on the smaller former between the two main coils.

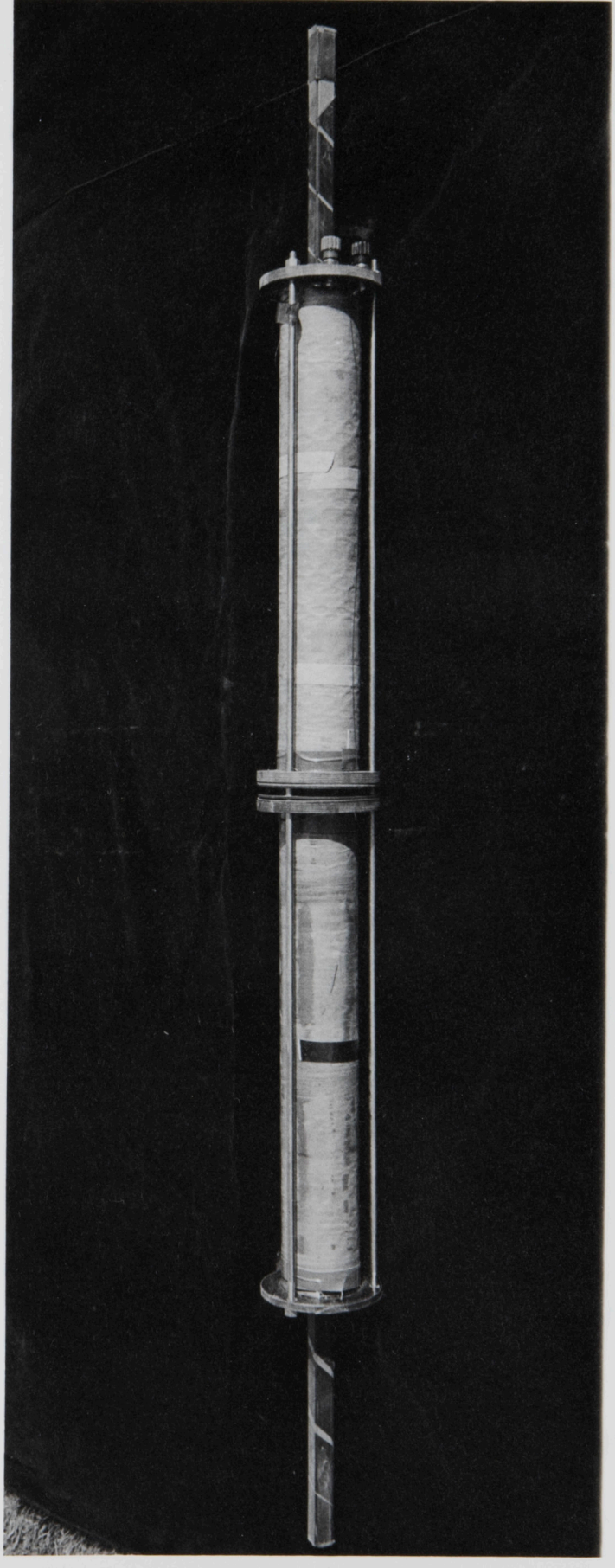

Figure A2.2 Galvanometer-photocell amplifier.

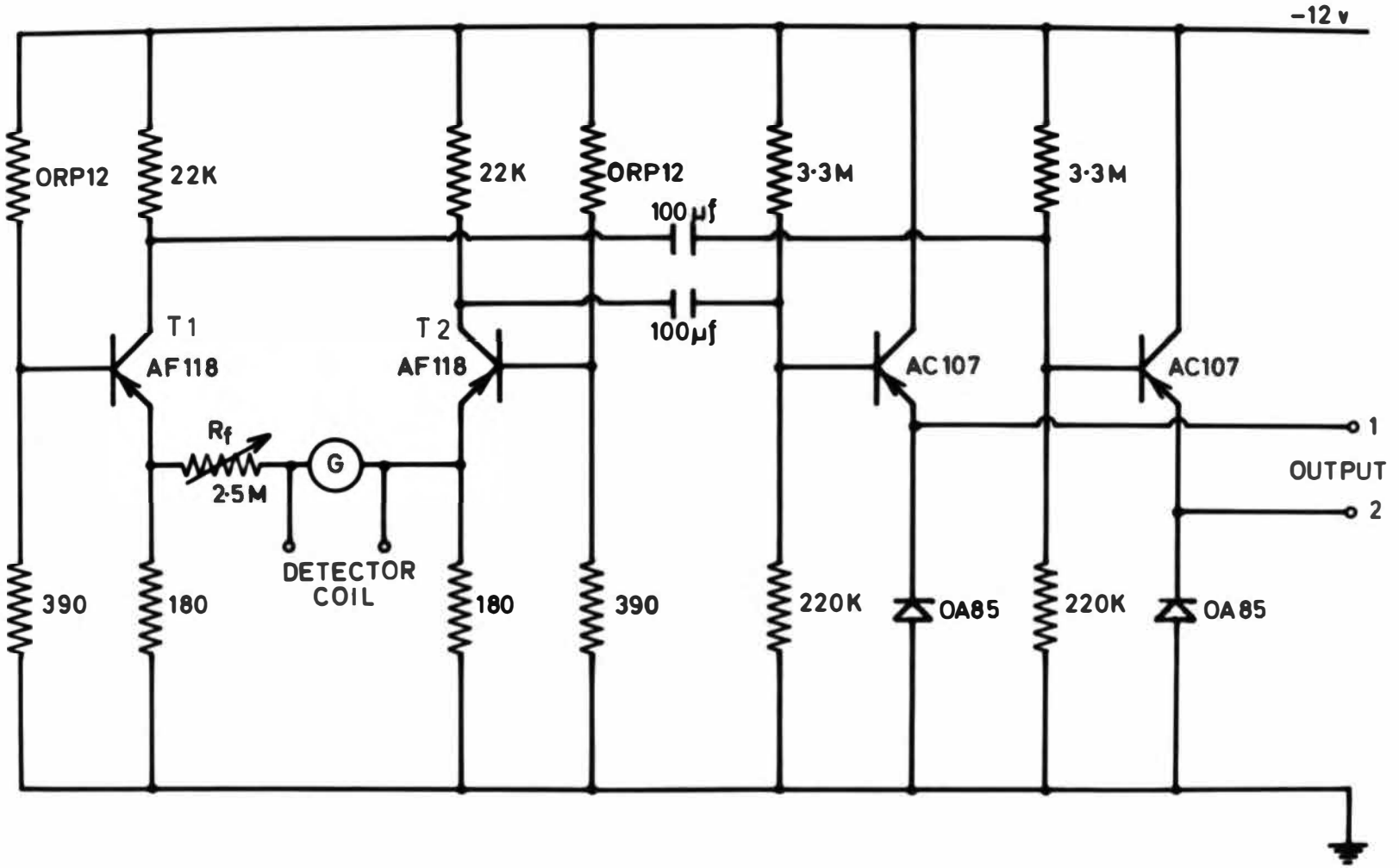
-12 v
ORP12
22K
22K
ORP12
3·3M
3·3M
100 µf
100µf
T1
AF118
T2
AF118
AC107
AC107
Rf
2·5M
G
1
OUTPUT
2
DETECTOR
COIL
390
180
180
390
220K
OA85
220K
OA85

Figure A2.3 Tape amplifier with high and low sensitivity data channels.

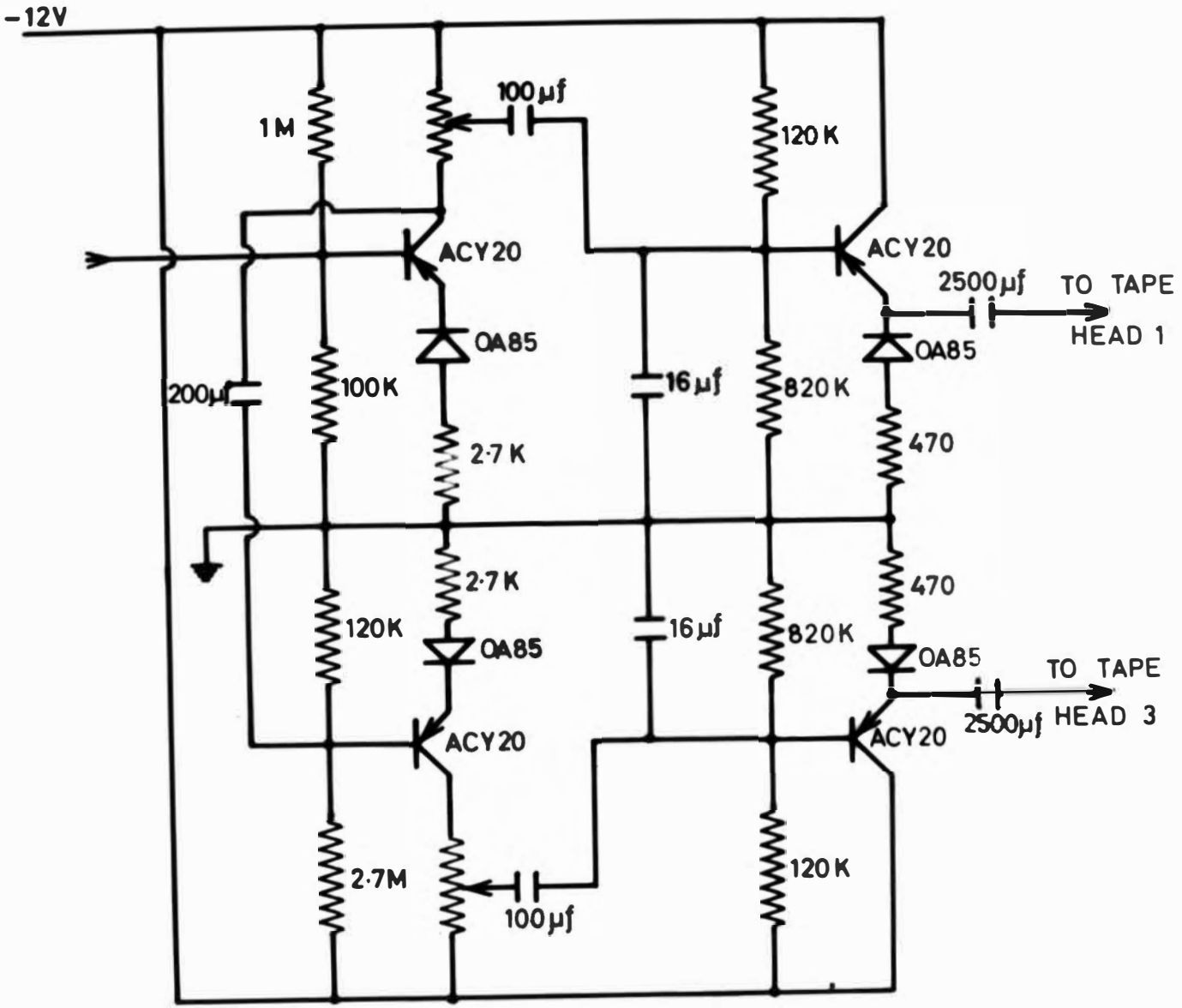
-12V
1M
100µf
120K
ACY20
ACY20
2500µf
TO TAPE
HEAD 1
OA85
OA85
200µf
100K
16µf
820K
2·7K
470
2·7K
470
120K
16µf
820K
OA85
OA85
TO TAPE
HEAD 3
ACY20
ACY20
2·7M
100µf
120K

Figure A2.4 Overall frequency response of the high sensitivity data recording channel. The 3db band-width is 0.08 - 3.3 cps.

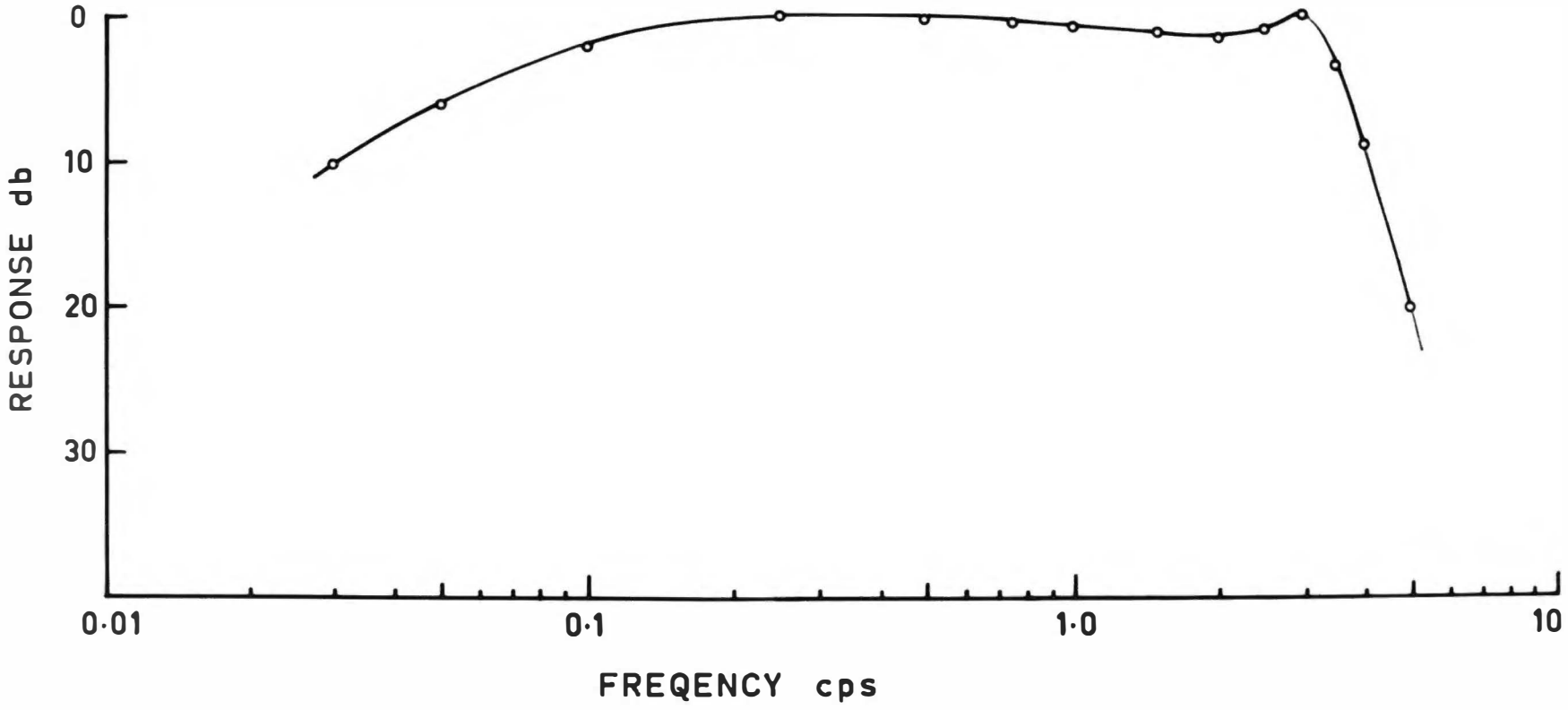
0
10
20
30
RESPONSE db
0·01
0·1
1·0
10
FREQENCY cps

Figure A2.5 500 cps bias oscillator and amplifier.

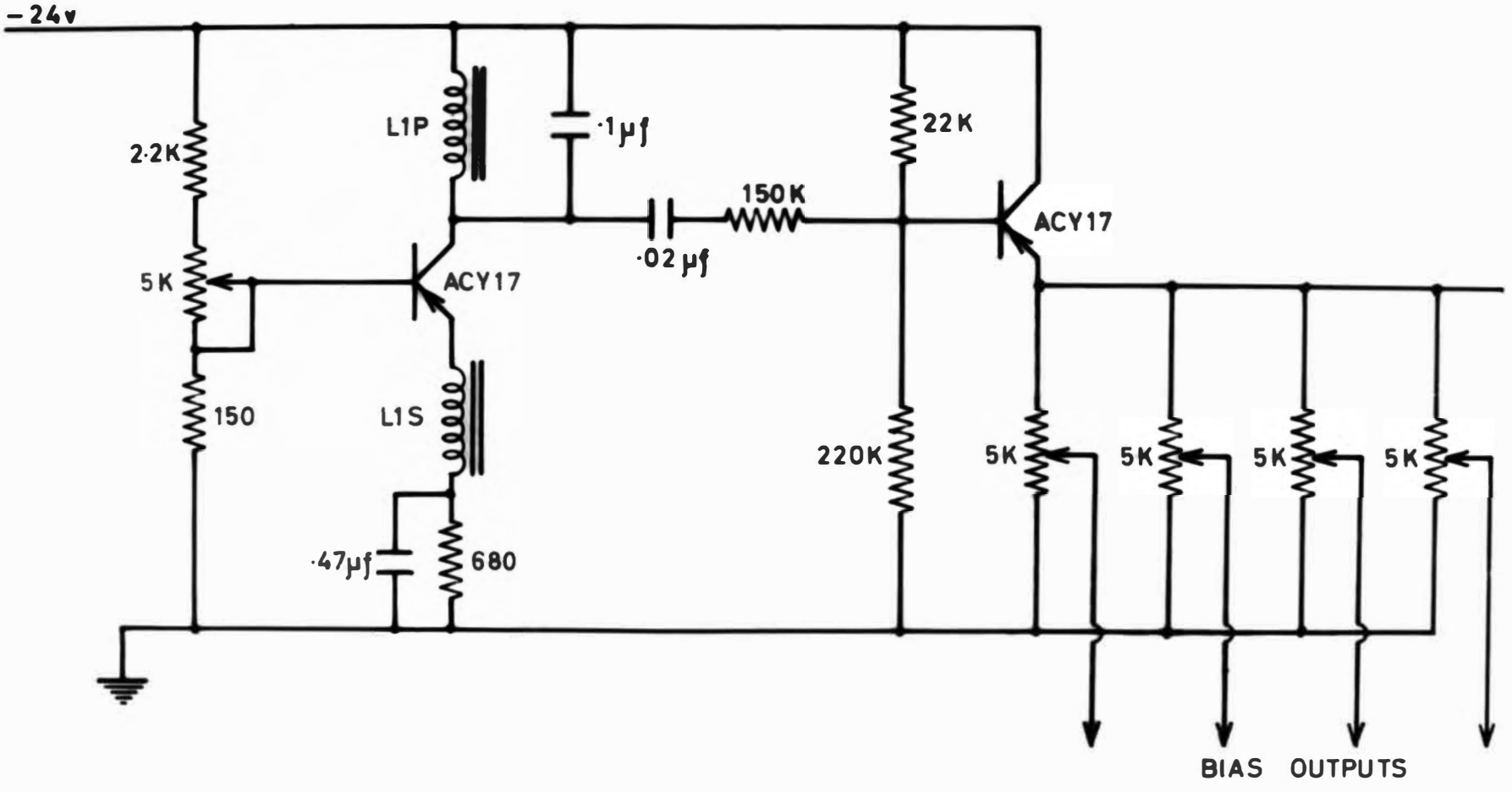
-24v
2·2K
L1P
·1µf
22K
150K
ACY17
·02 µf
5K
ACY17
150
L1S
220K
5K
5K
5K
5K
·47µf
680
BIAS
OUTPUTS

Figure A2.6. 50 cps squaring amplifier and motor drive power amplifier. The output of the squaring amplifier feeds to the frequency dividers providing the 2 ppm time signals. The power amplifier is rated at 1.5 W and drives the tape transport and calibration oscillator motors in parallel.

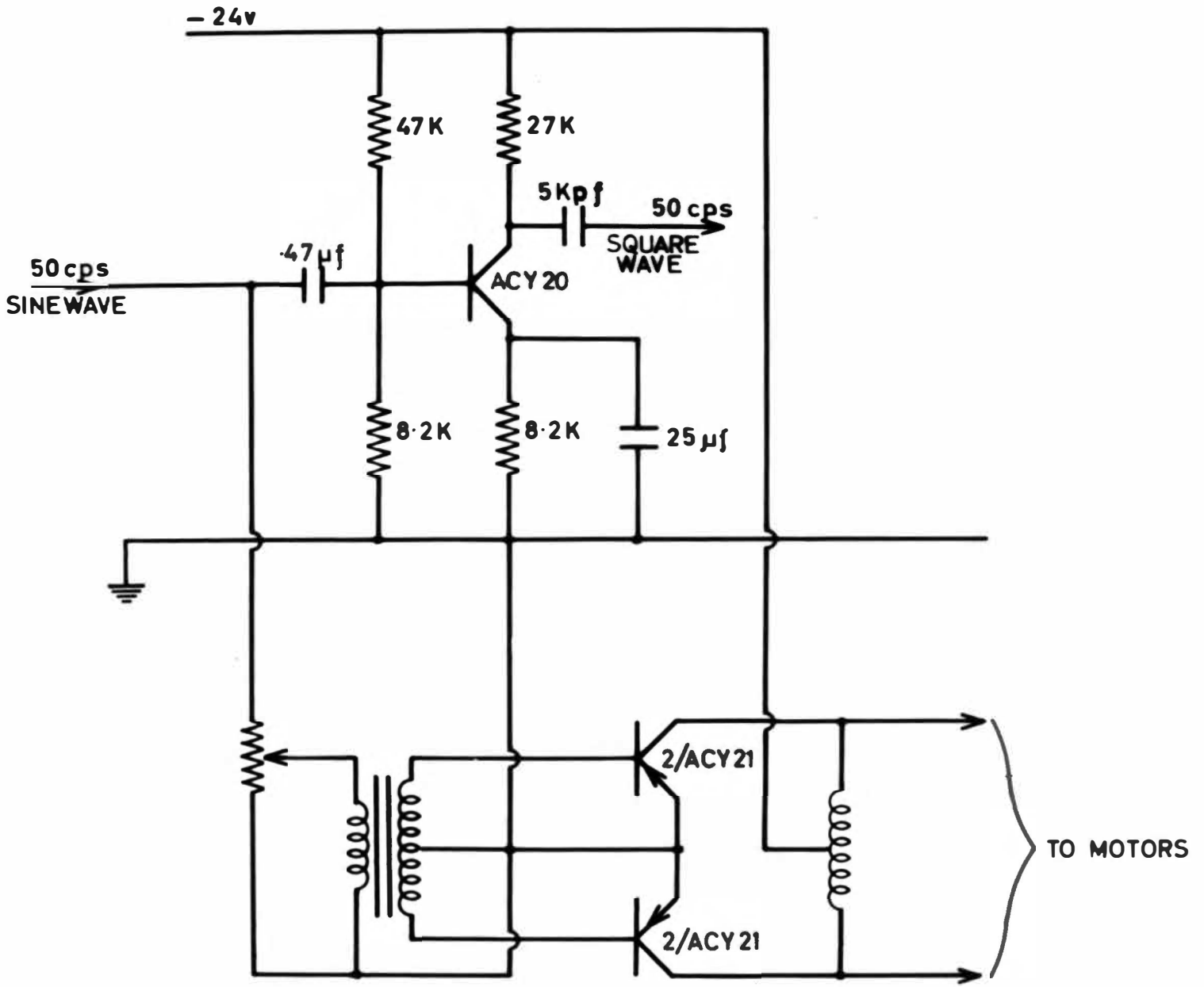
– 24v
47K
27K
5Kpf
50 cps
SQUARE WAVE
50 cps
SINEWAVE
·47µf
ACY20
8·2K
8·2K
25µf
2/ACY21
2/ACY21
TO MOTORS

Figure A2.7 Frequency division circuits for the time pulses. The 50 cps tuning fork signal is reduced to 2 ppm using four monostable circuits and three binary circuits. Details of the monostable circuits are listed below.

	Division Factor	R_1 (hi stab.)	C_1 (μf)
M1	5	283 K	0.47
M2	5	47 K	10
M3	5	100 K	25
M4	3	100 K	50

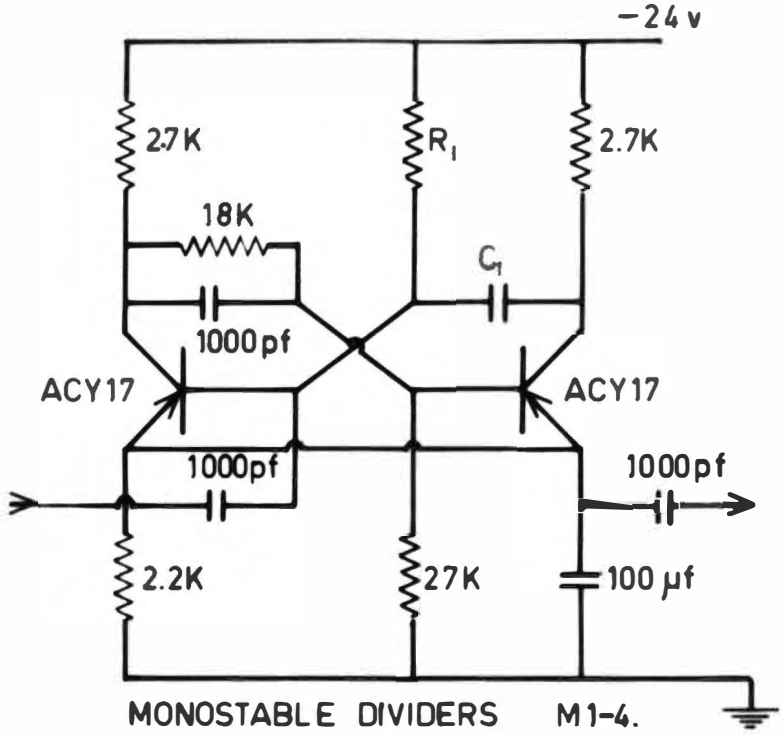

MONOSTABLE DIVIDERS M1-4.

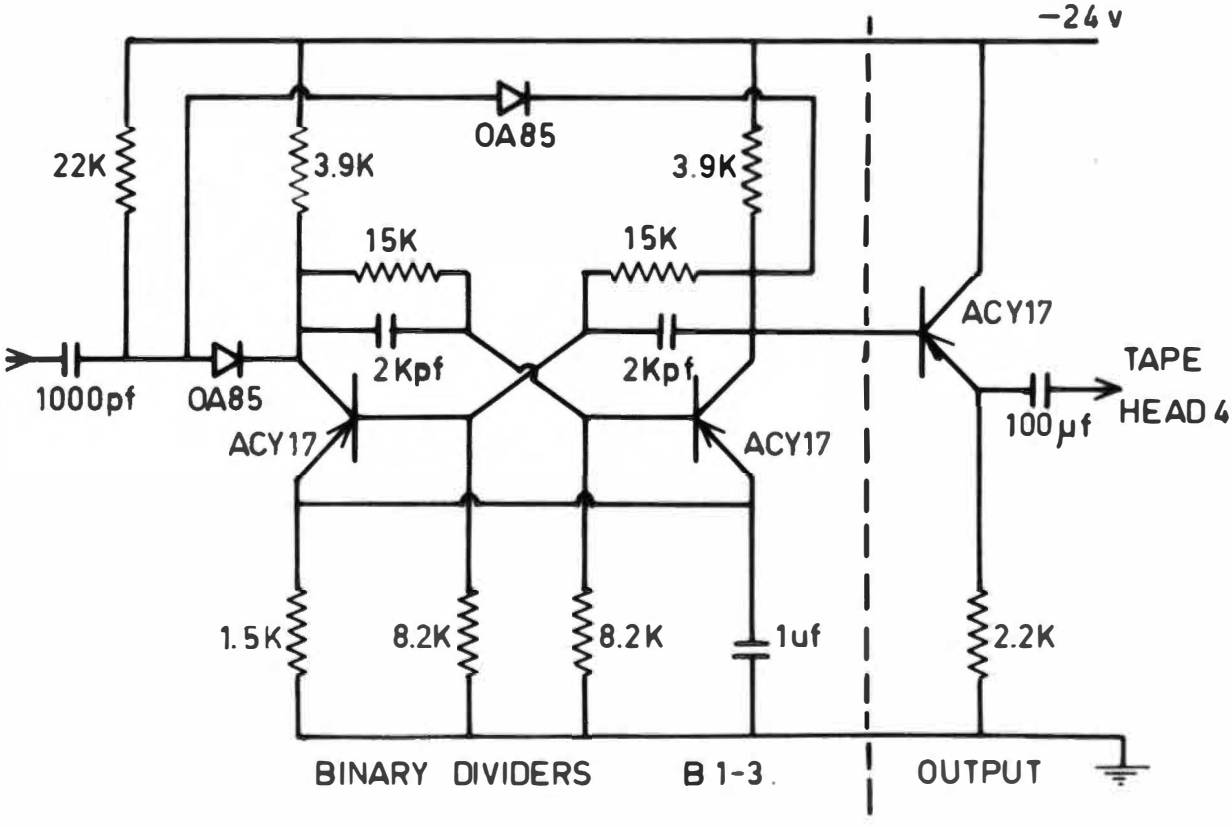

BINARY DIVIDERS B 1-3. OUTPUT

Figure A2.8 1000 cps filter amplifier and output stages. The amplifier has a Q-factor of 8.

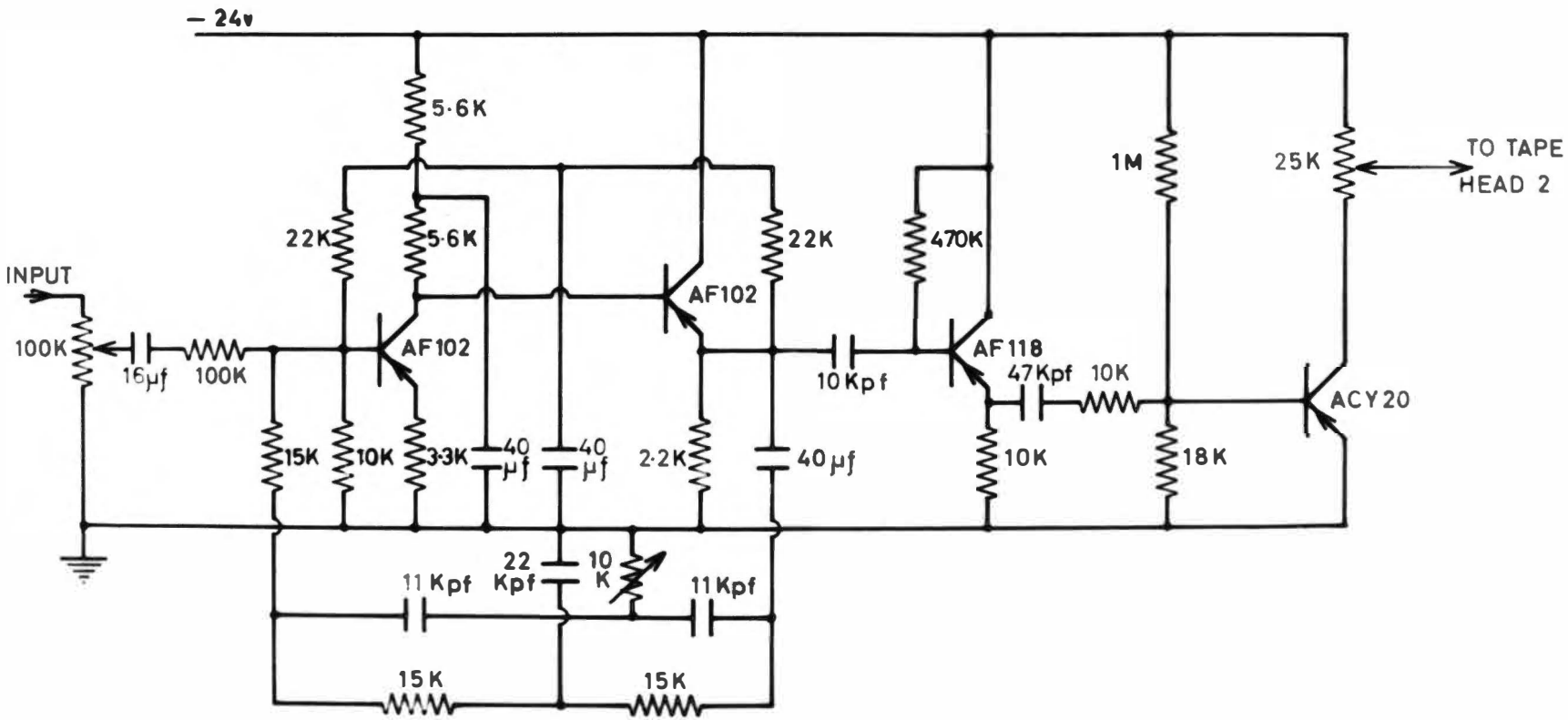
– 24v
5·6K
22K
5·6K
22K
470K
1M
25K
TO TAPE
HEAD 2
INPUT
100K
16µf
100K
AF102
AF102
AF118
10Kpf
47Kpf
10K
ACY20
15K
10K
3·3K
40 µf
40 µf
2·2K
40 µf
10K
18K
22 Kpf
10 K
11 Kpf
11 Kpf
15K
15K

Figure A2.9 Battery voltage regulator.

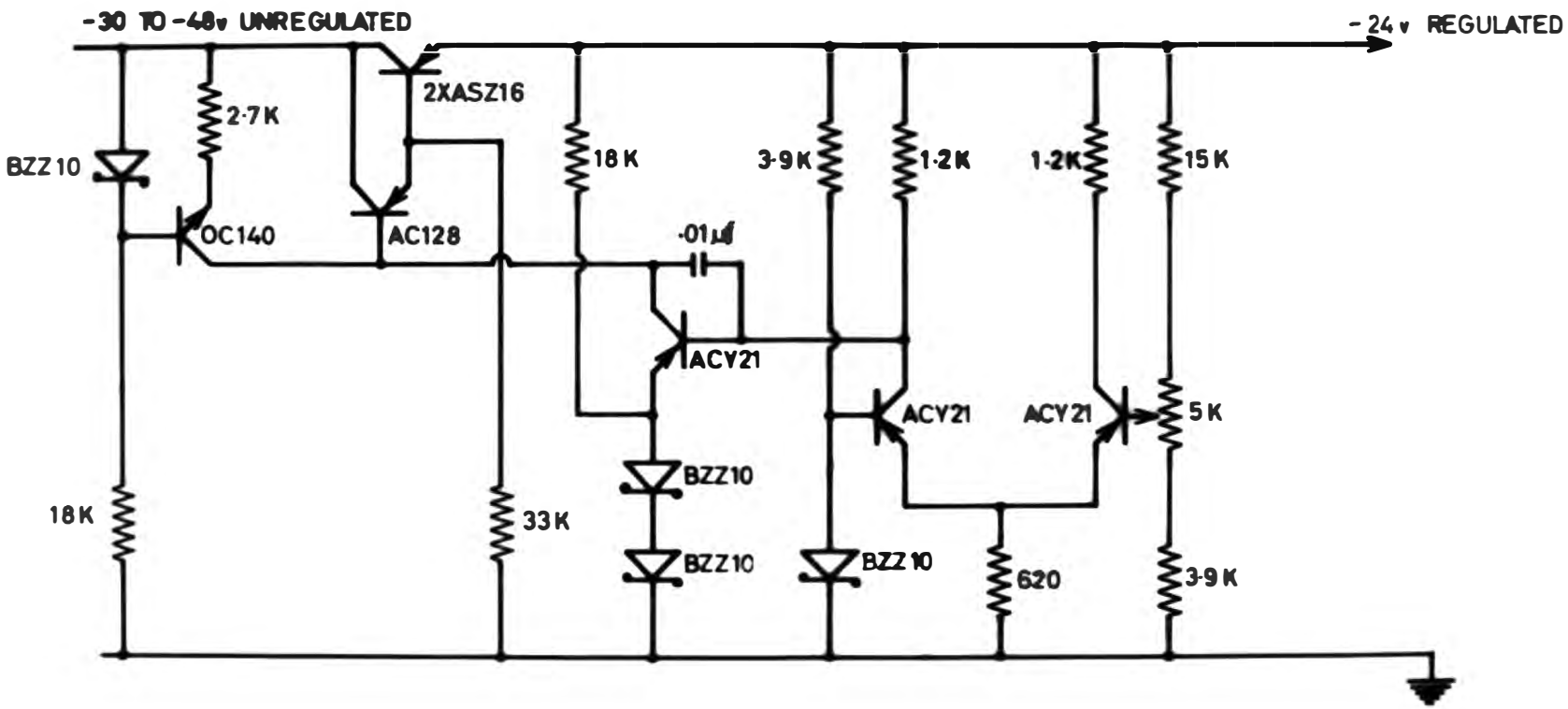
-30 TO -48v UNREGULATED
-24v REGULATED
2XASZ16
2·7K
BZZ10
OC140
AC128
18K
·01µF
3·9K
1·2K
1·2K
15K
ACY21
ACY21
ACY21
5K
BZZ10
18K
33K
BZZ10
BZZ10
620
3·9K

Figure A3.1 Equalization amplifier.

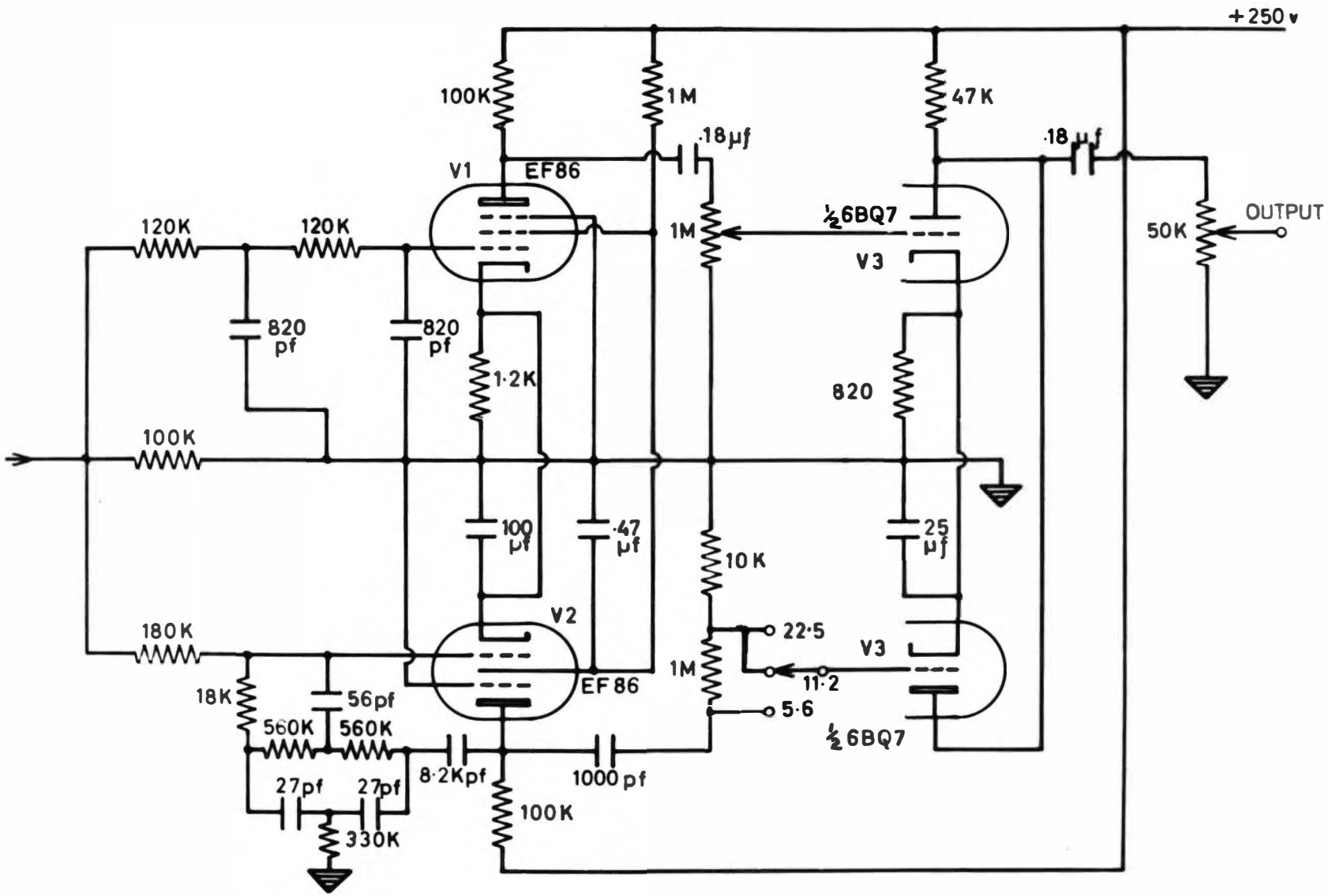
+250 v
100K
1M
47K
.18µf
.18 µf
V1
EF86
½6BQ7
V3
OUTPUT
50K
120K
120K
1M
820 pf
820 pf
1·2K
820
100K
100 µf
·47 µf
10K
25 µf
V2
22·5
180K
V3
11·2
1M
18K
56pf
EF 86
5·6
560K
560K
½6BQ7
8·2Kpf
1000 pf
27pf
27pf
100K
330K

Figure A3.2 Frequency response of the equalization amplifier.

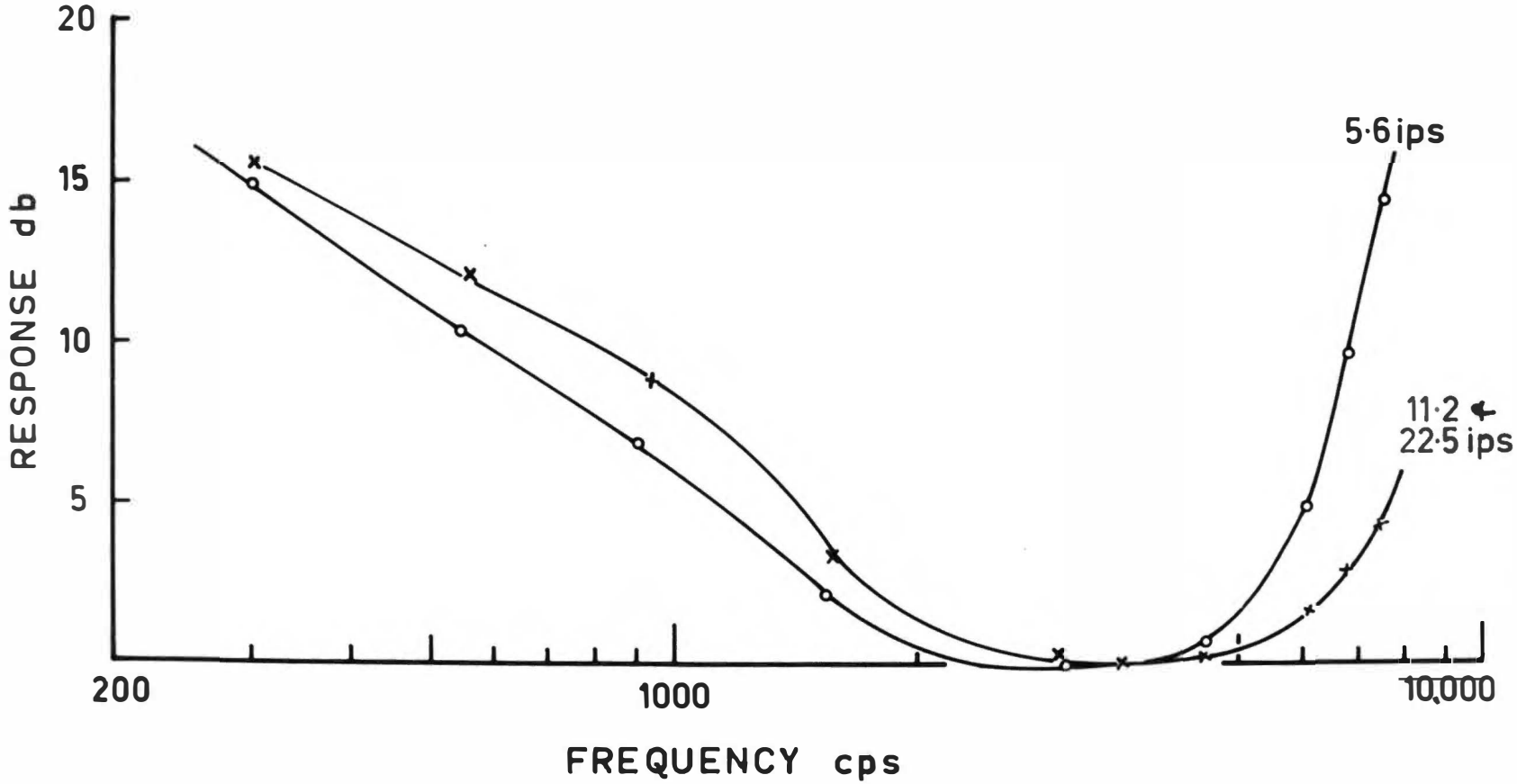
20
15
10
5
RESPONSE db
5·6ips
11·2
22·5 ips
200
1000
10,000
FREQUENCY cps

figure A3.3. Pulse shaping amplifier.

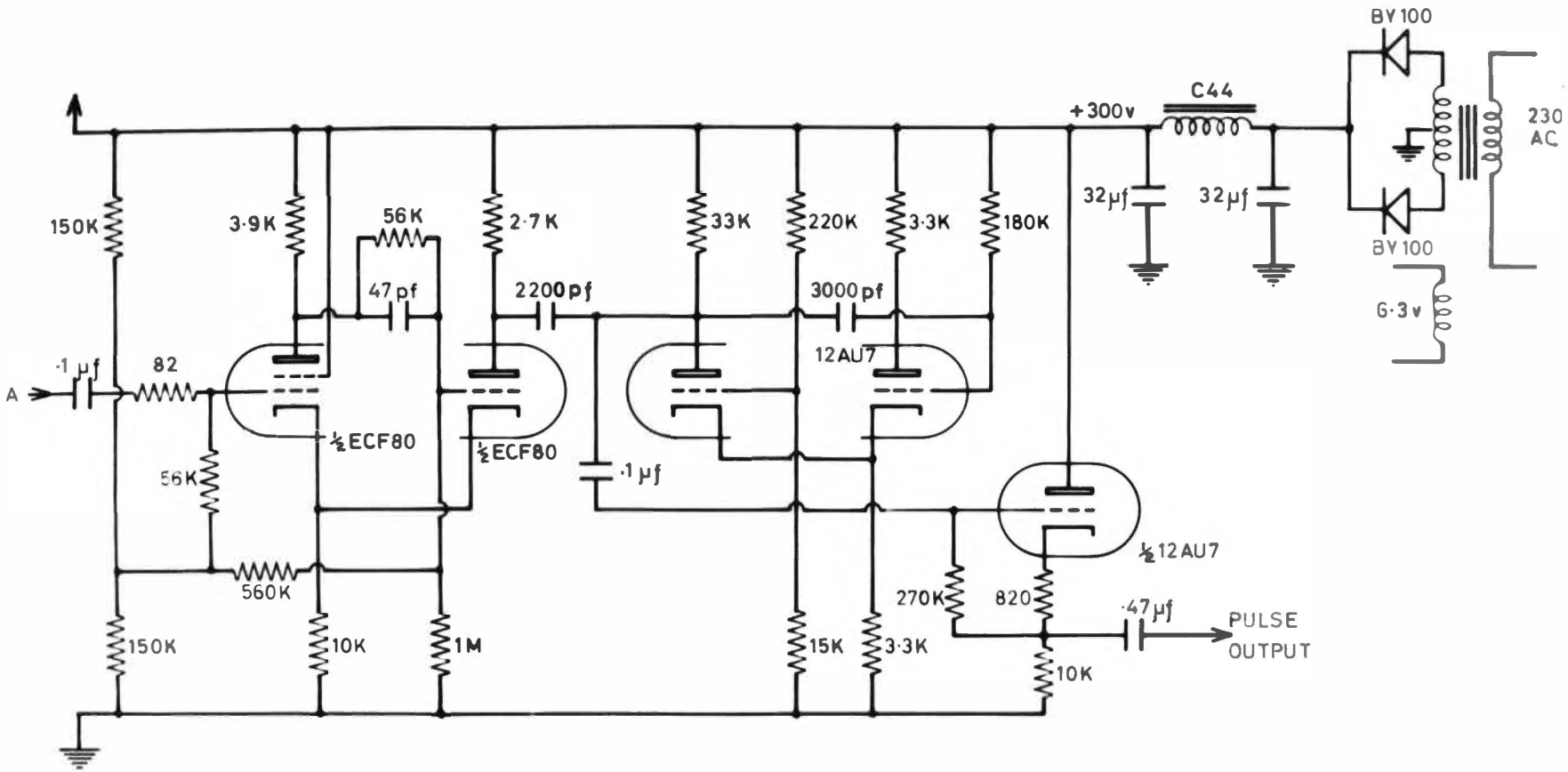
BY100
C44
+300v
230
AC
150K
3·9K
56K
2·7K
33K
220K
3·3K
180K
32µf
32µf
BY100
6·3v
47pf
2200pf
3000pf
12AU7
·1µf
82
A
½ECF80
½ECF80
56K
·1µf
560K
½12AU7
270K
820
·47µf
PULSE
OUTPUT
150K
10K
1M
15K
3·3K
10K

Figure A3.4. Block diagram of the pulse counter.

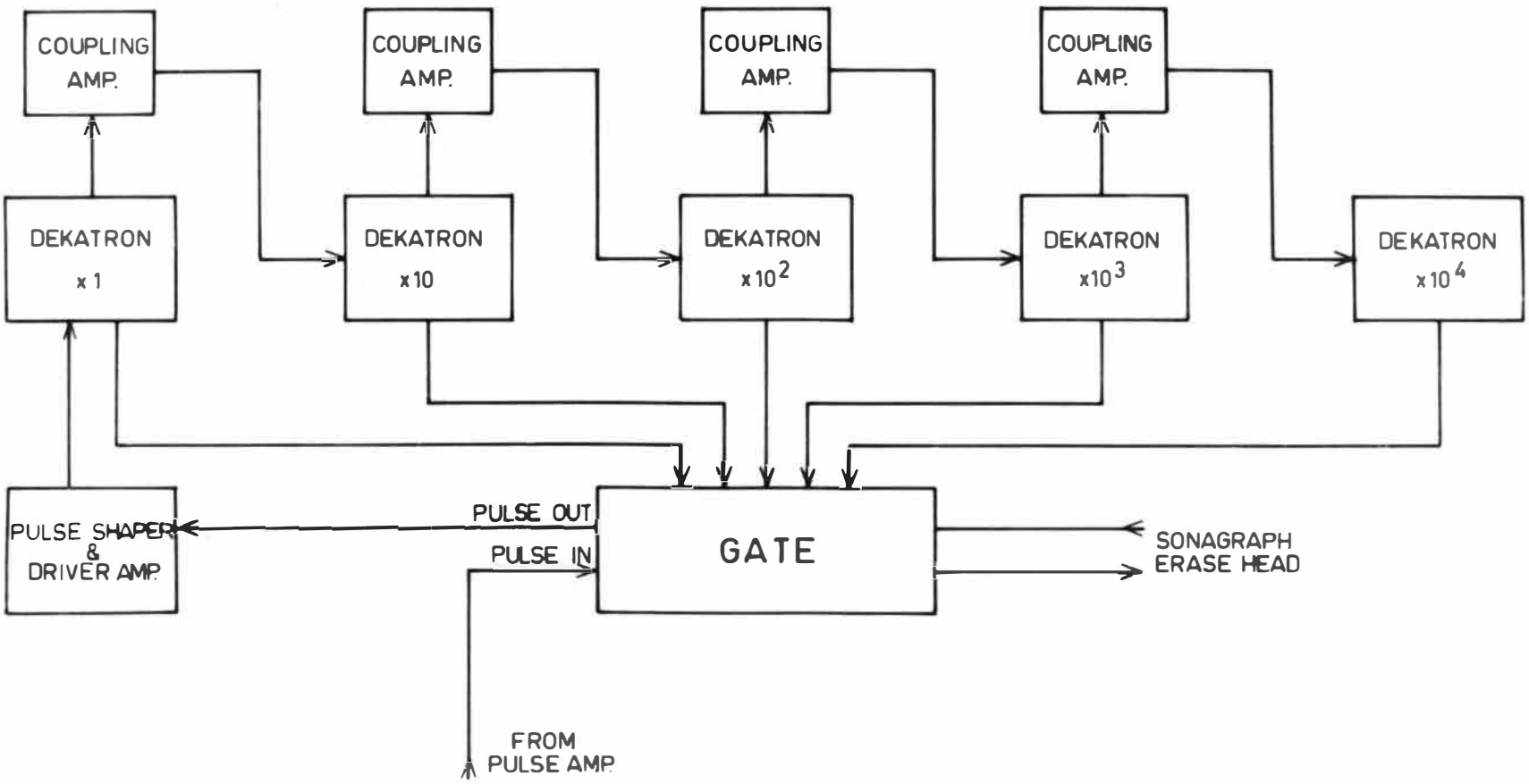
COUPLING AMP.
COUPLING AMP.
COUPLING AMP.
COUPLING AMP.
DEKATRON x 1
DEKATRON x10
DEKATRON x10 2
DEKATRON x10 3
DEKATRON x10 4
PULSE SHAPER & DRIVER AMP.
PULSE OUT
PULSE IN
GATE
SONAGRAPH ERASE HEAD
FROM PULSE AMP.

Figure A3.5. The pulse counter gate circuit.

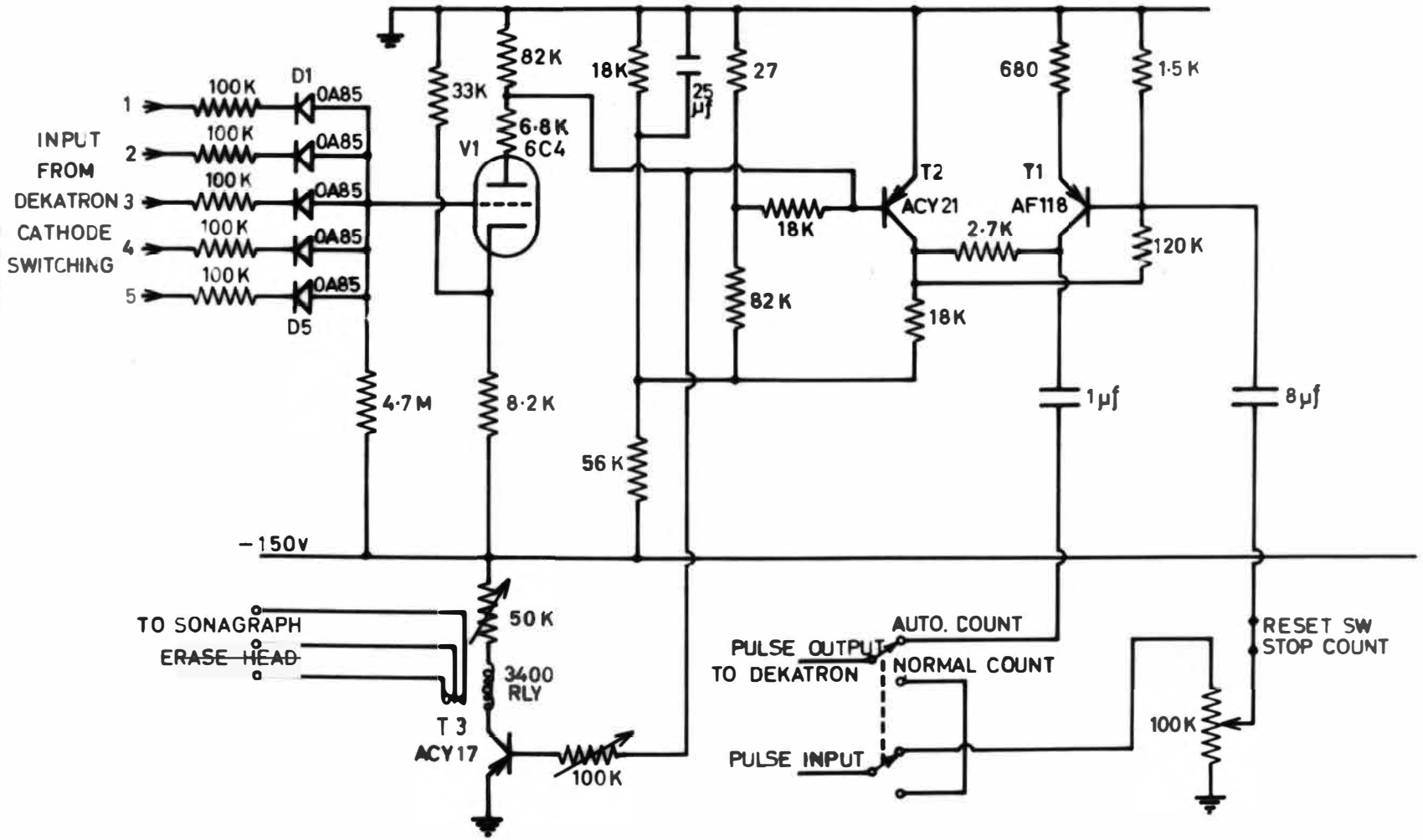
INPUT FROM DEKATRON CATHODE SWITCHING
1
2
3
4
5
100K
D1
0A85
D5
33K
82K
6·8K
6C4
V1
18K
25 µf
27
680
1·5K
T2
ACY21
T1
AF118
2·7K
120K
18K
82K
18K
4·7M
8·2K
56K
1µf
8µf
−150v
TO SONAGRAPH
ERASE HEAD
50K
3400 RLY
T3
ACY17
100K
AUTO. COUNT
PULSE OUTPUT TO DEKATRON
NORMAL COUNT
PULSE INPUT
RESET SW
STOP COUNT
100K